

AWARD NUMBER: W81XWH-13-1-0193

TITLE: Clinical Development of Gamitrinib, a Novel Mitochondrial-Targeted Small Molecule Hsp90 Inhibitor

PRINCIPAL INVESTIGATOR: Dario C. Altieri

CONTRACTING ORGANIZATION: The Wistar Institute
Philadelphia, PA 19104

REPORT DATE: September 2015

TYPE OF REPORT: Annual

PREPARED FOR: U.S. Army Medical Research and Materiel Command
Fort Detrick, Maryland 21702-5012

DISTRIBUTION STATEMENT: Approved for Public Release;
Distribution Unlimited

The views, opinions and/or findings contained in this report are those of the author(s) and should not be construed as an official Department of the Army position, policy or decision unless so designated by other documentation.

REPORT DOCUMENTATION PAGE

Form Approved
OMB No. 0704-0188

Public reporting burden for this collection of information is estimated to average 1 hour per response, including the time for reviewing instructions, searching existing data sources, gathering and maintaining the data needed, and completing and reviewing this collection of information. Send comments regarding this burden estimate or any other aspect of this collection of information, including suggestions for reducing this burden to Department of Defense, Washington Headquarters Services, Directorate for Information Operations and Reports (0704-0188), 1215 Jefferson Davis Highway, Suite 1204, Arlington, VA 22202-4302. Respondents should be aware that notwithstanding any other provision of law, no person shall be subject to any penalty for failing to comply with a collection of information if it does not display a currently valid OMB control number. **PLEASE DO NOT RETURN YOUR FORM TO THE ABOVE ADDRESS.**

1. REPORT DATE (DD-MM-YYYY) September 2015			2. REPORT TYPE Annual		3. DATES COVERED (From - To) 1 Sep 2014 – 31 Aug 2015	
4. TITLE AND SUBTITLE Clinical Development of Gamitrinib, a Novel Mitochondrial-Targeted Small Molecule Hsp90 Inhibitor					5a. CONTRACT NUMBER	
					5b. GRANT NUMBER W81XWH-13-1-0193	
					5c. PROGRAM ELEMENT NUMBER	
6. AUTHOR(S) Dario C. Altieri email: daltieri@wistar.org					5d. PROJECT NUMBER	
					5e. TASK NUMBER	
					5f. WORK UNIT NUMBER	
7. PERFORMING ORGANIZATION NAME(S) AND ADDRESS(ES) The Wistar Institute Philadelphia, PA 19104					8. PERFORMING ORGANIZATION REPORT NUMBER	
9. SPONSORING / MONITORING AGENCY NAME(S) AND ADDRESS(ES) U.S. Army Medical Research and Materiel Command Fort Detrick, Maryland 21702-5012					10. SPONSOR/MONITOR'S ACRONYM(S)	
					11. SPONSOR/MONITOR'S REPORT NUMBER(S)	
12. DISTRIBUTION / AVAILABILITY STATEMENT Approved for public release; distribution is unlimited.						
13. SUPPLEMENTARY NOTES						
14. ABSTRACT The past funding cycle of the present award has supported important advances in each of the milestones and specific tasks set forth in the original SOW. Work supported by the present award focused on three directions with the overarching goal of completing the original specific aim 2 of the application. First, we continued the preclinical characterization of Gamitrinib as a unique anticancer agent. Published in the premiere, peer-reviewed literature (<i>JNCI, PNAS and Sci Signal</i>), these studies demonstrated that the combination of Gamitrinib plus small molecule inhibitors of PI3K/Akt/mTOR pathway currently in the clinic delivered potent and synergistic anticancer activity in preclinical models (i), suppressed adaptive mitochondrial reprogramming of enhanced tumor cell survival (ii) and blocked a novel pathway of prostate cancer invasion and metastasis supported by mitochondrial bioenergetics at the cortical cytoskeleton (iii). Second, an initial non-GLP 7-day repeated dose toxicology study in rats using Gamitrinib formulated in the original formulation (75% DMSO- 25% PBS) demonstrated toxicity at the highest dose used of 6 mg/kg/daily after 4 repeated i.v. doses. Third, and in light of these initial results, we identified and characterized a novel, non-DMSO-based emulsion of Gamitrinib, which retained anticancer activity. This novel emulsion-based formulation of Gamitrinib will be used in the next budget cycle for new non-GLP repeated-dose toxicology in suitable animal species, as anticipated in the original SOW.						
15. SUBJECT TERMS Mitochondria, oxidative phosphorylation, Hsp90, advanced prostate cancer, Gamitrinib						
16. SECURITY CLASSIFICATION OF:				17. LIMITATION OF ABSTRACT UU	18. NUMBER OF PAGES 49	19a. NAME OF RESPONSIBLE PERSON USAMRMC
a. REPORT U	b. ABSTRACT U	c. THIS PAGE U	19b. TELEPHONE NUMBER (include area code)			

TABLE OF CONTENTS

Page

1. Introduction
2. Keywords
3. Accomplishments
4. Impact
5. Changes/Problems
6. Products
7. Participants & Other Collaborating Organizations
8. Special Reporting Requirements
9. Appendices

1. **INTRODUCTION.** The present research project is designed to reach a complete preclinical characterization (formulation studies, pharmacokinetics analysis, toxicology profile and identification and validation of suitable biomarkers) of Gamitrinib (GA mitochondrial matrix inhibitor), a first-in-class, mitochondrial-targeted small molecule inhibitor of Heat Shock Protein-90 (Hsp90) chaperones. Extensive preliminary data in support of the application have demonstrated that Gamitrinib has a unique mechanism of action, penetrating the mitochondria and selectively inhibiting the ATPase activity of a pool of Hsp90 and Hsp90-homolog TRAP-1 (TNFR-Associated Protein-1, TRAP-1) chaperones localized within the mitochondrial matrix and inner membrane. In turn, this causes catastrophic loss of protein folding quality control selectively within mitochondria, collapse of tumor bioenergetics, massive activation of apoptosis and potent single-agent and combination cytotoxic anticancer activity, in vivo. As Hsp90 chaperones are selectively enriched in tumor mitochondria, as opposed to normal tissues, Gamitrinib has shown good tolerability in preclinical xenograft and genetic tumor models, in vivo. The overarching goal of the proposal is to complete all of the preclinical characterization of Gamitrinib in order to support filing of an Investigational New Drug (IND) Application with the US Food and Drug Administration (FDA). This will fulfill key regulatory requirements in anticipation of the clinical testing of Gamitrinib in patients with advanced, castrate-resistant and metastatic prostate cancer.
2. **KEYWORDS.** Mitochondria, oxidative phosphorylation, Hsp90, metabolomics, advanced prostate cancer, Gamitrinib
3. **ACCOMPLISHMENTS.**
 - **What were the major goals of the project?**

Consistent with the original SOW of the application, studies proposed for the past budget cycle focused on the characterization of an effective formulation of Gamitrinib (i), suitability of Gamitrinib detection in dog plasma in anticipation of pharmacokinetics studies (ii), and initial, non-GLP 7-day repeated dose studies of Gamitrinib toxicity in rats (iii). In parallel, we continued our in-depth characterization of Gamitrinib unique anticancer activity, with respect to mechanism of action, suitability for combination regimens with other targeted agents and modulation of tumor cell migration and invasion for potential anti-metastatic strategies (iv).
 - **What was accomplished under these goals?**
 1. Major activities.

Studies reported in the 2015 quarterly report for this award demonstrated that a formulation of DMSO-PBS (75%-25%) provided optimal solubilization of Gamitrinib, stability of the solution over a 2-week interval at 4°C and the strongest anticancer activity against prostate cancer cell types. Other FDA-approved formulations were tested in these experiments, but none generated better results compared to the DMSO-PBS formulation. Based on these results, initial experiments were carried out during the past budget period to establish the suitability of Gamitrinib detection in dog plasma in anticipation of a complete pharmacokinetics profile. These studies utilized plasma samples collected from Beagle dogs spiked with increasing concentrations of Gamitrinib formulated in the DMSO-PBS formulation followed by tandem mass spectrometry. Second, we carried out 7-day repeated dose toxicity study of Gamitrinib formulated in the DMSO-PBS formulation administered daily i.v. to Sprague rats. Third, a new series of mechanistic experiments was carried out during the last budget cycle to further advance the preclinical characterization of Gamitrinib, specifically focused on novel combination.
 2. Specific objectives.

The specific objectives of these experiments were as follows. (1) **Establish the feasibility of Gamitrinib detection in samples of Beagle dog plasma using tandem mass spectrometry.** These studies were carried out as a feasibility step in anticipation of the full pharmacokinetics profile of Gamitrinib that is planned in the next budget cycle of the present application. (2) **Test the toxicity profile of Gamitrinib formulated in a DMSO-PBS formulation in a 7-day repeated dose study in Sprague rats.** All of the anticancer efficacy studies of Gamitrinib in rodents were carried out using a Cremophore formulation, which cannot be utilized in dogs for the risk of life-threatening anaphylactic reactions. The non-GLP studies carried out in the previous budget cycle examined the safety and suitability of a DMSO-based formulation of Gamitrinib in a 7-day repeated dose study in rats. (3) **Continue the preclinical characterization of Gamitrinib, and test its suitability in novel combination strategies with other molecularly-targeted drugs currently in the clinic, and as a potential inhibitor of prostate cancer metastasis.** Preliminary studies demonstrated that combination approaches of Gamitrinib with other anticancer drugs is feasible and may deliver more potent, synergistic anticancer activity in preclinical models. The studies carried out in the last budget

cycle followed up on this concept and utilized an unbiased high-throughput drug screen to identify novel combinations of Gamitrinib plus approved anticancer agents. Additional studies further examined the ability of Gamitrinib to suppress the bioenergetics requirements of prostate cancer migration and invasion, and potentially function as a first-in-class anti-metastatic agent.

3. Significant Results.

(1) Feasibility of detection of Gamitrinib formulated in 75%DMSO-25% PBS in dog plasma by mass spectrometry.

These studies were carried out to determine the feasibility of Gamitrinib detection in Beagle dog plasma.

Gamitrinib was formulated in a 75% DMSO-25% PBS formulation and added (spiked) to samples (50 µl) of Beagle dog plasma (K₂ EDTA, Matrix) over a range of concentrations between 20-20,000 ng/ml. A d15-labeled variant of Gamitrinib was synthesized for these experiments and used as an internal standard. Gamitrinib detection was carried out using a validated liquid chromatography-tandem mass spectrometry (LC-MS/MS) method. The endpoints for these experiments included the following parameters: Injection Matrix Integrity (IMI, 9 d stability at 4°C); Short-Term Matrix Stability (STMS, 24 h stability at 22°C –room temperature), Freeze-Thaw Matrix Stability (FTMS, 3 repeated cycles of freezing and thawing at -80°C), and Long-Term Matrix Stability (LTMS, 42 days stability at -80°C). The results of these experiments collectively demonstrated that detection of Gamitrinib in dog plasma is feasible, highly accurate and reproducible over increasing time intervals of storage of the primary samples. The results of the calibration standard of Gamitrinib in dog plasma is presented in [Table 1](#).

Table 1. Calibration Standard Results and Statistics of Gamitrinib in Dog Plasma

Watson Run ID	Concentration (ng/mL)									
	20.0	40.0	80.0	200	600	1600	4000	10000	16000	20000
01	20.3	39.5	79.0	190	557	2080 ^b	3933	9977	17288	21411
02	19.9	41.1	76.1	201	605	2050 ^b	4178	9757	15288	20692
03	20.1	41.3	75.4	190	597	2051 ^b	4056	10257	16355	20292
04	20.0	40.4	77.5	203	609	2042 ^b	4220	10109	15404	19192
05	20.4	39.2	77.6	190	621	1924 ^b	4036	9879	16381	20477
Mean	20.2	40.3	77.1	195	598	a	4084	9996	16143	20413
S.D.	0.215	0.943	1.42	6.78	24.5	a	115	195	820	803
% CV	1.1	2.3	1.8	3.5	4.1	a	2.8	1.9	5.1	3.9
% Bias	0.8	0.8	-3.6	-2.6	-0.3	a	2.1	0.0	0.9	2.1
n	5	5	5	5	5	a	5	5	5	5

a Not applicable, result not included in the statistical calculations.

b Outside of acceptance criteria; result not included in the statistical calculations.

As shown in [Table 2](#), the detection of Gamitrinib in dog plasma remained stable during short-term storage of the samples (24 h at room temperature) ([Table 2](#)).

Table 2 Short-term Matrix Stability at Ambient Room Temperature for 24 Hours

Theoretical concentration (ng/mL)	Measured concentration (ng/mL)	Relative error (%)	Average relative error (%)	CV (%)
60.0	56.1	-6.5	-7.1	2.5
	58.0	-3.3		
	54.6	-9.1		
	56.3	-6.2		
	54.3	-9.5		
	55.1	-8.1		
15000	15423	2.8	1.1	1.7
	15016	0.1		
	14785	-1.4		
	15412	2.7		
	15263	1.8		
	15067	0.4		

In addition, as shown in [Table 3](#), Gamitrinib detection in dog plasma was stable after a 9-day storage at 4°C ([Table 3](#)). All other parameters investigated in this study concurred to demonstrate the feasibility and reproducibility of Gamitrinib detection in dog plasma using LC/MS methods.

Table 3 Injection Medium Integrity at Approximately 4°C for 9 Days

Theoretical concentration (ng/mL)	Measured concentration fresh (ng/mL)	Relative error (%)	Measured concentration after storage (ng/mL)	Relative error (%)
60.0	60.1	0.2	61.5	2.5
	59.1	-1.4	59.1	-1.5
	58.0	-3.3	61.0	1.6
	62.0	3.4	59.1	-1.5
1400	1361	-2.8	1395	-0.4
	1345	-4.0	1362	-2.7
	1448	3.4	1407	0.5
	1389	-0.8	1437	2.7
15000	15100	0.7	15017	0.1
	13211	-11.9	13457	-10.3
	15560	3.7	15577	3.8
	15857	5.7	15185	1.2

(2) *Preliminary toxicity of Gamitrinib in rats.* A second series of experiments investigated the suitability of the Gamitrinib formulation in DMSO-PBS for IND-directed toxicology studies in rats. For these experiments, non-GLP grade Gamitrinib was formulated in the DMSO-PBS formulation as above and injected i.v. into Sprague rats in a 7-day repeated dose study. The concentrations of Gamitrinib used for these studies were 0 (Group 1 –DMSO-PBS formulation), 10 mg/kg/daily (Group 2) and 20 mg/kg daily (Group 3). Both male (6 animals) and female (6 animals) rats were used in each of the treatment group. The results of these experiments were as follows:

- (1) Repeated administration of Gamitrinib in the DMSO-based formulation is feasible.
- (2) The dose of Gamitrinib in Group 2 animals (10 mg/kg/daily/i.v.) generated one unexplained animal death on day 1 (after one dose) and one animal death on day 5 (after 5 doses).
- (3) The dose of Gamitrinib in Group 3 animals generated three unexplained animal deaths on day 5 (after 5 doses) and one additional animal death on day 6 (after 6 doses).
- (4) At necropsy, the cause of animal deaths in both Groups was not determined.
- (5) There was a 5% decrease in overall body weight in Group 2 animals and a 12% decrease in Group 3 animals after 7 day repeated dosing of Gamitrinib (Figure 1).
- (6) Despite the unexplained animal deaths in both groups, bone marrow function parameters in Group 2 and Group 3 animals examined at the end of the 7-repeated doses was comparable to those in control Group 1 animals (Figure 2).
- (7) Despite the unexplained animal deaths in both groups, clinico-chemistry parameters of liver and kidney function in Group 2 and Group 3 animals examined at the end of the 7-day repeated doses was comparable to those of Group 1 animals (Figure 3)

(7) **Conclusion:** The formulation of Gamitrinib in high concentrations of DMSO (75%) produces toxicity in rats, independently of the dose administered. A toxic effect of the formulation is consistent with extensive evidence in the literature indicating that DMSO-based formulations are not well tolerated in rats and cannot be used in dogs.

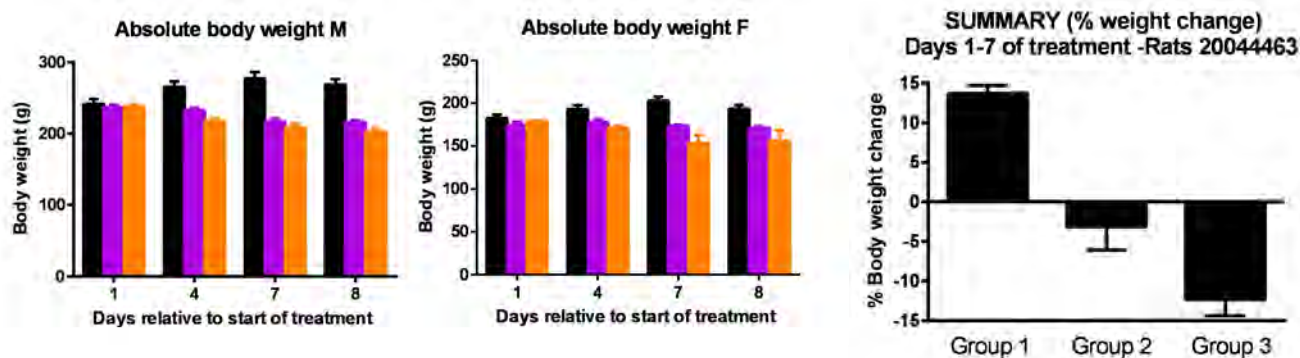


Figure 1. Effect of Gamitrinib administration on animal body weight after 7 repeated administrations. Group 1 – Formulation (BLACK); Group 2 -10 mg.kg/daily i.v. (PURPLE); Group 3 -20 mg/kg/daily/i.v. (ORANGE). Right, summary of body weight changes. M, males; F, females.

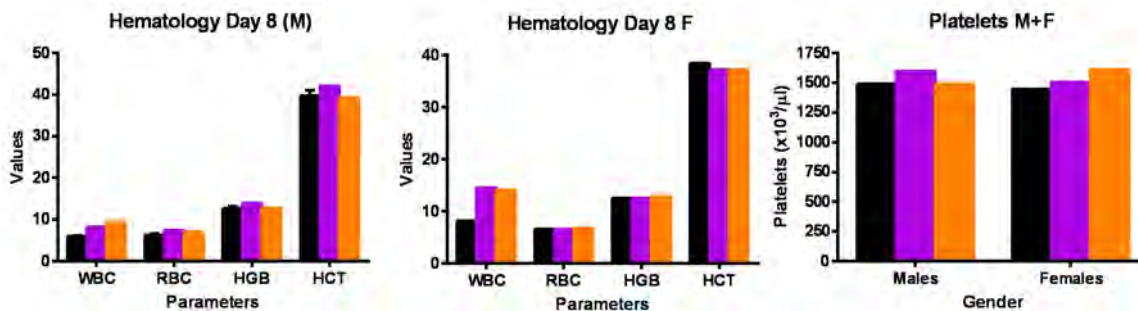


Figure 2. Effect of Gamitrinib administration on hematologic parameters and bone marrow function after 7 repeated administrations. Group 1 –Formulation (BLACK); Group 2 -10 mg.kg/daily i.v. (PURPLE); Group 3 -20 mg/kg/daily/i.v. (ORANGE). M, males; F, females.

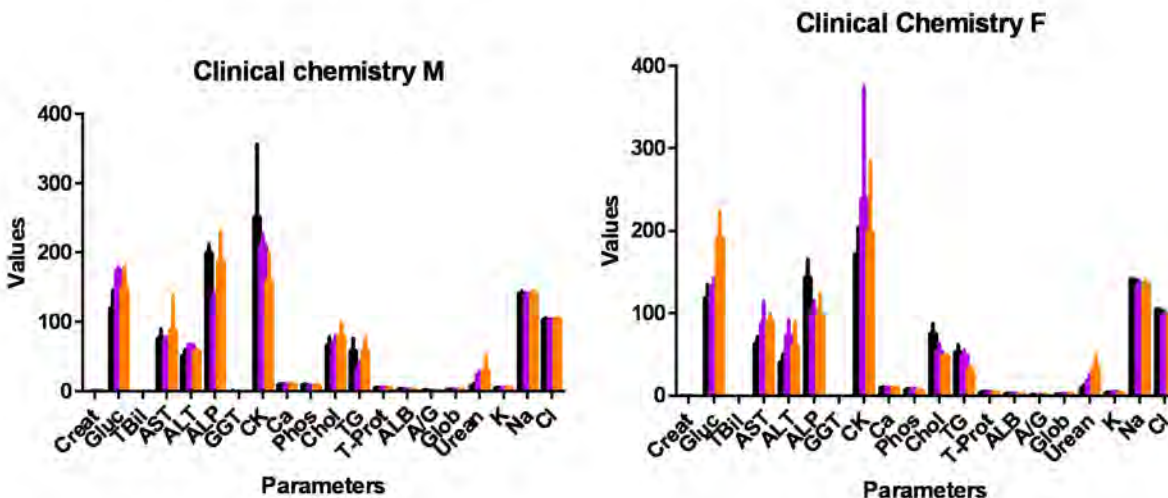


Figure 3. Effect of Gamitrinib administration on hematologic parameters and bone marrow function after 7 repeated administrations. Group 1 –Formulation (BLACK); Group 2 -10 mg.kg/daily i.v. (PURPLE); Group 3 -20 mg/kg/daily/i.v. (ORANGE). M, males; F, females

Based on these preliminary results, future studies will examine a novel Gamitrinib formulation as a micellar emulsion. This formulation is based on the Lipoid S-100 emulsificant and reduces the concentration of DMSO in the formulation from 75% to 2.5%. Preliminary experiments carried out during the last budget cycle have demonstrated that Gamitrinib formulated in the Lipoid S-100 emulsion retains full anticancer activity against prostate cancer cell types, indistinguishably from the original DMSO-PBS formulation. Toxicity experiments including new repeated dose studies will be carried out during the next budget cycle using the new emulsion-based formulation of Gamitrinib.

- (3) *Characterization of the anticancer activity of Gamitrinib.* Supported by the present award, additional mechanistic studies were carried out during the last budget cycle to further characterize the anticancer activity of Gamitrinib. These studies identified three novel aspects of Gamitrinib that enhances its spectrum of activity and first-in-class potential as a unique anticancer agent in humans.

First, using an unbiased high-throughput drug screen, we demonstrated that the combination of Gamitrinib plus small molecule inhibitors of the PI3K/Akt/mTOR pathway currently in the clinic produced strong and synergistic tumor cell killing. In contrast, none of the other targeted agents examined in the screen was effective in synergizing with Gamitrinib. Mechanistically, the combination of Gamitrinib plus PI3K inhibitors induced massive activation of mitochondrial apoptosis, prevented adaptive pathways of increased tumor cells survival and resulted in strong inhibition of tumor growth in vivo (Ghosh JC, Siegelin MD, Vaira V, Favarsani A, Tavecchio M, Chae YC, Lisanti S, Rampini P, Giroda M, Caino MC, Seo JH, Kossenkov AV, Michalek RD, Schultz DC, Bosari S, Languino LR, and Altieri DC (2015) Adaptive mitochondrial reprogramming and resistance to PI3K therapy *JNCI* 107 pii: dju502. doi: 10.1093/jnci/dju502 2015).

Second, we discovered that in response to stress stimuli typically found in the tumor microenvironment, including hypoxia and exposure to molecular therapy, prostate cancer cells reposition energetically active mitochondria to the cortical cytoskeleton. Juxtaposed to cellular protrusions implicated in cell movements, these *cortical* mitochondria provide a concentrated, *regional* energy source to fuel membrane lamellipodia dynamics, turnover of focal adhesion complexes, and increased tumor cell migration and invasion. Conversely, treatment of tumor cells with non-toxic

concentrations of Gamitrinib that do not induce tumor cell killing suppressed oxidative phosphorylation, prevented the repositioning of mitochondria to the cortical cytoskeleton and potentially inhibited tumor cell migration and invasion (Caino MC, Ghosh JC, Chae YC, Vaira V, Rivadeneira DB, Favarsani A, Rampini P, Kossenkov AV, Aird KM, Zhang R, Webster MR, Weeraratna AT, Bosari S, Languino LR, and Altieri DC (2015) PI3K therapy reprograms mitochondrial trafficking to fuel tumor cell invasion. *Proc Natl Acad Sci USA* 112:8638-8643. PMID: PMC4507184).

Third, we elucidated the biochemical requirements of mitochondrial trafficking to the cortical cytoskeleton as a regional source of energy for increased tumor cell migration and invasion. In these studies, we identified a novel role of the mitochondrial pool of the apoptosis regulator, survivin that helped maintain the folding and stability of oxidative phosphorylation Complex II subunit, SDHB in cooperation with mitochondrial Hsp90s. Accordingly, genetic or pharmacologic inhibition of mitochondrial survivin or targeting mitochondrial Hsp90s with Gamitrinib resulted in inhibition of mitochondrial trafficking to the cortical cytoskeleton, suppression of tumor cell migration and invasion and ablation of metastatic dissemination in a model of liver metastasis in vivo (Rivadeneira DB, Caino MC, Seo JH, Angelin A, Wallace DC, Languino LR, and Altieri DC (2015) Survivin promotes oxidative phosphorylation, subcellular mitochondrial repositioning, and tumor cell invasion. *Sci Signal* 8(389):ra80. PMID: PMC4539531).

The conclusions from these mechanistic studies are as follows: (1) We identified and validated a novel, rational combination strategy of Gamitrinib plus small molecule inhibitors of the PI3K/Akt/mTOR pathway that abolishes adaptive mechanisms of tumor compensation and delivers potent and synergistic anticancer activity, in vivo. (2) We characterized a novel mechanism of metastatic competency based on subcellular trafficking of mitochondria and generation of an efficient, *regional* energy source to fuel the machinery of tumor cell motility. (3) We validated the role of Gamitrinib as a potent suppressor of mitochondrial bioenergetics, including oxidative phosphorylation. The ability of Gamitrinib to inhibit membrane dynamics and tumor cell motility validates its indication in advanced disease settings, potentially as a novel anti-metastatic strategy.

4. Other Achievements.

Initial characterization of a novel, non-DMSO formulation of Gamitrinib based on Lipoid S-100 emulsification and formation of a micellar suspension with retained anticancer activity.

- **What opportunities for training and professional development has the project provided?**

The present application is not designed to provide a training and professional development environment. Nothing to report.

- **How were the results disseminated to communities of interest?**

The mechanistic studies on the further characterization of Gamitrinib anticancer activity, including synergistic combination therapies with small molecule inhibitors of PI3K/Akt/mTOR (i), identification of *regional* mitochondrial bioenergetics as a novel mechanism to fuel membrane dynamics of cell motility and increased tumor cell invasion (ii), and the biochemical role of the survivin-mitochondrial Hsp90 complex in supporting oxidative phosphorylation and increased tumor cell invasion (iii) were published in the premiere, peer-reviewed literature (*JNCI* 107 pii: dju502. doi: 10.1093/jnci/dju502 2015; *Proc Natl Acad Sci USA* 112:8638; *Sci Signal* 8(389):ra80). In addition, the PI on the present application presented some of these experimental results at the 2015 Banbury Conference on Mitochondria and Cancer (Cold Spring Harbor Laboratory, September 1-4, 2015).

- **What do you plan to do during the next reporting period to accomplish the goals?**

Studies will be carried out during the next budget cycle to accomplish the goals in specific aim 2 of the original SOW. Specifically, we will first test the novel, non-DMSO Lipoid S-100 emulsion formulation of Gamitrinib in a non-GLP repeated dose study in Sprague rats with evaluation of animal survival and functional parameters of liver, kidney and bone marrow function. Second, we will use this emulsion formulation of Gamitrinib in Lipoid S-100 to reach a comprehensive pharmacokinetics profile in rats. Third, we will continue our mechanistic studies on the role of *regional* mitochondrial bioenergetics as a mechanism to support tumor cell motility and metastasis, and further validate the role of Gamitrinib as a potential anti-metastatic agent, alone or in combination with other molecularly-targeted agents.

4. IMPACT

- **What was the impact on the development of the principal disciplines of the project?**

The studies summarized above had considerable impact on the principal disciplines of the project. First, we validated a highly reproducible and reliable tandem mass spectrometry method to detect a broad range of Gamitrinib concentrations spiked in dog plasma. Several parameters examined in these studies demonstrated that detection of Gamitrinib in plasma is feasible, reproducible and stable over long-term storage of the plasma samples. Second, these results emphasized the importance of optimal formulation development of Gamitrinib for IND-directed toxicity studies. Previous efficacy data of Gamitrinib in rodents utilized a Cremophore-based formulation, which unsuitable for the present studies, especially in dogs due to acute onset of life-threatening allergic reactions. To address this limitation, we carried out additional formulation development studies during the past budget cycle, and identified a 75% DMSO-25% PBS formulation as the best solvent for Gamitrinib. Although Gamitrinib solubilization was achieved also with other FDA-approved solvents, the high DMSO

formulation was the most effective to enable the production of highly concentrated drug stock solutions for use in animals. However, the results of the non-GLP repeated dose study in rats presented here demonstrated that Gamitrinib formulated in high concentrations of DMSO resulted in unexplained acute animal death, in the absence of obvious defects in tissue and organ function and with only a 5% decrease in overall animal weight (Group 2). In consultation with the *Gamitrinib development team*, we have concluded that the acute toxicity observed was independent of dose and likely due to the high concentration of DMSO (75%) in which Gamitrinib was formulated. This conclusion led to the additional studies carried out in the previous funding cycle that identified a low-DMSO (2.5%) emulsion formulation of Gamitrinib that utilizes Lipoid S-100 emulsificant as a base constituent. In this emulsion, Gamitrinib retained solubility at high concentrations (10 mg/kg) and anticancer activity comparable to the high DMSO formulation.

- **What was the impact on other disciplines?**

The results summarized above had significant impact for other disciplines, in particular for establishing a novel role of mitochondrial bioenergetics in fueling the process of metastasis in prostate cancer. In this context, the role of mitochondria in cancer has been controversial in the literature, as most tumors rewire their energy requirements to utilize glycolysis at the expense of mitochondrial oxidative phosphorylation (the so-called “Warburg effect”). Surprisingly, however, the basic question of how tumors that rely on an inefficient glycolytic metabolism support highly energy-intensive processes of cell migration, invasion and metastasis has not been answered. Our results identify a novel concept of metastatic competency, in which energetically active mitochondria reposition to the cortical cytoskeleton in physical proximity to subcellular sites of high energy demands. In turn, these *cortical* mitochondria provide a concentrated, *regional* energy source to power membrane dynamics of cell motility, lamellipodia dynamics and increased tumor cell migration and invasion. Consistent with the ability of Gamitrinib to inhibit mitochondrial respiration characterized in previous studies, results obtained in the previous budget cycle demonstrated that non-toxic concentrations of Gamitrinib suppressed mitochondrial oxidative phosphorylation, prevented mitochondrial repositioning to the cortical cytoskeleton and abolished tumor cell migration and invasion. These results introduce a novel concept of *spatiotemporal* mitochondrial bioenergetics as an indispensable requirement for tumor cell migration and invasion and therapeutic target in advanced disease, and validate the potential utility of Gamitrinib for novel anti-metastatic approaches.

- **What was the impact on technology transfer?**

Based on the novel results summarized above, a new US patent application was filed during the last budget cycle that focused on the contribution of subcellular mitochondrial bioenergetics in supporting metastatic competency, and the role of Gamitrinib as a potential, first-in-class anti-metastatic agent for advanced prostate cancer.

- **What was the impact on society beyond science and technology?**

These studies may open new, concrete prospect for the management of patients with advanced prostate cancer. Although early-stage prostate cancer is successfully managed and these patients are offered a range of options, more advanced disease settings carry significant morbidity and mortality due to disease dissemination to bones and visceral organs, with limited, if any, meaningful therapeutic options. The identification of a novel mechanism of *spatiotemporal* mitochondrial bioenergetics that supports metastasis, and the characterization of Gamitrinib as an inhibitor of this process, suggests a novel therapeutic strategy of cutting off energy supplies of tumor cell motility as a novel, first-in-class approach to anti-metastatic therapies in advanced cancer patients.

5. CHANGES/PROBLEMS.

- **Changes in approach and reasons for change.**

As detailed above, the initial formulation of Gamitrinib in high concentration of DMSO (75%) was found to be unsuitable for the further preclinical development of this agent in rats. Accordingly, the approach will be changed in the next budget cycle, and new non-GLP repeated dose studies are being currently planned that involve the novel emulsion formulation of Gamitrinib with the Lipoid S-100 micellar emulsificant. Preliminary experiments carried out in the past budget cycle have demonstrated that this new emulsion formulation of Gamitrinib is stable, allows the generation of high stock drug concentrations, and preserves anticancer activity against prostate cancer cell types, comparably to the high-DMSO formulation. In this context, the Lipoid S-100 emulsion of Gamitrinib lowers the DMSO concentration in the formulation from 75% to 2.5%, thus eliminating potential DMSO-related acute toxicity in rats observed in the previous budget cycle.

- **Actual or anticipated problems or delays and actions or plans to resolve them.**

We do not anticipate problems or delays in testing the new emulsion formulation of Gamitrinib with Lipod S-100 emulsificant in a new non-GLP repeated dose study in Sprague rats. Similar to the past budget cycle, these studies will be completed with a full toxicology profile in the various treatment groups, monitoring of animal weight throughout treatment duration, and analysis of liver, kidney and bone marrow function.

- **Changes that had a significant impact on expenditures.**

None reported

- **Significant changes in use or care of human subjects, vertebrate animals, biohazards, and/or select agents.**

None reported

6. PRODUCTS

• Publications, conference papers, and presentations

Journal Publications

1. Ghosh JC, Siegelin MD, Vaira V, Favarsani A, Tavecchio M, Chae YC, Lisanti S, Rampini P, Giroda M, Caino MC, Seo JH, Kossenkov AV, Michalek RD, Schultz DC, Bosari S, Languino LR, and Altieri DC (2015) Adaptive mitochondrial reprogramming and resistance to PI3K therapy *JNCI* 107 pii: dju502. doi: 10.1093/jnci/dju502 2015. PMID: 25650317. PMCID In Progress.
2. Trerotola M, Ganguly KK, Fazli L, Lu H, Dutta A, Liu Q, De Angelis T, Robio N, Gleave ME, Zoubeidi A, Altieri DC, and Languino LR (2015) Trop-2 is up-regulated in aggressive prostate cancer and interacts with $\alpha 5\beta 1$ integrin. *Oncotarget* 6:14318-1428. PMCID PMC4546469.
3. Caino MC, Ghosh JC, Chae YC, Vaira V, Rivadeneira DB, Favarsani A, Rampini P, Kossenkov AV, Aird KM, Zhang R, Webster MR, Weeraratna AT, Bosari S, Languino LR, and Altieri DC (2015) PI3K therapy reprograms mitochondrial trafficking to fuel tumor cell invasion. *Proc Natl Acad Sci USA* 112:8638-8643. PMCID: PMC4507184.
4. Rivadeneira DB, Caino MC, Seo JH, Angelin A, Wallace DC, Languino LR, and Altieri DC (2015) Survivin promotes oxidative phosphorylation, subcellular mitochondrial repositioning, and tumor cell invasion. *Sci Signal* 8(389):ra80. PMCID: PMC4539531.

Books or other non-periodical, one-time publications

Not applicable

Other publications, conference papers, and presentations

Invited speaker, 2015 Banbury Conference *Mitochondria and Cancer*, September 1-4, Cold Spring Harbor Laboratory, New York. Title of presentation: *Regulators of Mitochondrial Metabolism and Cancer Therapy*.

Websites or other Internet sites.

Not applicable

Technologies or techniques.

Time-lapse videomicroscopy of mitochondrial trafficking to the cortical cytoskeleton; stroboscopic imaging and quantification of membrane lamellipodia dynamics; high-throughput drug screen of the combination of Gamitrinib plus small molecule inhibitors of PI3K/Akt/mTOR pathway,

Inventions, patent applications, and/or licenses.

A new US provisional patent application has been filed based on the observations reported in the past budget cycle that tumor cells exposed to stress stimuli typically found in the tumor microenvironment, including molecular therapy, reposition their mitochondria to the cortical cytoskeleton, where they fuel membrane dynamics of cell motility, turnover of focal adhesions complexes, and increased tumor cell migration and invasion (named inventors, Altieri, DC and Caino MC).

Other Products

Not applicable

7. PARTICIPANTS & OTHER COLLABORATING ORGANIZATIONS

• What individuals have worked on the project?

Name:	Dario C. Altieri, M.D.
Project Role:	Principal Investigator
Researcher Identifier (e.g. ORCID ID):	
Nearest person month worked:	2
Contribution to Project:	Dr. Altieri coordinated and oversaw all of the studies of preclinical development of Gamitrinib, metabolomics screening and characterization of a biomarker signature of Gamitrinib anticancer activity in TRAMP mice
Funding Support:	In addition to the present award, these studies are also supported by NIH NCI CA78810 and CA14004. There is no scientific or budgetary overlap with any of these grants.
Name:	Young Chan Chae, Ph.D.
Project Role:	Postdoctoral Fellow
Researcher Identifier (e.g. ORCID ID):	
Nearest person month worked:	6
Contribution to Project:	Dr. Chae participated in the characterization of Gamitrinib regulation of mitochondrial bioenergetics, metabolomics profiling, and identification of a mitochondrial Hsp90 proteome

Funding Support: In addition to the present award, these studies are also supported by NIH NCI CA78810 and CA140043. There is no scientific or budgetary overlap with any of these grants.

Name: Qin Liu, Ph.D.
Project Role: Biostatistician
Researcher Identifier (e.g. ORCID ID):
Nearest person month worked: 1
Contribution to Project: As Director of the Biostatistics Unit of the Wistar Cancer Center Dr. Liu reviewed power of analysis, sample size calculations and provided statistical input for the in vivo experiments of bioenergetics requirements of metastatic dissemination.

Funding Support: In addition to the present award, these studies are also supported by NIH NCI CA140043. There is no scientific or budgetary overlap with this grant.

Name: Jody Hohenbrink, M.A.; Kelly Landin, M.A.
Project Role: Project Coordinators –Charles River Laboratory
Researcher Identifier (e.g. ORCID ID):
Nearest person month worked: 1
Contribution to Project: As Project Coordinators for the Gamitrinib development team, Ms. Hohenbrink and Landing oversaw the non-GLP preclinical evaluation of Gamitrinib in a 7-day repeated dose study in Sprague rats and the validation of tandem mass spectrometry for the detection of Gamitrinib in Beagle dog plasma.
Funding support: Present award.

- **Has there been a change in the active other support of the PD/PI(s) or senior/key personnel since the last reporting period?**
Nothing to report.

- **What other organizations were involved as partners?**
Organization: Thomas Jefferson University, Department Nuclear Medicine
Location: Philadelphia, PA
Contribution: Collaboration on the ¹⁸F-FDG-PET studies on WT and TRAP-1 knockout mice.

Organization: University of Pennsylvania Veterinary School
Location: Philadelphia, PA
Contribution: Collaboration on histologic characterization of TRAP-1 knockout mice.

Organization: Charles River Laboratory
Location: Spencerville, OH
Contribution: Preclinical characterization of Gamitrinib in Sprague rats.

8. SPECIAL REPORTING REQUIREMENTS

Nothing to report

9. APPENDICES

PDFs are attached for papers identified in #6 of this report.

ARTICLE

Adaptive Mitochondrial Reprogramming and Resistance to PI3K Therapy

Jagadish C. Ghosh, Markus D. Siegelin, Valentina Vaira, Alice Faversani, Michele Tavecchio, Young Chan Chae, Sofia Lisanti, Paolo Rampini, Massimo Giroda, M. Cecilia Caino, Jae Ho Seo, Andrew V. Kossenkov, Ryan D. Michalek, David C. Schultz, Silvano Bosari, Lucia R. Languino, Dario C. Altieri

Affiliations of authors: Prostate Cancer Discovery and Development Program (JCG, MT, YCC, SL, MCC, JHS, LRL, DCA), Tumor Microenvironment and Metastasis Program (JCG, MT, YCC, SL, MCC, JHS, DCA), Center for Systems and Computational Biology (AVK), and Center for Chemical Biology and Translational Medicine (DCS), The Wistar Institute, Philadelphia, PA; Department of Pathology and Cell Biology, Columbia University Medical Center, New York, NY (MDS); Istituto Nazionale Genetica Molecolare "Romeo and Enrica Invernizzi," Milan, Italy (VV); Division of Pathology (VV, AF, SB), Division of Neurosurgery (PR), and Division of Surgery (MG), Fondazione IRCCS Ca' Granda Ospedale Maggiore Policlinico, Milan, Italy; Metabolon, Inc. Durham, NC (RDM); Department of Pathophysiology and Organ Transplant, University of Milan, Milan, Italy (SB); Department of Cancer Biology, Kimmel Cancer Center, Thomas Jefferson University, Philadelphia, PA (LRL).

Correspondence to: Dario C. Altieri, MD, The Wistar Institute Cancer Center, 3601 Spruce St, Philadelphia, PA (e-mail: daltieri@wistar.org).

Abstract

Background: Small molecule inhibitors of phosphatidylinositol-3 kinase (PI3K) have been developed as molecular therapy for cancer, but their efficacy in the clinic is modest, hampered by resistance mechanisms.

Methods: We studied the effect of PI3K therapy in patient-derived tumor organotypic cultures (from five patient samples), three glioblastoma (GBM) tumor cell lines, and an intracranial model of glioblastoma in immunocompromised mice (n = 4–5 mice per group). Mechanisms of therapy-induced tumor reprogramming were investigated in a global metabolomics screening, analysis of mitochondrial bioenergetics and cell death, and modulation of protein phosphorylation. A high-throughput drug screening was used to identify novel preclinical combination therapies with PI3K inhibitors, and combination synergy experiments were performed. All statistical methods were two-sided.

Results: PI3K therapy induces global metabolic reprogramming in tumors and promotes the recruitment of an active pool of the Ser/Thr kinase, Akt2 to mitochondria. In turn, mitochondrial Akt2 phosphorylates Ser31 in cyclophilin D (CypD), a regulator of organelle functions. Akt2-phosphorylated CypD supports mitochondrial bioenergetics and opposes tumor cell death, conferring resistance to PI3K therapy. The combination of a small-molecule antagonist of CypD protein folding currently in preclinical development, Gamitrinib, plus PI3K inhibitors (PI3Ki) reverses this adaptive response, produces synergistic anticancer activity by inducing mitochondrial apoptosis, and extends animal survival in a GBM model (vehicle: median survival = 28.5 days; Gamitrinib+PI3Ki: median survival = 40 days, $P = .003$), compared with single-agent treatment (PI3Ki: median survival = 32 days, $P = .02$; Gamitrinib: median survival = 35 days, $P = .008$ by two-sided unpaired t test).

Conclusions: Small-molecule PI3K antagonists promote drug resistance by repurposing mitochondrial functions in bioenergetics and cell survival. Novel combination therapies that target mitochondrial adaptation can dramatically improve on the efficacy of PI3K therapy in the clinic.

The phosphatidylinositol-3 kinase (PI3K) pathway (1) is a universal signaling node that integrates environmental cues of cellular growth with downstream networks of cell proliferation, survival, and bioenergetics (2). Exploited in virtually every human cancer, in some cases through the acquisition of activating mutations (3), PI3K signaling and its effectors Akt and mammalian target of rapamycin (mTOR) (4) are validated therapeutic targets, and several small molecule antagonists of this pathway have entered clinical testing (5).

However, the response to PI3K therapy in the clinic has been inferior to expectations, with modest single-agent activity, statistically significant toxicity, and short-lived patient benefits (6). The basis for this treatment resistance is unknown (7), and strategies to guide patient selection or incorporate PI3K therapy in more effective combination regimens have remained elusive (8). In this context, there is evidence that small-molecule inhibitors of PI3K/Akt/mTOR activate a broad transcriptional and signaling program in tumors, culminating with a paradoxical (re)activation of Akt in treated patients (9–11). How (and whether) this process contributes to drug resistance has not been clearly elucidated, but it is possible that it provides a general adaptive response to “environmental stress” imposed by molecular therapy (12). In this context, mechanisms of adaptation are important drivers of tumor diversity and treatment failure (13), hinging on a tight control of the protein-folding environment (14) by molecular chaperones of the Heat Shock Protein-90 (Hsp90) family (15).

In this study, we hypothesized that clinical resistance to small molecule PI3K antagonists depends on reprogramming of metabolic and survival networks in tumor cells and that this adaptive response may be exploited for novel drug combination strategies in the clinic.

Methods

Patients

Fresh, patient-derived and treatment-naïve tissues obtained from surgical resections of colon adenocarcinoma (one case), infiltrating ductal breast adenocarcinoma (four cases), non-small cell lung adenocarcinoma (three cases), and grade IV glioblastoma (GBM) (five cases) were used in this study. Informed consent was obtained from all patients, and the study was approved by an Institutional Review Board at the Fondazione IRCCS Ca' Granda hospital (Milan, Italy). The clinicopathological characteristics of the patient series used in this study are presented in [Supplementary Table 1](#) (available online).

Organotypic cultures

Short-term organotypic cultures from primary patient samples were established as described (16). Cultures were supplemented with vehicle (DMSO, 2.5 μ L), pan-PI3K inhibitor LY294002 (50 or 100 μ M) or PX-866 (2.5, 5, or 10 μ M), mitochondrial-targeted Hsp90 inhibitor, Gamitrinib (10 or 25 μ M) (17), or the combination of PX-866 plus Gamitrinib (each used at 10 μ M). At the end of the experiment, one tissue slice per condition was formalin fixed and paraffin embedded and was further processed for morphological and immunohistochemical analysis. An additional tissue slice was embedded in optimal cutting temperature, and snap-frozen for molecular or immunofluorescence studies.

Statistical Methods

Data were analyzed using the two-sided unpaired t tests using a GraphPad software package (Prism 4.0) for Windows. Data

are expressed as mean \pm SD of replicates from a representative experiment out of at least two independent determinations. A *P* value of less than or equal to .05 was considered as statistically significant.

All other methods are described in detail in the [Supplementary Methods](#) (available online).

Results

PI3K Therapy and Mitochondrial Metabolism

To study how PI3K therapy affects tumor behavior, we first profiled the metabolome (18) of GBM LN229 cells in response to PX-866, a small-molecule antagonist of all PI3K subunits, currently in clinical trials (6). PI3K inhibition induced extensive defects in tumor mitochondrial metabolism. These included impaired oxidative phosphorylation (19), with reduced levels of pyruvate, α -ketoglutarate, succinate, fumarate, and malate ([Figure 1A](#); [Supplementary Figure 1A](#) and [Supplementary Table 2](#), available online), and defective arginine metabolism, with decreased expression of polyamines, agmatine, spermidine, putrescine, and 5'-deoxy-5'-(methylthio)adenosine (MTA) ([Figure 1B](#); [Supplementary Figure 1B](#) and [Supplementary Table 2](#), available online). Conversely, PI3K therapy resulted in higher levels of carnitine conjugates required for mitochondrial fatty acid β -oxidation ([Figure 1C](#); [Supplementary Figure 1C](#) and [Supplementary Table 2](#), available online), and elevation of long-chain fatty acids ([Figure 1C](#); [Supplementary Figure 1D](#) and [Supplementary Table 2](#), available online). Consistent with these findings, LN229 or prostate adenocarcinoma PC3 cells exposed to PI3K inhibitors, including PX-866, AZD6482, or GDC0941 (6), exhibited defects in glycolysis, with reduced glucose utilization ([Figure 1D](#)) and lactate production ([Figure 1E](#)), and inhibition of oxygen consumption ([Figure 1F](#)), a marker of oxidative phosphorylation (19). As a result of these bioenergetics defects, PI3K therapy considerably reduced adenosine triphosphate (ATP) production in tumor cells ([Figure 1G](#)).

Despite these bioenergetics defects, PI3K therapy did not appreciably kill tumor cells ([Supplementary Figure 2A](#), available online) and only caused reduced cell proliferation ([Supplementary Figure 2B](#), available online) because of G1 cell cycle arrest ([Supplementary Figure 2, C and D](#), available online). These cytostatic effects were transient, as the long-term colony-forming ability of tumor cells treated with PI3K inhibitors was unaffected compared with control cultures ([Supplementary Figure 2E](#), available online).

Akt Regulation During PI3K Therapy

We next searched for potential mediator(s) of resistance to PI3K therapy in cancer, and we focused on Akt, which becomes paradoxically reactivated under these conditions (9,10,20). A 48-hour exposure of organotypic cultures of GBM (16) ([Figure 2A](#), [Supplementary Figure 3A](#), available online) to PI3K inhibitors, PX-866, or LY294002 induced strong (re)phosphorylation of Akt (10,20) (vehicle vs PX-866 2.5 μ M, *P* = .03; vehicle vs PX-866 5 μ M, *P* = .005; vehicle vs PX-866 10 μ M, *P* = .04 by two-sided unpaired t test) ([Figure 2B](#)) (vehicle vs LY294002 50 μ M, *P* = .002; vehicle vs LY294002 100 μ M, *P* \leq .001 by two-sided unpaired t test) ([Supplementary Figure 3B](#), available online) and higher levels of phosphorylated mTOR (vehicle vs LY294002 50 μ M, *P* \leq .001; vehicle vs LY294002 100 μ M, *P* \leq 0.001 by two-sided unpaired t test) ([Supplementary Figure 3B](#), available online). PI3K inhibition also induced increased Ser473 phosphorylated Akt in organotypic cultures of breast adenocarcinoma ([Supplementary](#)

Figure 3C, available online) (vehicle vs LY294002 50 μM , $P \leq .001$; vehicle vs LY294002 100 μM , $P = .007$ by two-sided unpaired t test) (Supplementary Figure 3D, available online), or colon adenocarcinoma (Supplementary Figure 3E, available online) (vehicle vs LY294002 50 μM , $P = .02$, by two-sided unpaired t test) (Supplementary Figure 3F, available online). Other molecular therapies, including inhibition of cytosolic Hsp90 with 17-allylamino-demethoxygeldanamycin (17-AAG), had no effect on Akt or MTOR phosphorylation (Figure 2B).

As an alternative experimental approach, we next silenced the expression of PI3K p110 α subunit by small interfering RNA (siRNA), and looked at changes in signaling pathways. Similar to the results obtained with pharmacologic inhibition, PI3K knockdown in PC3 cells resulted in increased phosphorylation of Akt2 (see below), MTOR and its downstream effector, S6K (Supplementary Figure 3G, available online). This response was also associated with increased phosphorylation, ie, activation of ERK1/2 (Supplementary Figure 3G, available online), in agreement

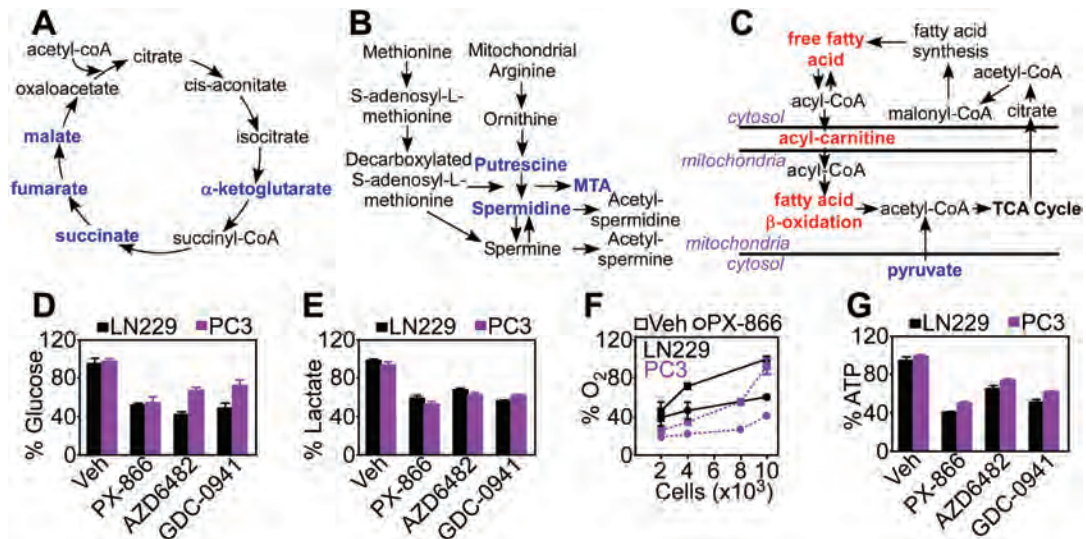


Figure 1. PI3K therapy and mitochondrial metabolic reprogramming. A-C) LN229 cells treated with PX-866 (10 μM for 48 hours) were analyzed in a global metabolomics screening ($n = 5$). Changes in expression levels of metabolites implicated in oxidative phosphorylation (A), polyamine metabolism (B), and fatty acid β -oxidation (C) are shown. Red, upregulation; blue, downregulation. D-G) LN229 or PC3 cells were treated with vehicle or PI3K inhibitors, PX-866 (10 μM), AZD6482 (10 μM), or GDC0942 (2 μM) and analyzed after 48 hours for changes in glucose utilization (D), lactate generation (E), oxygen consumption (F), or ATP production (G). Mean \pm SD of at least two independent determinations. MTA = 5'-deoxy-5'-(methylthio)adenosine; Veh = vehicle.

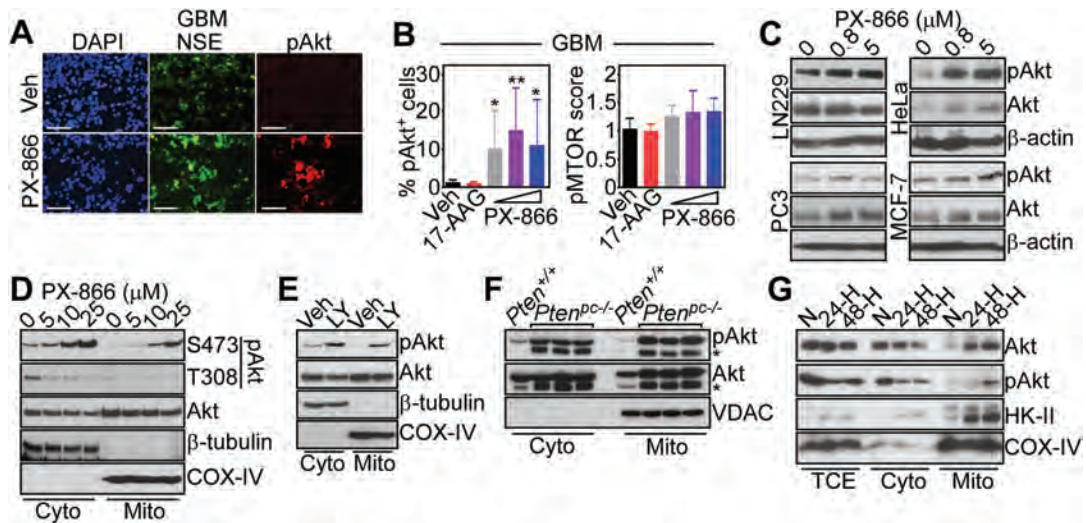


Figure 2. PI3K therapy and regulation of Akt signaling. A) Glioblastoma (GBM) organotypic cultures treated with vehicle or PX-866 (10 μM for 48 hours) were analyzed by immunofluorescence microscopy. DNA was counterstained with DAPI. Scale bar = 100 μm . B) The percentage of pAkt⁺ cells or a pMTOR immunohistochemical score was quantified in GBM organotypic cultures (PX-866, 2.5, 5, 10 μM , 17-AAG, 20 μM). None = untreated. Mean \pm SD of at least three independent determinations. * $P = .03$ -.04; ** $P = .005$ by two-sided unpaired t test. C) The various tumor cell lines were treated with the indicated increasing concentrations of PX-866 and analyzed by western blotting. D) LN229 cells were treated with the indicated increasing concentrations of PX-866 and cytosol or mitochondrial fractions were analyzed by western blotting. E) LN229 cells were treated with vehicle or LY294002 (LY, 50 μM for 48 hours), fractionated in cytosol or mitochondrial extracts, and analyzed by western blotting. For (D) and (E), Cox-IV and β -tubulin were used as mitochondrial or cytosolic markers, respectively. F) Cytosol or mitochondrial fractions from prostate tissues of wild-type (Pten^{+/+}) or Pten^{pc/-} mice (three mice per condition) were analyzed by western blotting. * = nonspecific. VDAC was a mitochondrial marker. G) LN229 cells were incubated in normoxia or hypoxia (H, 0.5% O_2) conditions for 24 to 48 hours, fractionated in cytosol or mitochondrial extracts and analyzed by western blotting. HK-II was used as a control for a hypoxia-regulated mitochondrial-associated protein. Cyto = cytosol; GBM = glioblastoma; Mito = mitochondrial; N = normoxia; NSE = neuron-specific enolase; pAkt = Ser473-phosphorylated Akt; TCE = total cell extracts; Veh = vehicle.

with previous observations (20). Consistent with these findings, PI3K therapy-induced Akt phosphorylation was observed in genetically heterogeneous tumor cell lines (Figure 2C), regardless of the presence of oncogenic “driver” mutation(s), for instance BRAF V600E melanoma cells (Supplementary Figure 3H, available online) and in response to structurally diverse PI3K antagonists currently in the clinic, including AZD6482, GDC0942, and BKM120 (Supplementary Figure 3I, available online). Both high (10 μ M) and low (0.8 μ M) concentrations of PX-866 induced Akt phosphorylation in tumor cells within 24 hours of treatment (Supplementary Figure 3J, available online).

In addition to Akt activation in cytosol (10,20), PI3K inhibitors induced the phosphorylation of a pool of Akt in mitochondria of tumor cells (Figure 2, D and E) (21). This involved the MTORC2 phosphorylation site on Akt (Ser473), whereas the PDK1 phosphorylation site (Thr308) was unaffected (Figure 2D). Mitochondrial Akt comprised predominantly the Akt2 isoform, whereas Akt1 was expressed at low levels in mitochondria (Supplementary Figure 4A, available online) (22). Accordingly, PI3K therapy with PX-866 resulted in robust and concentration-dependent isoform-specific phosphorylation of Akt2 on Ser474 in cytosol and mitochondrial extracts of treated tumor cells (Supplementary Figure 4B, available online), as well as primary GBM organotypic cultures (Supplementary Figure 4C, available online). In terms of submitochondrial localization, Akt2 predominantly accumulated in the organelle inner and outer membranes, and intermembrane space (Supplementary Figure 4D, available online), largely protected from proteinase K-dependent proteolysis of the outer membrane (Supplementary Figure 4E, available online). Akt is a known client protein for Hsp90 (15), and accordingly pretreatment of tumor cells with 17-AAG abolished the accumulation of phosphorylated Akt in cytosol, as well as mitochondria in response to PX-866 (Supplementary Figure 4F, available online). Mitochondrial Akt2 was broadly expressed in normal and tumor cell lines (Supplementary Figure 4G, available online) and in all normal mouse tissues examined (Supplementary Figure 4H, available online).

We next looked for other pathophysiological conditions that may activate mitochondrial Akt, independently of PI3K therapy. First, mice with prostate-specific deletion of *Pten*, an antagonist of the Akt pathway often deleted in tumors (23), showed constitutively high levels of Ser473-phosphorylated Akt in mitochondria (Figure 2F). Second, exposure of tumor cells to stress conditions, including hypoxia (Figure 2G) or glucose starvation induced by the nonmetabolizable analog, 2-deoxyglucose (2-DG), increased Akt recruitment to mitochondria and its phosphorylation on Ser473 (Figure 2G and Supplementary Figure 4I, available online). In contrast, ER (thapsigargin) or oxidative (H_2O_2) stress had no effect on Akt localization to mitochondria (Supplementary Figure 4I, available online).

Modulation of CypD Phosphorylation

We next searched public databases of mitochondria-localized proteins for the presence of potential Akt consensus phosphorylation site(s). We found that Cyclophilin D (CypD), a mitochondrial regulator of apoptosis (24) and bioenergetics (25), contained two potential Akt phosphorylation sites on Ser31 and Ser123 (Supplementary Figure 5A, available online). In immunoprecipitation (Figure 3A) and pull-down experiments (Figure 3B; Supplementary Figure 5B, available online), CypD formed a complex with Akt in tumor mitochondria. In addition, recombinant, active Akt1 (Supplementary Figure 5C, available online) or Akt2 (Supplementary Figure 5D) readily phosphorylated recombinant

CypD, as well as its known substrate GSK3 β in kinase assays. We next carried out mutagenesis studies to identify the Akt phosphorylation site(s) on CypD (Supplementary Figure 5A, available online). In kinase assays, recombinant Akt2 phosphorylated wild-type (WT) CypD or a CypD Ser123 \rightarrow Ala mutant (Figure 3C). In contrast, Akt2 phosphorylation of CypD Ser31 \rightarrow Ala mutant or a CypD Ser31/Ser123 \rightarrow Ala double mutant was abolished, and vehicle had no effect on CypD phosphorylation (Figure 3C).

To assess the status of CypD phosphorylation *in vivo*, we next reconstituted CypD^{-/-} mouse embryonic fibroblasts (MEFs) (Supplementary Figure 5E, available online) or LN229 cells with stable knockdown of CypD with WT or mutant CypD cDNAs (Supplementary Figure 5F, available online). Treatment with PX-866 did not affect the levels of endogenous or overexpressed CypD in reconstituted cells (Supplementary Figure 5E, available online). Under these conditions, WT CypD immunoprecipitated from reconstituted LN229 cells reacted with an antibody to phosphorylated Ser (Figure 3D). In contrast, immune complexes containing CypD Ser31 \rightarrow Ala mutant did not react with phosphorylated Ser, and immune precipitates with nonbinding IgG were ineffective (Figure 3D). Similarly, WT CypD immunoprecipitated from reconstituted LN229 cells after treatment with PX-866 showed increased reactivity with an antibody to pSer, compared with control transfectants (Figure 3E). In contrast, pSer reactivity of CypD Ser31 \rightarrow Ala mutant was abolished in PX-866-treated cells, and exposure to vehicle did not affect CypD phosphorylation (Figure 3E).

Mitochondrial Tumor Reprogramming

We next studied how CypD phosphorylation by Akt affected mitochondrial functions. First, transfection of WT CypD in CypD^{-/-} MEFs restored CypD peptidyl prolyl *cis, trans* isomerase (PPIase) activity to the levels of CypD^{+/+} MEFs (Figure 3F). In contrast, expression of a CypD Ser31 \rightarrow Ala mutant failed to restore PPIase activity in CypD^{-/-} MEFs (Figure 3F). As control, reconstitution of CypD^{-/-} MEFs with a PPIase-defective CypD His168 \rightarrow Gln mutant was also ineffective (Figure 3F). CypD PPIase activity is important for mitochondrial bioenergetics (25), as well as permeability transition-regulated apoptosis (24). Accordingly, expression of CypD Ser31 \rightarrow Ala mutant in CypD-depleted LN229 cells induced loss of the first enzyme of the glycolytic cascade, hexokinase-II (HK-II) (25), from the mitochondrial outer membrane (Figure 3G), resulting in decreased HK-II activity (WT CypD vs S31A CypD, $P = .001$ by two-sided unpaired t test) (Figure 3H), compared with WT CypD transfectants. The localization of HK-I was not affected (Figure 3G). Consistent with these data, tumor cells expressing CypD Ser31 \rightarrow Ala mutant exhibited defective mitochondrial bioenergetics, with reduced glucose utilization (WT CypD vs S31A CypD, $P = .04$ by two-sided unpaired t test) (Supplementary Figure 6A, available online), impaired oxygen consumption (WT CypD vs S31A CypD, $P = .001$ by two-sided unpaired t test) (Supplementary Figure 6B, available online), and decreased ATP production (WT CypD vs S31A CypD, $P = .004$ by two-sided unpaired t test) (Supplementary Figure 6C, available online), thus mimicking the bioenergetics defects induced by PI3K therapy (Figure 1).

When analyzed for markers of mitochondrial permeability transition (24), reconstitution of CypD-depleted LN229 cells with CypD Ser31 \rightarrow Ala mutant resulted in loss of organelle membrane potential (Supplementary Figure 6D, available online), reactivity for Annexin V (Supplementary Figure 6E, available online), and discharge of cytochrome c in the cytosol, compared with control transfectants (Supplementary Figure 6F, available online). As a result, expression of CypD Ser31 \rightarrow Ala mutant in CypD-depleted LN229 cells (WT CypD vs S31A CypD, $P < .001$ by two-sided

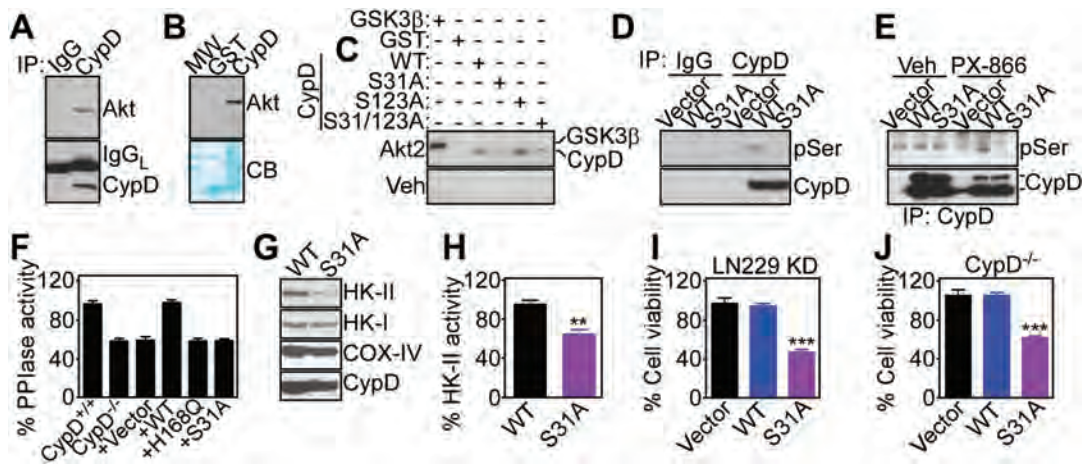


Figure 3. CypD phosphorylation. **A)** Mitochondrial extracts from LN229 cells were immunoprecipitated (IP) with IgG or an antibody to CypD, and pellets were analyzed by Western blotting. **B)** Recombinant GST-CypD or GST was incubated with mitochondrial extracts of LN229 cells, and bound proteins were analyzed by western blotting. **C)** The indicated recombinant proteins were incubated with recombinant active Akt2 or vehicle in a kinase assay, and radioactive proteins were visualized by autoradiography. GSK3 β was a control Akt substrate. **D)** LN229 cells with stable CypD knockdown were reconstituted with the indicated CypD cDNAs, immunoprecipitated with IgG or an antibody to CypD, and pellets were analyzed with an antibody to phosphorylated Ser (pSer) by western blotting. **E)** LN229 cells with stable shRNA knockdown of CypD were transfected with the indicated FLAG-tagged CypD cDNAs, treated with vehicle or PX-866, and immunoprecipitated with anti-FLAG-M2 gel followed by western blotting with anti-pSer antibody. The position of full-length or mature CypD band is shown. **F)** CypD^{+/+} or CypD^{-/-} mouse embryonic fibroblasts (MEFs) were transfected with wild-type or CypD mutant cDNAs and analyzed for peptidyl prolyl *cis,trans* isomerase (PPIase) activity. PPIase-defective CypD H168Q mutant was used as a control. Mean \pm SD. **G and H)** LN229 cells with stable CypD knockdown were transfected with the indicated CypD cDNAs, and isolated mitochondrial extracts were analyzed by western blotting (**G**) or HK-II activity (**H**). Mean \pm SD of replicates from a representative experiment out of at least two independent determinations. ***P* = .001 by two-sided unpaired *t* test. **I and J)** LN229 cells with stable shRNA knockdown (KD) of CypD (**I**) or CypD^{-/-} MEFs (**J**) were transfected with the indicated CypD cDNAs and analyzed for cell viability by a 3-(4,5 dimethylthiazol-2-yl)-2,5 diphenyltetrazolium bromide (MTT) assay. Mean \pm SD of replicates from a representative experiment out of at least two independent determinations. ****P* < .001 by two-sided unpaired *t* test. CB = Coomassie blue staining; IgG_L = Ig light chain; IP = immunoprecipitated; MW = molecular weight markers; PPIase = peptidyl prolyl *cis,trans* isomerase; Veh = vehicle; WT = wild-type.

unpaired *t* test) (Figure 3I) or CypD^{-/-} MEFs (WT CypD vs S31A CypD, *P* < .001 by two-sided unpaired *t* test) (Figure 3J) reduced cell viability, whereas expression of WT CypD had no effect (Figure 3, I and J).

Mitochondrial Adaptation and PI3K Therapy

Many mitochondrial functions in tumors, including those mediated by CypD (18), depend on protein folding quality control maintained by mitochondrial-localized Hsp90 chaperones (26). Therefore, we asked whether this requirement provided new therapeutic opportunities, and we carried out a high-throughput drug screening of a small-molecule antagonist of mitochondrial Hsp90s, Gamitrinib (17), in combination with various molecular therapies (Figure 4A). In these experiments, Gamitrinib potently enhanced the anticancer activity of all structurally unrelated PI3K/Akt/MTOR pathway antagonists present in the screening (Figure 4, A and B). In contrast, other molecular therapies were not affected (Figure 4A). The combination of Gamitrinib plus PI3K inhibitor killed tumor cells via induction of mitochondrial apoptosis (24), with membrane depolarization (Figure 4C), increased Annexin V labeling (Figure 4D), and cleavage of effector caspase-3 and -7 and their substrate, poly-ADP ribose polymerase (PARP) (Supplementary Figure 7A, available online). Bliss independence analysis demonstrated that the combination of Gamitrinib plus PI3K inhibitor had synergistic anticancer activity (Supplementary Figure 7B, available online) and was associated with loss of antiapoptotic molecules implicated in tumor cell survival, including Bcl-2, XIAP, and survivin (Supplementary Figure 7C, available online).

To validate these observations independently of pharmacologic inhibitors, we next transfected tumor cells with a PI3K Δ -p85 dominant negative mutant that interferes with PI3K signaling (Supplementary Figure 7D, available online). Expression of this mutant in GBM cell types reduced Akt phosphorylation on

Ser473, but caused only modest activation of effector caspases (Supplementary Figure 7D, available online). In contrast, the combination of PI3K Δ -p85 mutant plus noncytotoxic concentrations of Gamitrinib increased caspase activation (Supplementary Figure 7D, available online), and enhanced tumor cell killing, compared with each treatment alone (Supplementary Figure 7E, available online). When analyzed in a preclinical model of intracranial GBM in mice, the combination of Gamitrinib plus a PI3K antagonist (NVP-BE2235) inhibited tumor growth as determined by bioluminescence imaging (vehicle vs BE2235, *P* = .08; vehicle vs Gamitrinib, *P* = .01; vehicle vs BE2235+Gamitrinib, *P* = .001; Gamitrinib vs BE2235+Gamitrinib, *P* = .04; BE2235 vs BE2235+Gamitrinib, *P* = .02, all by two-sided unpaired *t* test) (Figure 5, A and B; Supplementary Figure 8A, available online) and extended animal survival (vehicle: median survival = 28.5 days; Gamitrinib+BE2235: median survival = 40 days, *P* = .003 by log-rank Mantel-Cox test), compared with single-agent treatment (BE2235: median survival = 32 days, *P* = .02; Gamitrinib: median survival = 35 days, *P* = .008 by log-rank Mantel-Cox test) (Figure 5C). Histologic analysis of GBMs harvested from mice receiving the combination treatment showed extensive inhibition of cell proliferation (Supplementary Figure 8B, available online) and apoptosis (Supplementary Figure 8C, available online), compared with tumors in groups receiving each agent alone.

Synergistic Enhancement of PI3K Therapy

We next analyzed the impact of this novel combination on therapy adaptive signaling induced by PI3K therapy (9–11). When combined with Gamitrinib, PX-866 no longer promoted the reactivation of Akt (Ser473) (PX 10 μ M vs PX 10 μ M+Gam, *P* = .01 by two-sided unpaired *t* test), or the phosphorylation of MTOR (PX 10 μ M vs PX 10 μ M+Gam, *P* = .007 by two-sided unpaired *t* test) in breast cancer organotypic cultures (Figure 5, D and E;

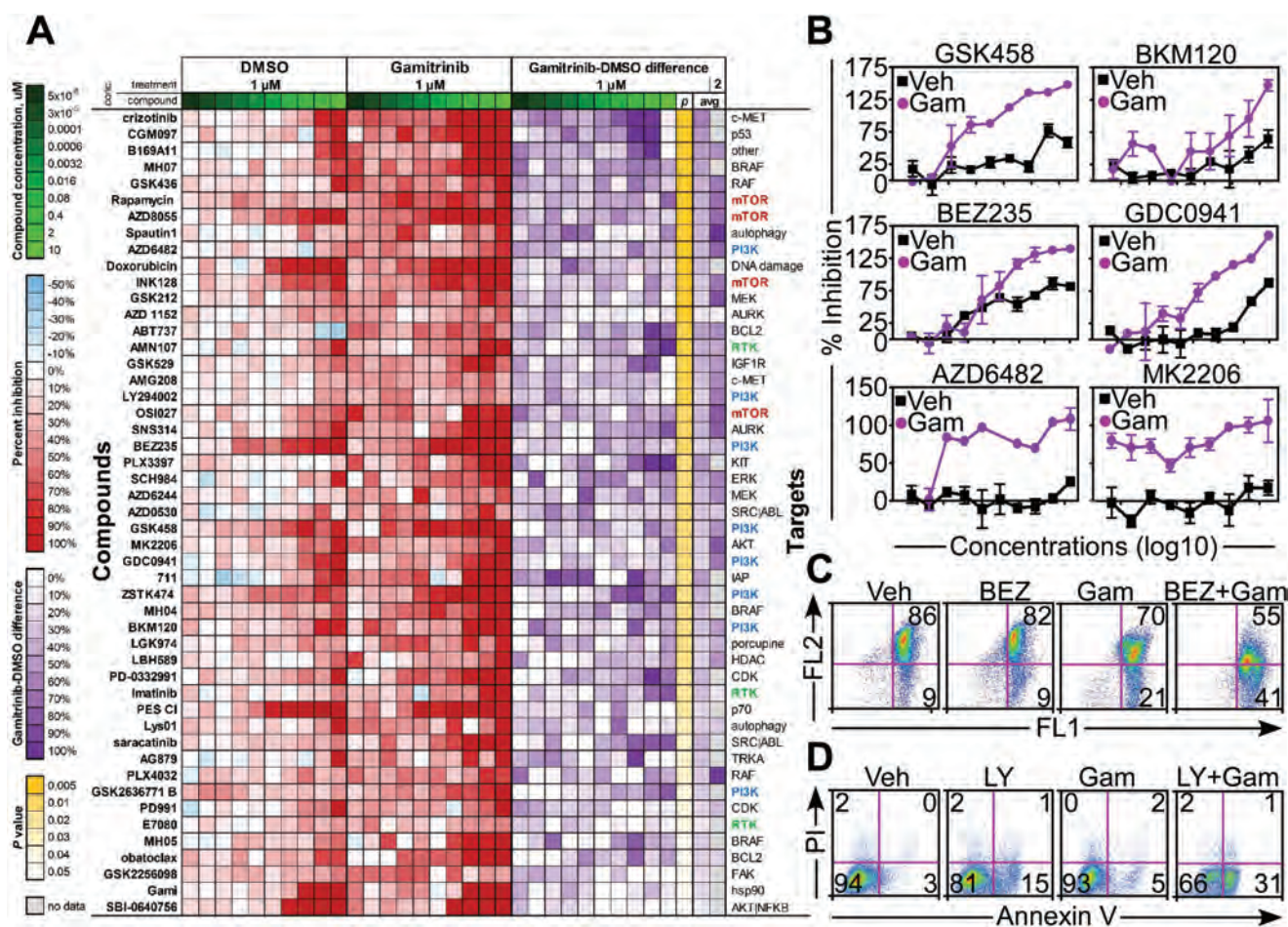


Figure 4. Mitochondrial adaptation and sensitivity to PI3K therapy. **A**) LN229 cells were incubated with the indicated small molecule targeted anticancer agents plus vehicle (DMSO) or a noncytotoxic concentration of Gamitrinib (Gam, 1 μ M) and analyzed for cell viability after 18 hours. The heatmap represents compounds with statistically significant ($P < .05$) increased inhibitory effect in the presence of Gamitrinib. P = P value (Wilcoxon test); avg = average difference between inhibition shown in Gamitrinib vs DMSO across all concentration points. 2 = results from the combination of targeted compounds plus 2 μ M Gamitrinib vs DMSO (only a subset of compounds were tested). **B**) LN229 cells were incubated with increasing concentrations of small molecule inhibitors of PI3K (GSK458, BKM120, BEZ235, GDC0941, AZD6482) or Akt (MK2206) in the presence of vehicle or Gamitrinib (Gam, 1 μ M) and analyzed for inhibition of cell viability by MTT after 18 hours. Mean \pm SD of two independent experiments. **C** and **D**) GBM U251 cells were treated with NVP-BEZ235 (BEZ, 0.5 μ M) or LY294002 (LY, 50 μ M), alone or in combination with Gamitrinib (0.5 μ M or 5 μ M, respectively), and analyzed for changes in mitochondrial membrane potential by JC1 staining (**C**) or Annexin V labeling (**D**) by multiparametric flow cytometry. The percentage of cells in each quadrant is indicated. Conc. = concentration; Veh = vehicle.

Supplementary Figure 8D, available online). When analyzed in a Reverse Phase Protein Array (RPPA) screening in different tumor cell types, the addition of Gamitrinib reversed many of the adaptive transcriptional and signaling responses induced by PI3K therapy (9–11), affecting Akt/MTOR (4EBP1, S6, RICTOR) and growth factor receptor (EGFR, ErbB2, ErbB3, NRG) signaling, effectors of cell invasion (Snail, Tyro3, Src, PAI1), cell cycle control (CDKN1A, MAPK8, MAPK14), and endogenous tumor suppression (PRKAA1) (Figure 5F; Supplementary Figure 8E, available online).

Discussion

In this study, we have shown that PI3K therapy currently in the clinic is a powerful driver of tumor adaptation, reprogramming mitochondrial functions in bioenergetics and apoptosis to promote cell survival and treatment resistance. This pathway is centered on a pool of Akt2 recruited to mitochondria, and its phosphorylation of the mitochondrial regulator, CypD, on Ser31. Conversely, the combination of PI3K therapy with an antagonist of CypD protein folding currently in preclinical development,

Gamitrinib, reverses this adaptive response and delivers potent, synergistic anticancer activity in vivo.

Despite their ability to target a fundamental cancer node (2), small-molecule inhibitors of PI3K/Akt/MTOR have shown modest efficacy in the clinic (6). The data presented here identify the paradoxical reactivation of Akt in response to PI3K therapy (9–11,20), as a pivotal effector of drug resistance to these regimens (8). Centered on the recruitment of Akt2 to mitochondria, this pathway differs from other mechanisms of drug resistance mediated by intratumor heterogeneity (27), acquisition of new mutations (28), or crosstalk within the tumor microenvironment (29).

Once in mitochondria, Akt2 associated with the organelle regulator CypD (30) and phosphorylated CypD on Ser31 to preserve its PPIase activity, maintain energy production, and antagonize apoptosis (24). There is prior evidence that post-translational modifications, for instance acetylation (31), affect CypD activity. Here, Ser31 is positioned at the NH_2 terminus of the mature form of CypD and becomes readily phosphorylated by Akt in vitro and in vivo. However, the complete Akt consensus phosphorylation site for Ser31 extends into the mitochondrial-import sequence, and it is possible that a fraction of CypD is phosphorylated on

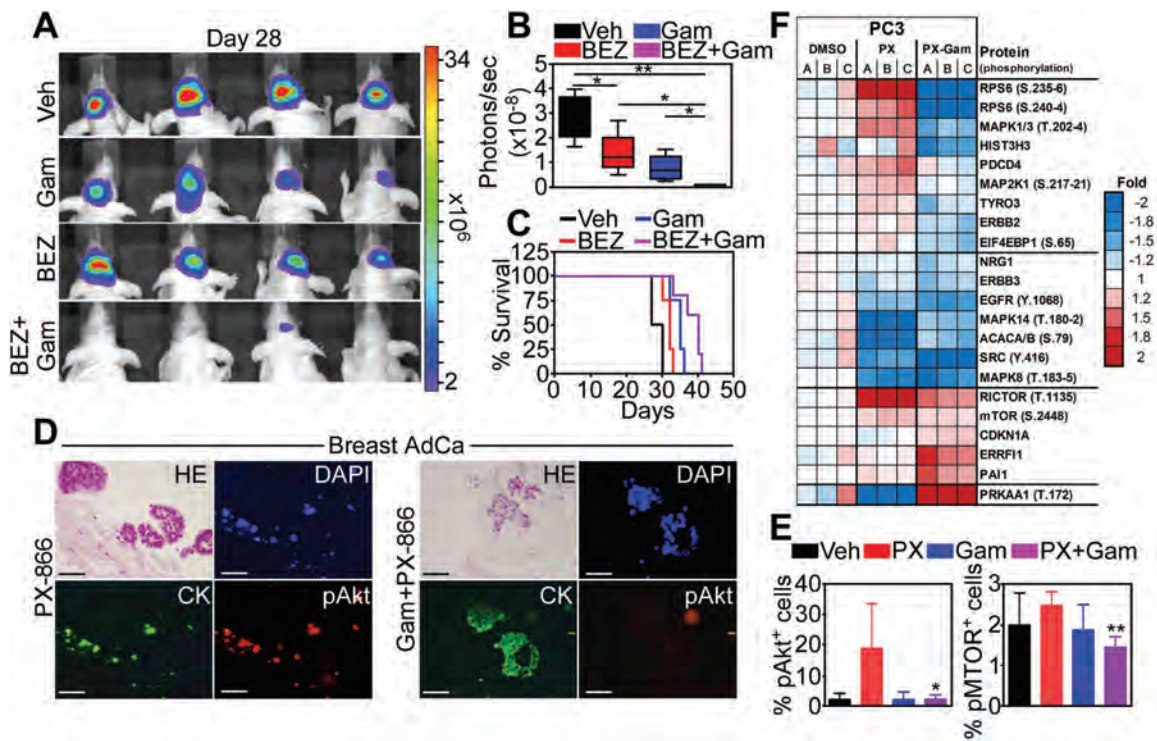


Figure 5. Mitochondrial reprogramming and efficacy of PI3K therapy. **A** and **B**) Nude mice injected with U87-Luc glioblastoma (GBM) cells in the right cerebral striatum were treated as indicated, and tumor growth was assessed by bioluminescence imaging 28 days after injection (**A**) and quantified (**B**). ** $P = .001$; * $P = .01-.04$ by two-sided unpaired t test. **C**) Overall survival of mice carrying intracranial GBMs in the various treatment groups. The statistical analysis by log-rank Mantel-Cox test among groups is as follows: Vehicle vs BEZ, $P = .02$ ($\chi^2 = 4.82$); Vehicle vs Gam, $P = .008$ ($\chi^2 = 6.94$); Vehicle vs Gam+BEZ, $P = .003$ ($\chi^2 = 8.35$); BEZ vs Gam+BEZ, $P = .008$ ($\chi^2 = 7.01$); Gam vs Gam+BEZ, $P = .003$ ($\chi^2 = 4.29$). See also [Supplementary Table 3](#) (available online) for the numbers of mice at risk in each group at various time points. **D** and **E**) Breast adenocarcinoma organotypic cultures treated with PX-866 (10 μM) alone (**left**) or in combination with Gamitrinib (10 μM , **right**) were analyzed by immunohistochemistry and fluorescence microscopy (**D**), and pAkt- or pMTOR-expressing cells were quantified (**E**). Cytokeratin was an epithelial marker. DNA was counterstained with DAPI. Scale bar = 100 μm . Mean \pm SD of individual replicates. * $P = .01$; ** $P = .007$ by two-sided unpaired t test. **F**) Heatmap of proteins statistically significantly different in expression and/or phosphorylation in PC3 cells treated with vehicle (DMSO), PX-866 alone (PX) or PX-866 in combination with Gamitrinib (PX-Gam), as determined by Reverse Phase Protein Arrays. Fold indicates protein expression/phosphorylation signal in a sample vs average DMSO. **A-C**), internal replicates ($n = 3$). CK = cytokeratin; HE = hematoxylin & eosin staining; pAkt = Ser473-phosphorylated Akt; PX = PX-866 alone; Veh = vehicle.

Ser31 during mitochondrial trafficking. Akt plays a central role in tumor bioenergetics (32), influencing aerobic glycolysis (33), as well as oxidative phosphorylation (34). An antiapoptotic role of Akt2 phosphorylation of CypD is also consistent with a physical assembly of CypD in a mitochondrial permeability transition pore (24) that regulates stress-associated cell death (30).

The functions of CypD in bioenergetics (25) and apoptosis (24) require protein folding quality control maintained by mitochondrial-localized Hsp90s (26). Accordingly, the combination of a small-molecule inhibitor of mitochondrial-localized Hsp90s currently in preclinical development, Gamitrinib (17), converted a transient, cytostatic effect of PI3K antagonists into potent, synergistic anticancer activity in vivo. The idea of targeting mitochondrial integrity for cancer therapy (19) has recently gained attention (35), and regulators of Bcl-2 proteins (36), oxidative phosphorylation (37), and redox mechanisms (38) have progressed through (pre)clinical development. Gamitrinib is an attractive candidate for this approach given its ability to simultaneously disable multiple pathways of mitochondrial homeostasis in bioenergetics, gene expression, and redox balance selectively in tumors (18).

In addition, the combination with Gamitrinib reversed adaptive tumor reprogramming induced by PI3K therapy, with respect to Akt (re)activation, growth factor receptor signaling, cell proliferation, and endogenous tumor suppression. Small-molecule inhibitors of PI3K (10,20), Akt (11), or MTOR (9) have

been shown to activate a broad gene expression program in tumor cells, potentially as a compensatory response via derepression of FOXO-dependent transcription. Our RPPA screening suggests that mitochondrial reprogramming maintained by organelle Hsp90s is important for this response, potentially via mitochondria-to-nuclei “retrograde” signaling (39). Accordingly, mitochondria-derived “retrograde” mediators that affect nuclear gene expression have been identified in model systems (40), and CypD contributes to retrograde signaling via activation of STAT3-dependent cell migration and invasion (41).

One limitation of our study is that the increased efficacy of PI3K therapy when combined with Gamitrinib was limited to mechanistic and preclinical readouts and not patient data. In addition, Gamitrinib—or other agents with comparable activity or specificity—is not yet available for clinical testing, as it is currently completing late stages for preclinical and safety evaluation.

In summary, Akt2-directed repurposing of mitochondrial functions provides a novel adaptive mechanism of tumor resistance to PI3K therapy. This pathway likely limits the activity of these agents in the clinic (8), but may confer a unique “addiction” of tumor cells to mitochondrial adaptation. In this context, the combination of small-molecule PI3K antagonists plus inhibitors of mitochondrial homeostasis (17,26), like Gamitrinib, may eliminate mitochondrial adaptation and dramatically improve on the efficacy of PI3K therapy in the clinic.

Funding

This work was supported by National Institutes of Health grants P01 CA140043 (DCA, LRL), R01 CA78810 (DCA), F32 CA177018 (MCC), R01 CA089720 (LRL), K08 NS083732 (MDS), American Association for Cancer Research-National Brain Tumor Society Career Development Award for Translational Brain Tumor Research (MDS), American Brain Tumor Association Translational Grant (MDS), and the Office of the Assistant Secretary of Defense for Health Affairs through the Prostate Cancer Research Program under Award No. W81XWH-13-1-0193 (DCA). Support for Core Facilities utilized in this study was provided by Cancer Center Support Grant (CCSG) CA010815 to The Wistar Institute.

Notes

The study sponsors had no role in the design of the study, the collection, analysis, or interpretation of the data, the writing of the manuscript, nor the decision to submit the manuscript for publication.

We thank Dr. Herlyn (The Wistar Institute) for melanoma cell lines, and the MD Anderson Cancer Center Reverse Phase Protein Array (RPPA) Facility for high-throughput analysis.

The authors declare no competing financial interest RDM is an employee of Metabolon, Inc. Correspondence and requests for materials should be addressed to DCA (daltieri@wistar.org).

References

- Engelman JA, Luo J, Cantley LC. The evolution of phosphatidylinositol 3-kinases as regulators of growth and metabolism. *Nat Rev Genet.* 2006;7(8):606–619.
- Manning BD, Cantley LC. AKT/PKB signaling: navigating downstream. *Cell.* 2007;129(7):1261–1274.
- Vivanco I, Sawyers CL. The phosphatidylinositol 3-Kinase AKT pathway in human cancer. *Nat Rev Cancer.* 2002;2(7):489–501.
- Guertin DA, Sabatini DM. Defining the role of mTOR in cancer. *Cancer Cell.* 2007;12(1):9–22.
- Liu P, Cheng H, Roberts TM, et al. Targeting the phosphoinositide 3-kinase pathway in cancer. *Nat Rev Drug Discov.* 2009;8(8):627–644.
- Rodon J, Dienstmann R, Serra V, et al. Development of PI3K inhibitors: lessons learned from early clinical trials. *Nat Rev Clin Oncol.* 2013;10(3):143–153.
- Janne PA, Gray N, Settleman J. Factors underlying sensitivity of cancers to small-molecule kinase inhibitors. *Nat Rev Drug Discov.* 2009;8(9):709–723.
- Fruman DA, Rommel C. PI3K and cancer: lessons, challenges and opportunities. *Nat Rev Drug Discov.* 2014;13(2):140–156.
- Carracedo A, Ma L, Teruya-Feldstein J, et al. Inhibition of mTORC1 leads to MAPK pathway activation through a PI3K-dependent feedback loop in human cancer. *J Clin Invest.* 2008;118(9):3065–3074.
- Chakraborty A, Sanchez V, Kuba MG, et al. Feedback upregulation of HER3 (ErbB3) expression and activity attenuates antitumor effect of PI3K inhibitors. *Proc Natl Acad Sci U S A.* 2012;109(8):2718–2723.
- Chandarlapaty S, Sawai A, Scaltriti M, et al. AKT inhibition relieves feedback suppression of receptor tyrosine kinase expression and activity. *Cancer Cell.* 2011;19(1):58–71.
- Meads MB, Gatenby RA, Dalton WS. Environment-mediated drug resistance: a major contributor to minimal residual disease. *Nat Rev Cancer.* 2009;9(9):665–674.
- Fodale V, Pierobon M, Liotta L, et al. Mechanism of cell adaptation: when and how do cancer cells develop chemoresistance? *Cancer J.* 2011;17(2):89–95.
- Balch WE, Morimoto RI, Dillin A, et al. Adapting proteostasis for disease intervention. *Science.* 2008;319(5865):916–919.
- Taipale M, Jarosz DF, Lindquist S. HSP90 at the hub of protein homeostasis: emerging mechanistic insights. *Nat Rev Mol Cell Biol.* 2010;11(7):515–528.
- Vaira V, Fedele G, Pyne S, et al. Preclinical model of organotypic culture for pharmacodynamic profiling of human tumors. *Proc Natl Acad Sci U S A.* 2010;107(18):8352–8356.
- Chae YC, Caino MC, Lisanti S, et al. Control of tumor bioenergetics and survival stress signaling by mitochondrial HSP90s. *Cancer Cell.* 2012;22(3):331–344.
- Chae YC, Angelin A, Lisanti S, et al. Landscape of the mitochondrial Hsp90 metabolome in tumours. *Nat Commun.* 2013;4:2139.
- Wallace DC. Mitochondria and cancer. *Nat Rev Cancer.* 2012;12(10):685–698.
- Serra V, Scaltriti M, Prudkin L, et al. PI3K inhibition results in enhanced HER signaling and acquired ERK dependency in HER2-overexpressing breast cancer. *Oncogene.* 2011;30(22):2547–2557.
- Miura T, Tanno M, Sato T. Mitochondrial kinase signalling pathways in myocardial protection from ischaemia/reperfusion-induced necrosis. *Cardiovasc Res.* 2010;88(1):7–15.
- Santi SA, Lee H. The Akt isoforms are present at distinct subcellular locations. *Am J Physiol Cell Physiol.* 2010;298(3):C580–C591.
- Song MS, Salmena L, Pandolfi PP. The functions and regulation of the PTEN tumour suppressor. *Nat Rev Mol Cell Biol.* 2012;13(5):283–296.
- Tait SW, Green DR. Mitochondria and cell death: outer membrane permeabilization and beyond. *Nat Rev Mol Cell Biol.* 2010;11(9):621–632.
- Vander Heiden MG, Cantley LC, Thompson CB. Understanding the Warburg effect: the metabolic requirements of cell proliferation. *Science.* 2009;324(5930):1029–1033.
- Kang BH, Plescia J, Dohi T, et al. Regulation of tumor cell mitochondrial homeostasis by an organelle-specific Hsp90 chaperone network. *Cell.* 2007;131(2):257–270.
- Gerlinger M, Rowan AJ, Horswell S, et al. Intratumor heterogeneity and branched evolution revealed by multiregion sequencing. *N Engl J Med.* 2012;366(10):883–892.
- Yates LR, Campbell PJ. Evolution of the cancer genome. *Nat Rev Genet.* 2012;13(11):795–806.
- Friedl P, Alexander S. Cancer invasion and the microenvironment: plasticity and reciprocity. *Cell.* 2011;147(5):992–1009.
- Baines CP, Kaiser RA, Purcell NH, et al. Loss of cyclophilin D reveals a critical role for mitochondrial permeability transition in cell death. *Nature.* 2005;434(7033):658–662.
- Shulga N, Wilson-Smith R, Pastorino JG. Sirtuin-3 deacetylation of cyclophilin D induces dissociation of hexokinase II from the mitochondria. *J Cell Sci.* 2010;123(Pt 6):894–902.
- Garcia-Cao I, Song MS, Hobbs RM, et al. Systemic elevation of PTEN induces a tumor-suppressive metabolic state. *Cell.* 2012;149(1):49–62.
- Elstrom RL, Bauer DE, Buzzai M, et al. Akt stimulates aerobic glycolysis in cancer cells. *Cancer Res.* 2004;64(11):3892–3899.
- Li C, Li Y, He L, et al. PI3K/AKT signaling regulates bioenergetics in immortalized hepatocytes. *Free Radic Biol Med.* 2013;60:29–40.
- Fulda S, Kroemer G. Mitochondria as therapeutic targets for the treatment of malignant disease. *Antioxid Redox Signal.* 2011;15(12):2937–2949.
- Czabotar PE, Lessene G, Strasser A, et al. Control of apoptosis by the BCL-2 protein family: implications for physiology and therapy. *Nat Rev Mol Cell Biol.* 2014;15(1):49–63.
- Kluckova K, Bezawork-Geleta A, Rohlena J, et al. Mitochondrial complex II, a novel target for anti-cancer agents. *Biochim Biophys Acta.* 2013;1827(5):552–564.

38. Trachootham D, Alexandre J, Huang P. Targeting cancer cells by ROS-mediated mechanisms: a radical therapeutic approach? *Nat Rev Drug Discov.* 2009;8(7):579–591.
39. Butow RA, Avadhani NG. Mitochondrial signaling: the retrograde response. *Mol Cell.* 2004;14(1):1–15.
40. Haynes CM, Yang Y, Blais SP, et al. The matrix peptide exporter HAF-1 signals a mitochondrial UPR by activating the transcription factor ZC376.7 in *C. elegans*. *Mol Cell.* 2010;37(4):529–540.
41. Tavecchio M, Lisanti S, Lam A, et al. Cyclophilin D extramitochondrial signaling controls cell cycle progression and chemokine-directed cell motility. *J Biol Chem.* 2013;288(8):5553–5561.

Trop-2 is up-regulated in invasive prostate cancer and displaces FAK from focal contacts

Marco Trerotola^{1,2,6}, Kirat K. Ganguly^{1,2}, Ladan Fazli³, Carmine Fedele^{1,2}, Huimin Lu^{1,2}, Anindita Dutta^{1,2}, Qin Liu^{1,4}, Tiziana De Angelis^{1,2}, Luke W. Riddell^{1,2}, Natalia A. Riobo⁵, Martin E. Gleave³, Amina Zoubeidi³, Richard G. Pestell², Dario C. Altieri^{1,4} and Lucia R. Languino^{1,2}

¹ Prostate Cancer Discovery and Development Program, Thomas Jefferson University, Philadelphia, PA, USA

² Department of Cancer Biology, Sidney Kimmel Cancer Center, Thomas Jefferson University, Philadelphia, PA, USA

³ The Vancouver Prostate Centre, University of British Columbia, Vancouver, British Columbia, Canada

⁴ Tumor Microenvironment and Metastasis Program, The Wistar Institute Cancer Center, Philadelphia, PA, USA

⁵ Department of Biochemistry, Thomas Jefferson University, Philadelphia, PA, USA

⁶ Current address: Ce.S.I. – University of Chieti-Pescara, Chieti Scalo, Italy

Correspondence to: Lucia R. Languino, email: lucia.languino@jefferson.edu

Keywords: pT2/pT3/pT4 prostate cancer, metastasis, gleason grade, TRAMP, exosome

Received: December 30, 2014

Accepted: April 10, 2015

Published: April 29, 2015

This is an open-access article distributed under the terms of the Creative Commons Attribution License, which permits unrestricted use, distribution, and reproduction in any medium, provided the original author and source are credited.

ABSTRACT

In this study, we show that the transmembrane glycoprotein Trop-2 is up-regulated in human prostate cancer (PCa) with extracapsular extension (stages pT3/pT4) as compared to organ-confined (stage pT2) PCa. Consistent with this evidence, Trop-2 expression is found to be increased in metastatic prostate tumors of Transgenic Adenocarcinoma of Mouse Prostate mice and to strongly correlate with $\alpha 5\beta 1$ integrin levels. Using PCa cells, we show that Trop-2 specifically associates with the $\alpha 5$ integrin subunit, as binding to $\alpha 3$ is not observed, and that Trop-2 displaces focal adhesion kinase from focal contacts. In support of the role of Trop-2 as a promoter of PCa metastatic phenotype, we observe high expression of this molecule in exosomes purified from Trop-2-positive PCa cells. These vesicles are then found to promote migration of Trop-2-negative PCa cells on fibronectin, an $\alpha 5\beta 1$ integrin/focal adhesion kinase substrate, thus suggesting that the biological function of Trop-2 may be propagated to recipient cells. In summary, our findings show that Trop-2 promotes an $\alpha 5\beta 1$ integrin-dependent pro-metastatic signaling pathway in PCa cells and that the altered expression of Trop-2 may be utilized for early identification of capsule-invading PCa.

INTRODUCTION

The molecular mechanisms underlying the early phases of tumor invasion are not completely understood, although it is largely believed that acquisition of enhanced capacity to migrate through the extracellular matrix (ECM) is a critical step for the onset of the metastatic cascade. When diagnosed at a non-invasive stage, prostate cancer (PCa) is generally curable by surgical removal of the prostate gland. However, when PCa cells acquire the ability to break through the external capsule and invade the surrounding tissues, the chances to eradicate the

disease by radical prostatectomy are reduced, resulting in lower overall survival rates for patients with metastatic disease. Widely accepted tumor staging criteria establish that stage pT2 identifies PCa still confined within the prostatic gland, whereas stages pT3/pT4 refer to PCa that has spread through the capsule and has eventually invaded adjacent structures [1, 2]. Traditional disease monitoring approaches, including circulating prostate specific antigen (PSA) levels or Gleason scoring, do not discriminate between stage pT2 and stages pT3/pT4 [1, 2], thus hampering a central tenet for cancer patient stratification [3]. Therefore, developing molecular biomarkers that

Table 1: Correlation of Trop-2 expression with pT3/pT4 in extracapsular invasive human prostate cancer

Score	pT2 (N = 104)	pT3/pT4 (N = 44)	<i>P</i>
	n (% of N)	n (% of N)	
Trop-2 IHC Score			0.0002
< 1.5	73 (70.2)	8 (18.2)	
≥ 1.5	31 (29.8)	36 (81.8)	
Gleason Score			0.0940
6-7	72 (69.2)	24 (54.6)	
8-10	32 (30.8)	20 (45.4)	

Expression of Trop-2 was evaluated by IHC using 148 PCa specimens as described in Methods. Samples were categorized in groups based on Trop-2 expression measured using IHC (< 1.5 and ≥ 1.5) or Gleason (6-7 and 8-10) scores. *P*, *P* value was determined as described in the Methods section.

could identify specific stages of PCa progression remains an urgent, unmet medical need.

Previous studies have reported that the expression profile of many integrins, receptors for ECM substrates, becomes aberrant during cancer progression [4, 5]. In particular, the $\alpha 5\beta 1$ integrin heterodimer plays a pivotal role in development and progression of several types of carcinomas, including PCa [6, 7], and its expression correlates with reduced disease-free survival in several malignancies [7-9]. The $\alpha 5\beta 1$ integrin is implicated in cell proliferation and growth [10]. A function-blocking antibody against $\alpha 5\beta 1$ integrin significantly reduces tumor burden and metastasis in ovarian cancer models [7]. Additional studies demonstrate that the $\alpha 5\beta 1$ integrin directly supports cell migration/invasion and metastasis [11, 12].

Metastatic dissemination is also promoted by exosomes, vesicles of endosomal origin, which are believed to generate a suitable microenvironment in the pre-metastatic niche [13, 14] by mediating horizontal transfer of genetic material [15] as well as of signaling molecules [14].

The epithelial transmembrane glycoprotein Trop-2 functions as a key regulator of $\beta 1$ integrin activities by inducing cell detachment from ECM substrates and promoting motility of PCa cells [16, 17]. Trop-2 overexpression has been consistently linked to poor prognosis in many human cancers [18-21], suggesting a potential role of this molecule in metastatic dissemination. Specifically, we have previously shown that Trop-2 inhibits localization of $\beta 1$ integrins in focal adhesions (FAs) and induces hyperphosphorylation of focal adhesion kinase (FAK), deregulating cell-ECM interactions [17].

Altogether, the experimental findings presented here show that Trop-2 is a novel marker of capsule-invasive PCa, is found in PCa cell exosomes and may function as

mediator of PCa cell motility and metastasis.

RESULTS

Trop-2 expression is increased in stages pT3/pT4 of human PCa

Our previous findings demonstrate a role of Trop-2 as an anti-adhesive and pro-migratory regulator in PCa [16, 17]. Here, we hypothesized that up-regulation of Trop-2 promotes escape of PCa cells from the primary tumor microenvironment and accelerates the onset of the metastatic cascade. Hence, we performed an immunofluorescence (IF) analysis of human PCa tissues; as depicted in Figure 1A, an abundant distribution of Trop-2 is found in membrane rims of the transformed cell population, whereas no reactivity is detected in the stromal compartment. We next analyzed Trop-2 expression levels in human PCa tissues by immunohistochemistry (IHC) using a Tissue Microarray (TMA) containing 104 cores from stage pT2 (organ-confined) and 44 cores from stages pT3/pT4 (PCa with extracapsular extension) cancer specimens collected from radical prostatectomies (Table 1). An example of Trop-2 expression in stages pT3 and pT2 of PCa is shown in Figure 1B. The expression of Trop-2 in these specimens was evaluated as low (IHC score <1.5) or high (IHC score ≥1.5) and is reported in Table 1. In these experiments, we observe strong expression of Trop-2 in 29.8% of pT2 stage and 81.8% in pT3/pT4 stage samples (Fisher's exact test *P* = 0.0002). We analyzed in parallel the frequency of cases with high Gleason score (8-10) in stage pT2 and stages pT3/pT4 and found that the differences are not statistically significant (Fisher's exact test *P* = 0.0940). Our results show that

Trop-2 expression correlates with the stages pT3/pT4 in extracapsular invasive human PCa.

Trop-2 is up-regulated in prostate tumors of metastatic Transgenic Adenocarcinoma of Mouse Prostate (TRAMP) mice and forms a complex with the $\alpha 5\beta 1$ integrin in PCa cells

Although mouse models of spontaneous PCa progression to metastasis are limited [22], the TRAMP model is known to develop aggressive and metastatic PCa [23]. We observe Trop-2 expression in metastatic prostate tumors of TRAMP mice using IF staining of prostate tumor tissue sections (Figure 2A). Macroscopic organ dissection of TRAMP mice ($n = 69$) was performed and primary tumors as well as metastases were analyzed. Figure 2B shows a representative normal genito-urinary (GU) (top left panel) and a primary tumor (bottom left panel), and also metastases in lung (top right panel) and liver (bottom right panel). Hematoxylin and Eosin (H&E) analysis of non-metastatic (top left panel) and metastatic (bottom left panel) primary tumors is shown in Figure 2C. Analysis of lung (Figure 2C, top right panel) and liver (Figure 2C, bottom right panel) metastases are also shown.

We next analyzed the expression levels of Trop-2 and of $\alpha 5$, $\beta 1$, $\beta 5$, and αv integrin subunits in this experimental model, and compared metastatic ($n = 4$) with non-metastatic primary tumors ($n = 4$). As shown in Figure 3A, Trop-2 is highly expressed in metastatic tumor samples, but it is undetectable or expressed at low levels in non-metastatic tumors. Similarly, both $\alpha 5$ and $\beta 1$ integrin subunits are strongly up-regulated in metastatic prostate tumors as compared with non-metastatic tumors. These changes are found to be specific, as $\beta 5$, another integrin subunit, does not show appreciable variations in expression between metastatic and non-metastatic tumors. The αv integrin subunit, which does not associate with Trop-2 in PCa cells [16], was also preferentially expressed in metastatic tumors, suggesting the existence of additional regulatory mechanisms of this integrin subunit in PCa.

Since Trop-2 inhibits $\beta 1$ integrin-mediated PCa cell adhesion to fibronectin (FN) [17] and induces migratory phenotypes on this ECM ligand [16], we tested the ability of Trop-2 to interact with $\alpha 5\beta 1$. Co-immunoprecipitation experiments performed using PC3 human PCa cells demonstrate that Trop-2 specifically associates with the $\alpha 5$ integrin subunit (Figure 3B). In contrast, another $\beta 1$ -associated subunit, $\alpha 3$, does not interact with Trop-2 (Figure 3C). These results provide a biochemical basis for

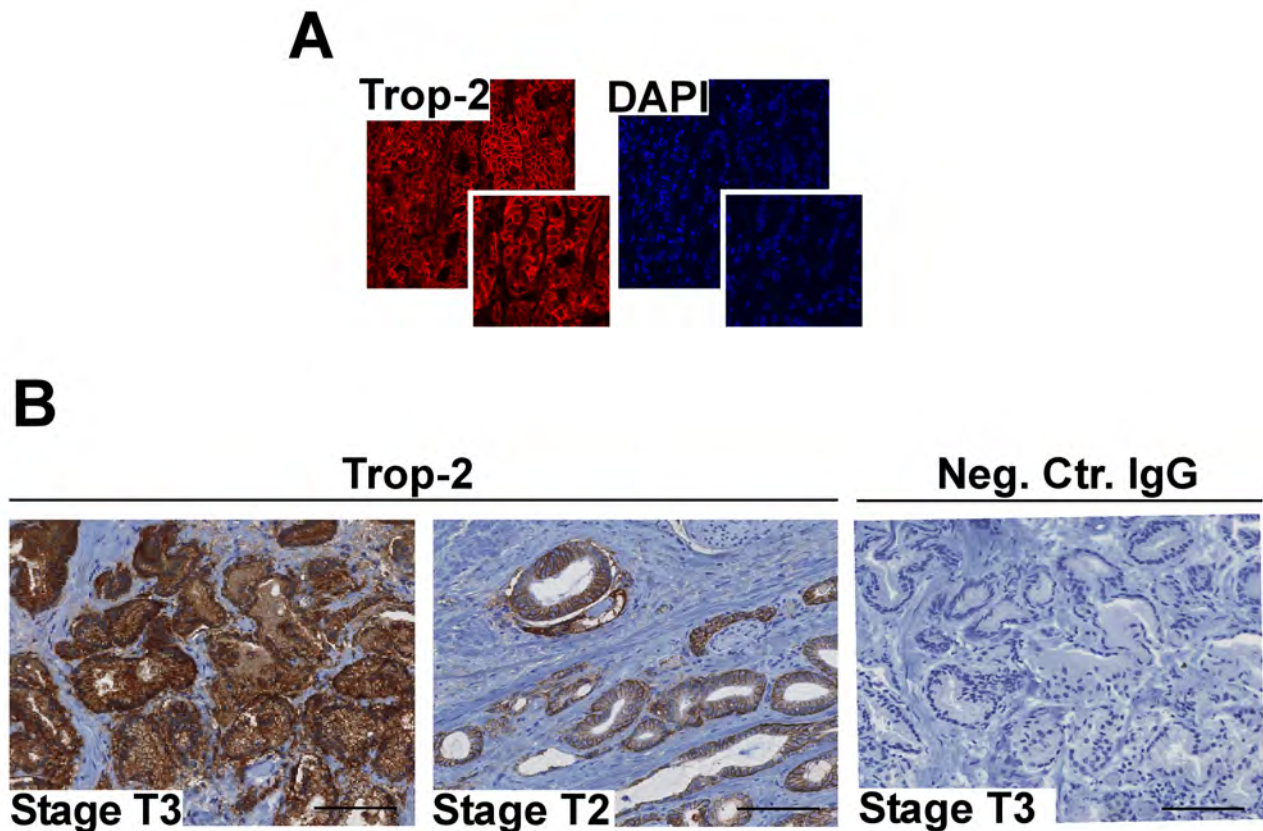


Figure 1: Trop-2 localization and expression in PCa. A. Localization of Trop-2 as investigated by IF staining and confocal microscopy in human PCa (pT3 stage, Gleason Score 9). B. Representative IHC staining for Trop-2 using specimens from patients at pT3 (left) and pT2 (middle) stages of PCa is shown. A non-immune IgG was used as negative control on a stage pT3 section (right). Bars, 100 μ m.

the ability of Trop-2 to specifically regulate $\alpha 5\beta 1$ integrin functions.

Trop-2 displaces focal adhesion kinase from focal contacts

Recent findings from our group have shown that Trop-2 inhibits accumulation of $\alpha 5\beta 1$ integrin at FA sites [16], and promotes FAK activation [17]. To test this model, we stably silenced the expression of Trop-2 in PCa cells and looked at the dynamics of FAK subcellular distribution. As shown in Figure 4 (right panel), the average number of FAK-containing FA sites is found to be

178.60 ± 0.53 per cell in PC3/Trop-2 shRNA cells (FAK-containing FAs, $n = 5,358/30$ cells) as compared with 30.57 ± 0.4 per cell in PC3/control shRNA (Ctr.shRNA) cells (FAK-containing FAs, $n = 917/30$ cells). Conversely, the average number of vinculin-containing FAs is 107.87 ± 0.50 per cell in PC3/Trop-2 shRNA cells (FAs, $n = 3,236/30$ cells) as compared with 110.53 ± 0.43 per cell in PC3/Ctr.shRNA cells (FA, $n = 3,316/30$ cells), confirming the specificity of the observed response (Figure 4).

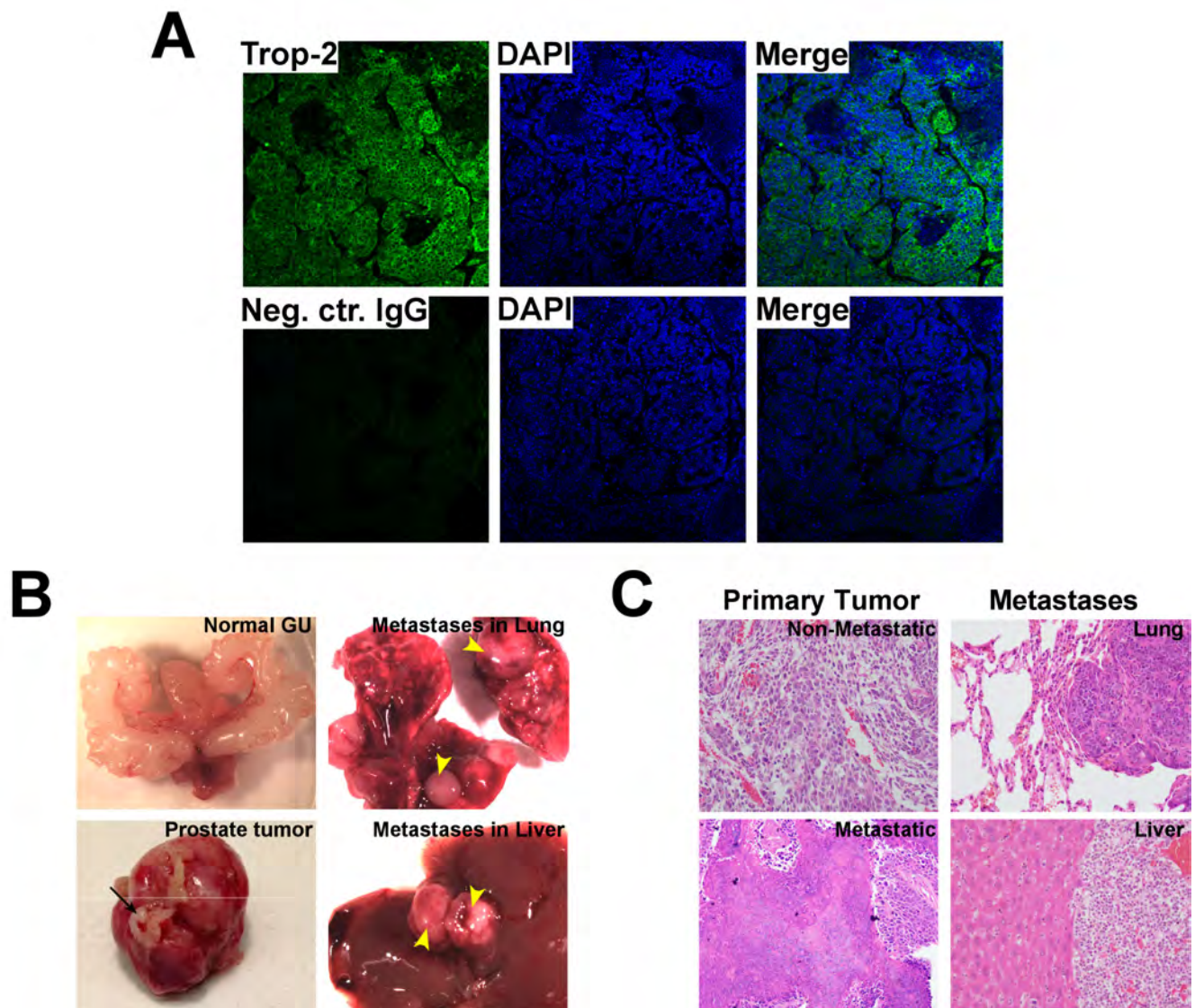


Figure 2: Analysis of Trop-2 expression in metastatic PCa from TRAMP mice. **A.** IF analysis of Trop-2 expression in metastatic prostate tumors from TRAMP mice (top). Cell nuclei were counterstained with DAPI. A non-immune goat IgG was used as a negative control Ab (bottom). **B.** Representative images of a dissected normal genito-urinary (GU) system (top left), primary prostate tumor (bottom left), and lung (top right) and liver (bottom right) macroscopic metastases. Seminal vesicles (black arrow); metastases (yellow arrowheads). **C.** H&E staining of non-metastatic (top left), metastatic primary prostate tumors (bottom left), and of metastases in lungs (top right) and liver (bottom right).

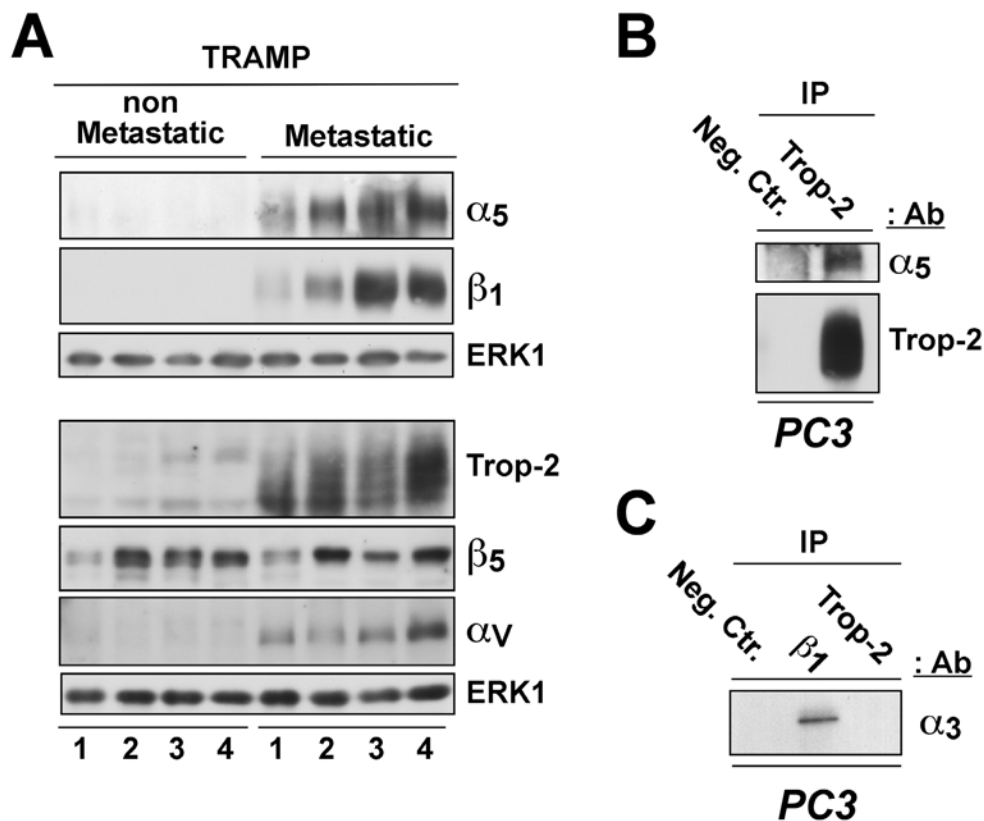


Figure 3: Correlation of Trop-2 and $\alpha5\beta1$ integrin expression in murine PCa. **A.** Analysis of $\alpha5$, $\beta1$ (top), αv and $\beta5$ (bottom) integrin subunits, as well as of Trop-2 (bottom) expression by IB using protein lysates from non-metastatic (left) and metastatic (right) prostate tumors collected from TRAMP mice. ERK1, control of protein loading. **B.** Protein lysates of PC3 cells endogenously expressing Trop-2 were immunoprecipitated using an Ab targeting Trop-2; a non-immune mouse IgG was used as a negative control Ab (Neg. Ctr.). The immunoprecipitates were then separated by SDS-PAGE and analyzed by IB for detection of the $\alpha5$ integrin subunit and Trop-2. **C.** Protein lysates of PC3 cells were immunoprecipitated using Abs targeting $\beta1$ integrins or Trop-2; a non-immune mouse IgG was used as a negative control Ab (Neg. Ctr.). The immunoprecipitates were then analyzed by IB for detection of the $\alpha3$ integrin subunit.

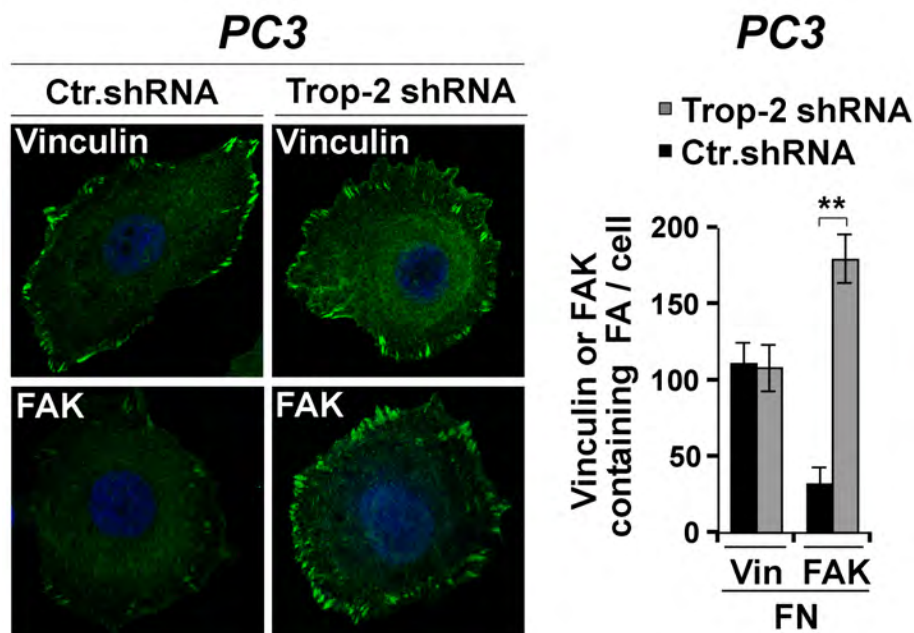


Figure 4: Trop-2-dependent modulation of FAK localization. Localization of vinculin and FAK in PC3/Ctr.shRNA and PC3/Trop-2 shRNA cells seeded on FN was analyzed by IF (left). Vinculin (Vin)- and FAK-containing FAs were counted, and the average numbers per cell are shown in the bar graph (right). Error bars, SEM. **, Student's *t*-test $P < 0.001$.

Trop-2 is recruited in PCa exosomes that stimulate cell migration on FN

Release of exosomes from cancer cells has been shown to efficiently contribute to induction of metastatic dissemination by favoring intercellular communication [14, 24]. We hypothesized that Trop-2 may be recruited to these cellular compartments, where $\beta 1$ integrins are also found [24-26]. Therefore, we isolated exosomes from PC3 culture supernatants and investigated by immunoblotting (IB) whether Trop-2 is recruited in these organelles as described in previous proteomic studies [27, 28]. Exosome preparations were characterized by IB analysis of exosomal markers: CD63, CD81 (Figure 5B); as control, IB analysis of Calnexin was performed to

exclude contamination of endoplasmic membranes (Figure 5A). Our results show specific recruitment of Trop-2 in exosomes (Figure 5A). To investigate whether exosomal Trop-2 might affect cell migration on FN, we incubated Trop-2-negative cells, PC3^{Trop-2-} or LNCaP cells, with or without exosomes purified from PC3 cells which either express Trop-2 (Parental, Ctr.shRNA) or lack Trop-2 (Trop-2 shRNA). After confirming down-regulation of Trop-2 in exosomes, characterized by IB analysis of the exosomal marker CD63 (Figure 5B), we next performed migration assays FN as substrate. We show that 24 h treatment with Trop-2 containing exosomes increases cell migration on FN of both cell lines (Figure 5C). These findings suggest that a functional Trop-2/ $\alpha 5\beta 1$ integrin complex may accumulate in exosomes and stimulate migration of recipient cells.

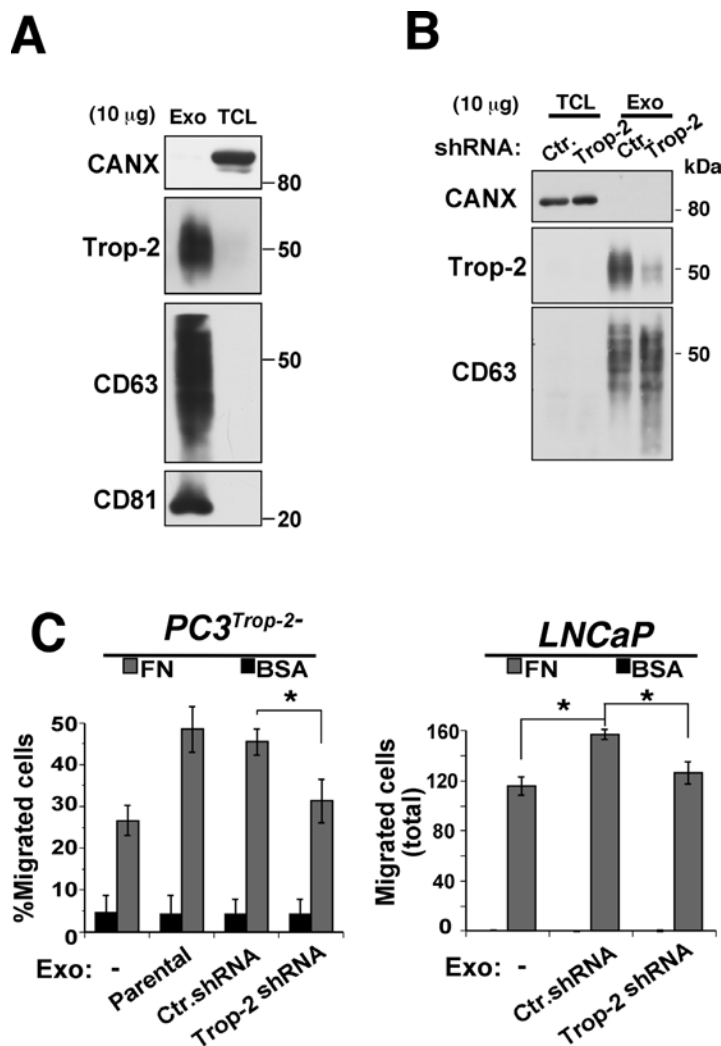


Figure 5: PC3 exosome uptake by PCa cells enhances cell migration on FN in a Trop-2-dependent manner. **A.** Analysis of Trop-2 levels in purified PC3 exosomal lysates separated by SDS-PAGE in non-reducing conditions and immunoblotted using an Ab to Trop-2; CD63 and CD81 were used as positive exosomal markers while calnexin (CANX) was used as a negative marker for exosomes. Exo, exosomes; TCL, total cell lysates. **B.** IB analysis of Trop-2 expression in exosomes secreted by PC3 cells (Ctr.shRNA and Trop-2 shRNA) using an Ab to Trop-2; CD63 was used as positive exosomal markers while calnexin (CANX) was used as a negative marker for exosomes. Exo, exosomes; TCL, total cell lysates. **C.** Migration assays of PC3^{Trop-2-} (left) or LNCaP (right) cells either untreated or treated with 10 µg/ml of PC3 exosomes (Exo) in which Trop-2 is expressed (Parental and Ctr.shRNA) or down-regulated (Trop-2 shRNA). Left, χ^2 test; right, Student's *t*-test. *, $P \leq 0.05$.

DISCUSSION

In this study, we demonstrate for the first time that Trop-2, an anti-adhesive and pro-migratory transmembrane protein, is up-regulated in human PCa with extracapsular extension (stages pT3/pT4) as compared to organ-confined (stage pT2) PCa, suggesting that this molecule plays a crucial role during cancer progression toward a metastatic phenotype. Mechanistically, we show that Trop-2 specifically binds the $\alpha 5 \beta 1$ integrin heterodimer and induces rearrangement of FA sites through displacement of FAK, thus perturbing the integrin signaling axis which is a major regulator of FA [29]. We finally find Trop-2 expression in exosomes secreted from PCa cells and demonstrate that Trop-2-containing exosomes stimulate migration of recipient Trop-2-negative cells on the $\alpha 5 \beta 1$ integrin substrate, FN.

The correlation between Trop-2 and disease progression suggests that this molecule is a novel biomarker of aggressive disease. During development, Trop-2 is expressed in the trophoblast, an actively invasive tissue at the interface between fetal and maternal circulation [30], whereas expression of this molecule in the adult is confined to a restricted number of tissues [21]. This pathway becomes exploited in malignancy, where Trop-2 is overexpressed in several human carcinomas, promotes accelerated tumor growth [21, 31], and correlates with unfavorable prognosis [18-20]. Our findings reinforce a role of this pathway in the progression from organ-confined to disseminated cancer and this phenotype appears to be more insightful than Gleason scores in the histopathological analysis of stages pT2 and pT3/pT4. It remains to be investigated whether Trop-2 overexpression may be predictive of biochemical recurrence after prostatectomy as Gleason scores are poor predictors of recurrence [32].

We find that the up-regulation of Trop-2 in metastatic tumors from TRAMP mice correlates with expression of $\beta 1$ integrins (Figure 3A). While the mechanisms of Trop-2 up-regulation during disease progression are not known, we hypothesize that $\beta 1$ integrins and Trop-2 expression may be co-regulated. Specifically, since previous studies from our group have shown that Insulin-like Growth Factor-1 Receptor (IGF-IR) plays a critical role in regulating $\beta 1$ integrin expression and since the absolute levels of IGF-IR increase during PCa progression in TRAMP tumors [33-35], we propose that IGF-IR may be an upstream regulator of Trop-2/ $\beta 1$ integrin levels in metastasis-prone tumor types.

The proposed mechanism of metastatic dissemination, as suggested here, requires also up-regulation of the $\alpha 5$ integrin subunit expression and appears specific since it does not affect the $\alpha 3$ integrin subunit. The acquisition of invasive potential by transformed cells has been linked to loss of E-cadherin-dependent cell-cell contacts, epithelial-to-mesenchymal

transition [36] and consequent up-regulation of $\alpha 5$ [7]. Consistently, we observe that $\alpha 5$ is overexpressed in metastatic versus non-metastatic PCa using TRAMP mice as a model of disease progression. This may involve, in addition to the previously reported ability of $\alpha 5 \beta 1$ to promote epithelial-to-mesenchymal transition during cancer progression [7], a direct role in leading PCa invasion through recognition sequences in FN for the $\alpha 5$ subunit [37]. Our previous findings that the reduced adhesive phenotype induced by Trop-2 results in a higher rate of cell migration on FN [16] are consistent with a model of Trop-2 modulation of $\alpha 5 \beta 1$ integrin signaling and selective displacement of FAK from FAs, that does not require changes in FAK expression as previously reported by our group [17].

We finally describe a novel mechanism involving accumulation of the Trop-2/ $\beta 1$ complex in secreted exosomes and demonstrate that exosomes containing Trop-2 impact neighboring tumor cells by enhancing their ability to migrate. These data suggest that therapeutics which interfere with the production, transfer or uptake of Trop-2-containing exosomes may attenuate tumor progression and metastasis.

Although more work is needed to fully elucidate the pro-invasive signaling pathways mediated by Trop-2 in PCa cells, the data presented here suggest that modulation of the Trop-2/ $\alpha 5 \beta 1$ complex may provide new insights in the functional stratification of PCa patients with higher metastatic propensity and, therefore, in need of more aggressive treatments.

MATERIALS AND METHODS

Cells and culture conditions

Cell lines and transfectants, as well as culture conditions have been described previously [16, 17]. Authentication of the cell lines was provided with their purchase from American Type Culture Collection. PC3/Ctr.shRNA and PC3/Trop-2 shRNA cells were generated as described previously [16, 21].

Mice

TRAMP mice, expressing SV40 large T antigen into the prostatic epithelium, were generated and characterized as described [23]. 23-54 week-old metastatic and non-metastatic TRAMP mice were used to isolate tumor samples and perform IB analysis. Distant sites were: liver and lungs. All mice were maintained under specific pathogen-free conditions. Care and handling of animals was in compliance with IACUC experimental protocols.

Reagents and antibodies

The T16 mouse monoclonal antibody (mAb) against Trop-2 (gift of Dr. S. Alberti) and the TS2/16 mAb against $\beta 1$ integrin (HB-243, ATCC) were used for IP. The following Abs were used for IB: mAbs against $\beta 1$ integrin subunit (610468, BD Transduction Laboratories), CD63 (Ab8219, Abcam), CD81 (Ab23505, Abcam); goat polyclonal Abs (pAbs) against human and murine Trop-2 (AF650 and AF1122, R&D Biosystems); rabbit antisera against $\alpha 3$ and αv integrin subunits; rabbit pAbs against $\alpha 5$ integrin subunit (sc-10729, Santa Cruz Biotechnology), $\beta 5$ integrin subunit (AB1926, Millipore), Calnexin (sc-11397, Santa Cruz Biotechnology) and ERK1/2 (sc-93, Santa Cruz Biotechnology). The goat pAb against human Trop-2 (AF650, R&D Biosystems), a mAb to Vinculin (MAB1624, Millipore) and a mAb to FAK (05-537, Millipore) were used for IF. A goat pAb against human Trop-2 (R&D Biosystems) was used for IHC. Non-immune goat IgG (SantaCruz), non-immune rabbit IgG (Sigma) and non-immune mouse IgG (Pierce) were used as negative control Abs. FN purification from human plasma has been previously described [17].

Immunohistochemical analysis

TMA were constructed at the Vancouver Prostate Cancer Centre (Vancouver, Canada) from 74 men with newly diagnosed, previously untreated, clinically localized high-risk PCa, who underwent radical prostatectomy at the same Center. Ethical approval was obtained from the Institutional Ethical Review Board.

Specimens were identified for benign and cancerous sites and marked in donor paraffin blocks using matching H&E-stained reference slides. The TMA were constructed using a manual tissue microarrayer (Beecher Instruments, Silver Spring, MD, USA). Each marked block for benign and cancerous sites was sampled two times with a core diameter of 0.6 mm arrayed in a rectangular pattern with 1 mm between the center of each core, creating a duplicate TMA layout with a total of 148 cores. The TMA paraffin block was sectioned into 5- μ m sections and mounted on positively charged slides.

IHC staining was conducted using a goat pAb to Trop-2 (AF650, R&D Biosystems, dilution 1:25) by a Ventana autostainer model Discover XTTM (Ventana Medical System, Tuscan, AZ, USA) with an enzyme-labelled biotin-streptavidin system and solvent-resistant 3,3'-diaminobenzidine Map kit. The slides were scanned on a BLISS system (Bacus Laboratory, North Lombard, IL, USA) and scored from 0 to +3 by a pathologist (L.F.) based on the staining intensity and the proportion of cells stained. Normal goat IgG was used as negative control Ab. All comparisons of staining intensities were made at 200X magnifications.

Immunofluorescence and confocal microscopy

Antigen retrieval was performed on rehydrated formalin-fixed paraffin-embedded sections from human or TRAMP mice PCa samples by incubation in 10 mM Sodium Citrate Buffer (pH 6.0) at 95°C for 23 min. The sections were blocked for 1 h at room temperature with PBS / 5% BSA. Staining was performed by incubation of tissue samples with primary Abs (1:100) for 1 h at room temperature, followed by incubation with Alexa Fluor 633-Donkey anti goat (1:250) for 20 min at room temperature. Nuclei were counterstained using DAPI. After three washes, coverslips were mounted on the sections using Pro-Long anti-fade reagent (Invitrogen), and slides were analyzed on an inverted confocal microscope (LSM510, Carl Zeiss). Immunofluorescence analysis of PC3 cells using Alexa Fluor 488 goat anti-mouse (1:250) for 60 min at room temperature was performed as described [16].

Generation of tumor lysates

Tumor lysates were prepared by homogenizing the tissues on ice using the following lysis buffer: 100 mM Tris-HCl (pH 7.4), 150 mM NaCl, 5% SDS, 0.1% Triton X-100, 1 mM benzamidine, 10 μ g/mL Soybean Trypsin Inhibitor, 10 μ g/mL leupeptin, 1 mM PMSF, 1 μ g/mL pepstatin A, and 1 μ M calpain inhibitor. The lysates were boiled for 5 min and centrifuged at 13,000 rpm for 20 min. Supernatants were collected and protein content was determined using the DC Protein Assay Kit (Bio-Rad). The protein samples (50 μ g per lane) were separated by SDS-PAGE and transferred onto PVDF membranes for IB.

Isolation and immunoblotting analysis of PCa exosomes

Exosomes were isolated from PCa cells as described [24, 38]. Purified exosomes were lysed with radioimmunoprecipitation assay buffer (10 mM Tris-HCl at pH 7.4, 150 mM NaCl, 1 mM EDTA, 0.1% SDS, 1% Triton X-100, and 1% sodium deoxycholate) supplemented with protease inhibitors. The protein samples (10 μ g per lane) were separated by SDS-PAGE under non-reducing conditions and transferred onto PVDF membranes for IB.

Immunoprecipitation

To collect nuclear and cytoplasmic fractions, cells were washed with cold PBS and lysed by scraping in 20 mM Tris-HCl (pH 7.4), 150 mM NaCl, 1mM CaCl_2 , 1mM MgCl_2 , 1% NP-40, 1 mM benzamidine, 10 μ g/ml leupeptin, 1 mM PMSF, 1 μ g/ml pepstatin A, 1 μ M calpain inhibitor, 1mM Na_3VO_4 , 1 mM $\text{Na}_4\text{O}_7\text{P}_2$. The

cells were subjected to 3 cycles of sonication (15 sec each) on ice. After 15 min incubation on ice, lysates were centrifuged at 12,000g for 10 min, and supernatants were collected and pre-cleared by two consecutive incubations with protein G-Sepharose at 4°C for 45 min. Binding to specific Abs was performed by incubation at 4°C for 3 h, followed by incubation with protein G-Sepharose at 4°C for 1 h. After six washes with lysis buffer, immunocomplexes were eluted with 100 mM glycine pH 2.5, followed by pH neutralization using Tris to a final concentration of 50 mM. The immunocomplexes were then separated by SDS-PAGE, transferred onto PVDF membrane, and subjected to analysis by IB.

Exosome treatment and migration assay

Cell treatment with exosomes was performed as previously described [24]. Briefly, LNCaP and PC3^{Trop-2-} cells were serum starved for 18 h, then treated for 24 h with 20 µg/ml of exosomes obtained from PC3 cells. The cells treated with PC3-derived exosomes were trypsinized, extensively washed with PBS and subsequently plated to perform the migration assay. Cell migration assays on FN has been performed as previously described using Millicell inserts (Millipore) with 8 (for LNCaP) or 12 µm (for PC3^{Trop-2-}) pores [16]. Briefly, chambers were coated on both top and bottom layers with FN (10 µg/mL) or 1% BSA overnight at 4°C. After cell detachment and trypsin inactivation, cells were seeded on coated transwell chambers at 37°C for 6 h. After fixation with 3.7% paraformaldehyde (PFA), cells attached on both layers of the porous filter were stained with 1 µg/mL 4',6-diamidino-2-phenylindole (DAPI) and pictures of nuclei were acquired by fluorescence microscopy. Then, cells on the top layer were removed using a cotton swab, and pictures of nuclei from cells migrated to the bottom layer were acquired. For each group of PC3^{Trop-2-} cells treated with or without exosomes, the ratio between number of cells migrated onto the bottom layer and total (top + bottom) number of cells attached on the filter was calculated. For LNCaP cells, only the total number of cells attached on the bottom layer was calculated.

Statistical analysis

For patients' samples, Fisher's exact test was used to examine the association between dichotomized biomarkers (Trop-2) and PCa stage (Gleason score). For FA analysis, *t*-test was used to evaluate the average numbers of FA per cell between PC3/Ctr.shRNA and PC3/Trop-2 shRNA cells. For migration assays χ^2 tests and *t*-test were used to compare the migration between treatments. Stata 12.0 (StatCORP LP, College Station, TX, USA) was used for data analysis. $P \leq 0.05$ was considered as statistical significance.

ACKNOWLEDGMENTS

We thank Dr. S. Alberti for providing the mAb (clone T16) against Trop-2 and Dr. L. Borgia for helpful discussion. The authors would like to thank Dr. A. Sayeed, as well as R. M. De Rita, A. N. Duffy and A. Singh in Languino's lab for constructive suggestions. We are also grateful to Mrs. M. Harden and Mrs. C. Deemer for their help with the preparation of the manuscript.

GRANT SUPPORT

This work was supported by NIH (LRL, DCA), NIH-R01CA109874 (LRL), NIH-R01CA089720 (LRL), NIH-R01CA086072 (RGP); the Office of the Assistant Secretary of Defense for Health Affairs through the Prostate Cancer Research Program under Award No. W81XWH-13-1-0193 (DCA), and by a Post-Doctoral Research Fellowship from the Italian Association for Cancer Research to M.T. and by a Post-Doctoral Research Fellowship from the American Italian Cancer Foundation to C.F. Research in this publication includes work carried out using the Sidney Kimmel Cancer Center Bioimaging Facility and the Translational Research & Pathology Shared Resource, which are supported in part by NCI Cancer Center Support Grant P30 CA56036 (RGP). This project is also funded, in part, under a Commonwealth University Research Enhancement Program grant with the Pennsylvania Department of Health (H.R.); the Department specifically disclaims responsibility for any analyses, interpretations or conclusions.

CONFLICTS OF INTEREST

The Authors do not have any conflicts of interest.

Abbreviations

PCa, prostate cancer; ECM, extracellular matrix; TNM, tumor, node and metastasis; PSA, prostate specific antigen; TRAMP, TRansgenic Adenocarcinoma of Mouse Prostate; IB, immunoblotting; mAb, monoclonal antibody; pAb, polyclonal antibody; IF, immunofluorescence; IHC, immunohistochemistry; TMA, Tissue Microarray; FAK, focal adhesion kinase; FN, fibronectin.

REFERENCES

1. Edge SB and American Joint Committee on Cancer. (2010). AJCC cancer staging manual. (New York: Springer).
2. Sobin LH, Gospodarowicz MK, Wittekind C and Cancer IUa. (2010). TNM classification of malignant tumours. (Chichester, West Sussex, UK ; Hoboken, NJ: Wiley-Blackwell).
3. Logothetis CJ, Gallick GE, Maity SN, Kim J, Aparicio

- A, Efstathiou E and Lin SH. Molecular classification of prostate cancer progression: foundation for marker-driven treatment of prostate cancer. *Cancer Discov.* 2013; 3:849-861.
4. Knox JD, Cress AE, Clark V, Manriquez L, Affinito KS, Dalkin BL and Nagle RB. Differential expression of extracellular matrix molecules and the alpha 6-integrins in the normal and neoplastic prostate. *Am J Pathol.* 1994; 145:167-174.
 5. Murant SJ, Handley J, Stower M, Reid N, Cussenot O and Maitland NJ. Co-ordinated changes in expression of cell adhesion molecules in prostate cancer. *Eur J Cancer.* 1997; 33:263-271.
 6. Goel HL, Underwood JM, Nickerson JA, Hsieh CC and Languino LR. $\beta 1$ integrins mediate cell proliferation in three-dimensional cultures by regulating expression of the sonic hedgehog effector protein, GLI1. *J Cell Physiol.* 2010; 224:210-217.
 7. Sawada K, Mitra AK, Radjabi AR, Bhaskar V, Kistner EO, Tretiakova M, Jagadeeswaran S, Montag A, Becker A, Kenny HA, Peter ME, Ramakrishnan V, Yamada SD and Lengyel E. Loss of E-cadherin promotes ovarian cancer metastasis via $\alpha 5$ -integrin, which is a therapeutic target. *Cancer Res.* 2008; 68:2329-2339.
 8. Adachi M, Taki T, Higashiyama M, Kohno N, Inufusa H and Miyake M. Significance of integrin $\alpha 5$ gene expression as a prognostic factor in node-negative non-small cell lung cancer. *Clin Cancer Res.* 2000; 6:96-101.
 9. Dingemans AM, van den Boogaart V, Vosse BA, van Suylen RJ, Griffioen AW and Thijssen VL. Integrin expression profiling identifies integrin $\alpha 5$ and $\beta 1$ as prognostic factors in early stage non-small cell lung cancer. *Mol Cancer.* 2010; 9:152.
 10. Kuwada SK and Li X. Integrin $\alpha 5/\beta 1$ mediates fibronectin-dependent epithelial cell proliferation through epidermal growth factor receptor activation. *Mol Biol Cell.* 2000; 11:2485-2496.
 11. Morozovich G, Kozlova N, Cheglakov I, Ushakova N and Berman A. Integrin $\alpha 5\beta 1$ controls invasion of human breast carcinoma cells by direct and indirect modulation of MMP-2 collagenase activity. *Cell Cycle.* 2009; 8:2219-2225.
 12. Akiyama SK. Integrins in cell adhesion and signaling. *Hum Cell.* 1996; 9:181-186.
 13. Luga V, Zhang L, Vitoria-Petit AM, Ogunjimi AA, Inanlou MR, Chiu E, Buchanan M, Hosein AN, Basik M and Wrana JL. Exosomes mediate stromal mobilization of autocrine Wnt-PCP signaling in breast cancer cell migration. *Cell.* 2012; 151:1542-1556.
 14. Peinado H, Aleckovic M, Lavotshkin S, Matei I, Costa-Silva B, Moreno-Bueno G, Hergueta-Redondo M, Williams C, Garcia-Santos G, Ghajar C, Nitadori-Hoshino A, Hoffman C, Badal K, Garcia BA, Callahan MK, Yuan J, et al. Melanoma exosomes educate bone marrow progenitor cells toward a pro-metastatic phenotype through MET. *Nat Med.* 2012; 18:883-891.
 15. Valadi H, Ekstrom K, Bossios A, Sjostrand M, Lee JJ and Lotvall JO. Exosome-mediated transfer of mRNAs and microRNAs is a novel mechanism of genetic exchange between cells. *Nat Cell Biol.* 2007; 9:654-659.
 16. Trerotola M, Jernigan DL, Liu Q, Siddiqui J, Fatatis A and Languino LR. Trop-2 promotes cancer metastasis by modulating $\beta 1$ integrin functions. *Cancer Res.* 2013; 73:3155-3167.
 17. Trerotola M, Li J, Alberti S and Languino LR. Trop-2 inhibits prostate cancer cell adhesion to fibronectin through the $\beta 1$ integrin-RACK1 axis. *J Cell Physiol.* 2012; 227:3670-3677.
 18. Fong D, Moser P, Krammel C, Gostner JM, Margreiter R, Mitterer M, Gastl G and Spizzo G. High expression of TROP2 correlates with poor prognosis in pancreatic cancer. *Br J Cancer.* 2008; 99:1290-1295.
 19. Kluger HM, Kluger Y, Gilmore-Hebert M, DiVito K, Chang JT, Rodov S, Mironenko O, Kacinski BM, Perkins AS and Sapi E. cDNA microarray analysis of invasive and tumorigenic phenotypes in a breast cancer model. *Lab Invest.* 2004; 84:320-331.
 20. Ohmachi T, Tanaka F, Mimori K, Inoue H, Yanaga K and Mori M. Clinical significance of TROP2 expression in colorectal cancer. *Clin Cancer Res.* 2006; 12:3057-3063.
 21. Trerotola M, Cantanelli P, Guerra E, Tripaldi R, Aloisi AL, Bonasera V, La Sorda R, Lattanzio R, de Lange R, Weidle U, Piantelli M and Alberti S. Upregulation of Trop-2 quantitatively stimulates human cancer growth. *Oncogene.* 2012; 32:222-233.
 22. Ellis L, Lehet K, Ku S, Azabdaftari G and Pili R. Generation of a syngeneic orthotopic transplant model of prostate cancer metastasis. *Oncoscience.* 2014; 1:609-613.
 23. Greenberg NM, DeMayo F, Finegold MJ, Medina D, Tilley WD, Aspinall JO, Cunha GR, Donjacour AA, Matusik RJ and Rosen JM. Prostate cancer in a transgenic mouse. *Proc Natl Acad Sci USA.* 1995; 92:3439-3443.
 24. Fedele C, Singh A, Zerlanko BJ, Iozzo RV and Languino LR. The $\alpha 5\beta 6$ Integrin Is Transferred Intercellularly via Exosomes. *J Biol Chem.* 2015; 290:4545-4551.
 25. Bijnsdorp IV, Geldof AA, Lavaei M, Piersma SR, van Moorselaar RJ and Jimenez CR. Exosomal ITGA3 interferes with non-cancerous prostate cell functions and is increased in urine exosomes of metastatic prostate cancer patients. *J Extracell Vesicles.* 2013; 2.
 26. Clayton A, Turkes A, Dewitt S, Steadman R, Mason MD and Hallett MB. Adhesion and signaling by B cell-derived exosomes: the role of integrins. *FASEB J.* 2004; 18:977-979.
 27. Chen CL, Lai YF, Tang P, Chien KY, Yu JS, Tsai CH, Chen HW, Wu CC, Chung T, Hsu CW, Chen CD, Chang YS, Chang PL and Chen YT. Comparative and targeted proteomic analyses of urinary microparticles from bladder cancer and hernia patients. *J Proteome Res.* 2012; 11:5611-

5629.

28. Tauro BJ, Greening DW, Mathias RA, Mathivanan S, Ji H and Simpson RJ. Two distinct populations of exosomes are released from LIM1863 colon carcinoma cell-derived organoids. *Mol Cell Proteomics*. 2013; 12:587-598.
29. Cox BD, Natarajan M, Stettner MR and Gladson CL. New concepts regarding focal adhesion kinase promotion of cell migration and proliferation. *J Cell Biochem*. 2006; 99:35-52.
30. Lipinski M, Parks DR, Rouse RV and Herzenberg LA. Human trophoblast cell-surface antigens defined by monoclonal antibodies. *Proc Natl Acad Sci USA*. 1981; 78:5147-5150.
31. Guerra E, Trerotola M, Dell' Arciprete R, Bonasera V, Palombo B, El-Sewedy T, Ciccimarra T, Crescenzi C, Lorenzini F, Rossi C, Vacca G, Lattanzio R, Piantelli M and Alberti S. A bicistronic CYCLIN D1-TROP2 mRNA chimera demonstrates a novel oncogenic mechanism in human cancer. *Cancer Res*. 2008; 68:8113-8121.
32. Bedolla R, Prihoda TJ, Kreisberg JI, Malik SN, Krishnegowda NK, Troyer DA and Ghosh PM. Determining risk of biochemical recurrence in prostate cancer by immunohistochemical detection of PTEN expression and Akt activation. *Clin Cancer Res*. 2007; 13:3860-3867.
33. Goel H, Sayeed A, Breen M, Zarif MJ, Garlick DS, Leav I, Davis RJ, Fitzgerald TJ, Morrione A, Liu Q, Dicker A, Altieri DC and Languino LR. β 1 integrins mediate resistance to ionizing radiation by inhibiting JNK. *J Cell Physiol*. 2013; 228:1601-1609.
34. Sutherland BW, Knoblaugh SE, Kaplan-Lefko PJ, Wang F, Holzenberger M and Greenberg NM. Conditional deletion of insulin-like growth factor-I receptor in prostate epithelium. *Cancer Res*. 2008; 68:3495-3504.
35. Goel HL, Breen M, Zhang J, Das I, Aznavoorian-Cheshire S, Greenberg NM, Elgavish A and Languino LR. β 1A integrin expression is required for type 1 insulin-like growth factor receptor mitogenic and transforming activities and localization to focal contacts. *Cancer Res*. 2005; 65:6692-6700.
36. Hanahan D and Weinberg RA. Hallmarks of cancer: the next generation. *Cell*. 2011; 144:646-674.
37. Aota S, Nomizu M and Yamada KM. The short amino acid sequence Pro-His-Ser-Arg-Asn in human fibronectin enhances cell-adhesive function. *J Biol Chem*. 1994; 269:24756-24761.
38. They C, Amigorena S, Raposo G and Clayton A. (2006). Isolation and characterization of exosomes from cell culture supernatants and biological fluids (John Wiley & Sons, Inc).

PI3K therapy reprograms mitochondrial trafficking to fuel tumor cell invasion

M. Cecilia Caino^{a,b}, Jagadish C. Ghosh^{a,b}, Young Chan Chae^{a,b}, Valentina Vaira^{c,d}, Dayana B. Rivadeneira^{a,b}, Alice Favarsani^d, Paolo Rampini^e, Andrew V. Kossenkov^f, Katherine M. Aird^g, Rugang Zhang^g, Marie R. Webster^b, Ashani T. Weeraratna^b, Silvano Bosari^{d,h}, Lucia R. Languino^{a,i}, and Dario C. Altieri^{a,b,†}

^aProstate Cancer Discovery and Development Program, The Wistar Institute, Philadelphia, PA 19104; ^bTumor Microenvironment and Metastasis Program, The Wistar Institute, Philadelphia, PA 19104; ^cIstituto Nazionale Genetica Molecolare "Romeo ed Enrica Invernizzi," Milan 20122, Italy; ^dDivision of Pathology, Fondazione Istituto di Ricovero e Cura a Carattere Scientifico (IRCCS) Ca' Granda Ospedale Maggiore Policlinico, Milan 20122, Italy; ^eDivision of Neurosurgery, Fondazione IRCCS Ca' Granda Ospedale Maggiore Policlinico, Milan 20122, Italy; ^fCenter for Systems and Computational Biology, The Wistar Institute, Philadelphia, PA 19104; ^gGene Expression and Regulation Program, The Wistar Institute, Philadelphia, PA 19104; ^hDepartment of Pathophysiology and Organ Transplant, University of Milan, Milan 20122, Italy; and ⁱDepartment of Cancer Biology, Kimmel Cancer Center, Thomas Jefferson University, Philadelphia, PA 19107

Edited by Vincent T. Marchesi, Yale University School of Medicine, New Haven, CT, and approved May 26, 2015 (received for review January 13, 2015)

Molecular therapies are hallmarks of "personalized" medicine, but how tumors adapt to these agents is not well-understood. Here we show that small-molecule inhibitors of phosphatidylinositol 3-kinase (PI3K) currently in the clinic induce global transcriptional reprogramming in tumors, with activation of growth factor receptors, (re)phosphorylation of Akt and mammalian target of rapamycin (mTOR), and increased tumor cell motility and invasion. This response involves redistribution of energetically active mitochondria to the cortical cytoskeleton, where they support membrane dynamics, turnover of focal adhesion complexes, and random cell motility. Blocking oxidative phosphorylation prevents adaptive mitochondrial trafficking, impairs membrane dynamics, and suppresses tumor cell invasion. Therefore, "spatiotemporal" mitochondrial respiration adaptively induced by PI3K therapy fuels tumor cell invasion, and may provide an important antimetastatic target.

mitochondria | molecular therapy | cytoskeleton | PI3K | cell invasion

The phosphatidylinositol 3-kinase (PI3K) is a universal tumor driver (1) that integrates growth factor signaling with downstream circuitries of cell proliferation, metabolism, and survival (2). Exploited in nearly every human tumor, including through acquisition of activating mutations (3), PI3K signaling is an important therapeutic target, and several small-molecule antagonists of this pathway have entered clinical testing (4). However, the patient response to these agents has been inferior to expectations (5), dampened by drug resistance (6) and potentially other mechanisms of adaptation by the tumor (7).

In this context, there is evidence that therapeutic targeting of PI3K promotes tumor adaptation, paradoxically reactivating protein kinase B (PKB/Akt) in treated cells (8) and reprogramming mitochondrial functions in bioenergetics and apoptosis resistance (9). How these changes affect tumor traits, however, is unclear. Against the backdrop of a ubiquitous "Warburg effect" (10), where tumors switch from cellular respiration to aerobic glycolysis, a role of mitochondria in cancer has not been clearly defined (11) and at times has been proposed as that of a tumor suppressor (12).

In this study, we examined the impact of mitochondrial reprogramming induced by PI3K therapy on mechanisms of tumor progression.

Results

PI3K Therapy Reactivates Akt and Mammalian Target of Rapamycin Signaling. Treatment of patient-derived glioblastoma (GBM) organotypic cultures (13) with PX-866, an irreversible pan-PI3K antagonist currently in the clinic (4), caused transcriptional up-regulation of multiple growth factor receptor pathways (Fig. 1*A*). This was associated with widespread phosphorylation, namely activation of the GBM kinome in primary organotypic cultures

(Fig. 1*B* and Table S1) as well as GBM LN229 cells (Fig. S1*A*). Consistent with previous observations (8), structurally diverse small-molecule PI3K antagonists induced robust (re)phosphorylation of Akt1 (S473) and Akt2 (S474) in tumor cells (Fig. 1*C* and Fig. S1*B*), as well as phosphorylation of downstream mammalian target of rapamycin (mTOR) and its effectors, 70S6K and 4EBP1 (Fig. 1*D* and Fig. S1*C*). Similar results were obtained in primary 3D GBM neurospheres, where PI3K therapy strongly induced Akt (Fig. 1*E*) and mTOR (Fig. 1*F*) phosphorylation. By transcriptome analysis, PI3K antagonists up-regulated two main gene networks of protection from apoptosis (9) and increased cell motility (Fig. 1*G*) in treated tumors.

Increased Tumor Cell Motility Mediated by PI3K Therapy. Consistent with these data, PI3K inhibitors vigorously stimulated tumor cell invasion across Matrigel-coated Transwell inserts (Fig. 2*A* and *B* and Fig. S1*D* and *E*) and in 3D tumor spheroids (Fig. 2*A* and *B*). Tumor cell proliferation was not significantly affected (Fig. S1*F*) (9). In addition, PI3K therapy dose-dependently increased the number and size of 3D GBM neurospheres (Fig. 2*C* and Fig. S1*G* and *H*).

Significance

Despite the promise of personalized cancer medicine, most molecular therapies produce only modest and short-lived patient gains. In addition to drug resistance, it is also possible that tumors adaptively reprogram their signaling pathways to evade therapy-induced "stress" and, in the process, acquire more aggressive disease traits. We show here that small-molecule inhibitors of PI3K, a cancer node and important therapeutic target, induce transcriptional and signaling reprogramming in tumors. This involves the trafficking of energetically active mitochondria to subcellular sites of cell motility, where they provide a potent, "regional" energy source to support tumor cell invasion. Although this response may paradoxically increase the risk of metastasis during PI3K therapy, targeting mitochondrial reprogramming is feasible, and could provide a novel therapeutic strategy.

Author contributions: M.C.C. and D.C.A. designed research; M.C.C., J.C.G., Y.C.C., V.V., D.B.R., A.F., K.M.A., R.Z., M.R.W., and A.T.W. performed research; P.R. contributed new reagents/analytic tools; P.R. provided primary, patient-derived glioblastoma samples; K.M.A. and R.Z. performed and analyzed quiescence studies in tumor cells; M.R.W. and A.T.W. performed and analyzed 3D cell invasion assays; M.C.C., A.V.K., S.B., L.R.L., and D.C.A. analyzed data; and M.C.C., J.C.G., and D.C.A. wrote the paper.

The authors declare no conflict of interest.

This article is a PNAS Direct Submission.

[†]To whom correspondence should be addressed. Email: daltieri@wistar.org.

This article contains supporting information online at www.pnas.org/lookup/suppl/doi:10.1073/pnas.1500722112/-DCSupplemental.

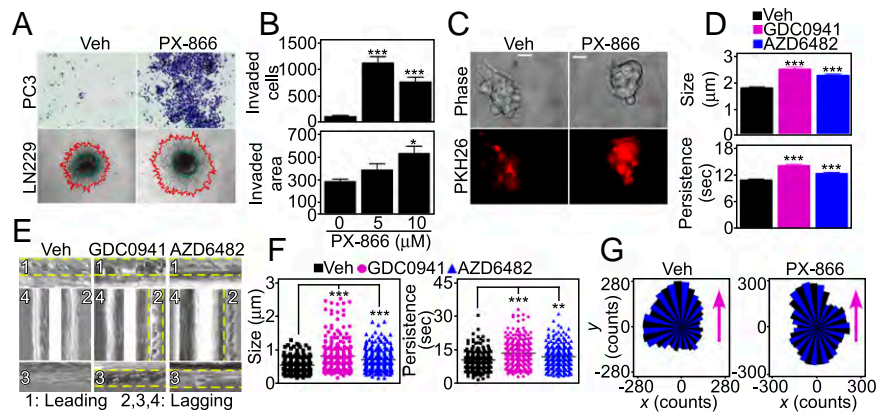


Fig. 2. PI3K therapy induces adaptive tumor cell motility and invasion. (A) Tumor cells treated with vehicle or 10 μ M PX-866 for 48 h were analyzed for invasion across Matrigel-coated Transwell inserts (Top) or in 3D spheroids (Bottom). Red, invasive edge; green, core. Representative images. Magnification, 10 \times . (B) PC3 (Top) or LN229 (Bottom) cells were treated with the indicated increasing concentrations of PX-866 and quantified for invasion across Matrigel (Top) or in 3D spheroids (Bottom). The distance between the core and edge of 3D spheroids was determined. Mean \pm SEM of replicates from a representative experiment. * $P = 0.02$; *** $P < 0.0001$. (C) Patient-derived GBM spheroids were treated with vehicle or PX-866 (0–10 μ M) for 48 h and analyzed by phase-contrast (Top) or fluorescence microscopy (Bottom). The vital dye PKH26 was used to counterstain live GBM neurospheres. (Scale bar, 20 μ m.) (D) Membrane ruffling was quantified in PC3 cells treated with vehicle or PI3K inhibitors for 48 h by SACED microscopy. Average values from at least 330 ruffles per treatment are shown for ruffle size (Top) and time of ruffle persistence (Bottom). Mean \pm SEM ($n = 15$). *** $P < 0.0001$. (E) Representative stroboscopic images from time-lapse video microscopy of PC3 cells treated with vehicle or PI3K inhibitors. Four SACED regions corresponding to the top (1), right (2), bottom (3), and left (4) of each cell are shown. The ruffling activity (broken yellow lines) is restricted to one main region (1) on the vehicle cell but is distributed equally between three regions (1–3) on cells treated with PI3K inhibitors. See also Movie S1. (F) PC3 cells were treated with vehicle or PI3K inhibitors, and membrane dynamics at lagging areas were quantified. Ruffle size (Left) or time of ruffle persistence (Right) from at least 205 individual lagging ruffles are shown. Mean \pm SEM ($n = 15$). ** $P = 0.0047$; *** $P < 0.0001$. (G) PC3 cells were treated with vehicle or PX-866 for 48 h and quantified for directional versus random cell migration by time-lapse video microscopy (8 h). Rose plots show the distribution of cells migrating along each position interval (range interval 10 $^\circ$, internal angle 60 $^\circ$). Arrows indicate the direction of chemotactic gradient.

therapy profoundly affected FA dynamics (Fig. 3H and Movie S2), increasing both the assembly and decay of FA complexes (Fig. S5D) and their turnover rate (Fig. S5E). In contrast, PI3K inhibition reduced the number of stable FA complexes (Fig. S5F).

Mitochondria are a primary source of reactive oxygen species (ROS), and these moieties have been implicated in tumor cell motility. PI3K antagonists increased the production of mitochondrial superoxide in tumor cells compared with untreated cultures (Fig. S6A and B), and this response was abolished by a mitochondrial-targeted ROS scavenger, mitoTEMPO (Fig. S6C). In contrast, ROS scavenging with mitoTEMPO did not affect mitochondrial repositioning to the cortical cytoskeleton (Fig. 4A and Fig. S6D and E) or tumor cell invasion (Fig. 4B) mediated by PI3K inhibitors. Increasing concentrations of the pan-antioxidant *N*-acetyl cysteine (NAC) had no effect on PI3K therapy-mediated tumor cell invasion (Fig. S6F). The increase in basal cell motility in the presence of antioxidants may reflect release of ROS-regulated inhibitory mechanisms of mitochondrial trafficking.

Role of Bioenergetics in Mitochondrial Trafficking and Tumor Cell Invasion. Next, we asked whether mitochondrial bioenergetics was important for this pathway, and generated LN229 cells devoid of oxidative phosphorylation ($\rho 0$ cells). Chemoattractant stimulation of respiration-competent LN229 cells induced repositioning of mitochondria to the cortical cytoskeleton (Fig. S7A) that colocalized with paxillin⁺ FA complexes (Fig. S7B). In contrast, respiration-deficient LN229 $\rho 0$ cells failed to reposition mitochondria to the cortical cytoskeleton (Fig. 4C). This absence of mitochondria proximal to FA complexes (Fig. 4D) was associated with loss of FA dynamics (Fig. S7C and D and Movie S3) and suppression of tumor cell invasion across Matrigel-containing inserts (Fig. 4E and Fig. S7E).

As an independent approach, we treated tumor cells with Gamitrinib, a mitochondrial-targeted small-molecule Hsp90 inhibitor that induces misfolding and degradation of the oxidative phosphorylation complex II subunit SDHB (19). Nontoxic

concentrations of Gamitrinib abolished the trafficking of mitochondria to pFAK-containing FA complexes in response to PI3K antagonists (Fig. 4F and G) and preserved a polarized and perinuclear mitochondrial distribution (Fig. S8A). Consistent with these findings, Gamitrinib abolished the increase in tumor cell invasion (Fig. 4H) and the expansion of primary GBM neurospheres (Fig. S8B and C) mediated by PI3K antagonists. To validate these findings, we next silenced the expression of TRAP-1 (Fig. S8D), a mitochondrial Hsp90-like chaperone targeted by Gamitrinib and implicated in complex II stability (19). TRAP-1 silencing in vehicle-treated cells did not affect mitochondrial localization (Fig. S8E, Left). In contrast, knockdown of TRAP-1 abolished mitochondrial trafficking to the cortical cytoskeleton in the presence of PI3K antagonists, increasing the fraction of polarized and perinuclear organelles in these cells (Fig. S8E, Right). Finally, treatment with small-molecule inhibitors of mitochondrial complex I (Rotenone), complex III (Antimycin A), or complex V (Oligomycin) or a mitochondrial uncoupler (carbonyl cyanide *m*-chlorophenyl hydrazine; CCCP) inhibited mitochondrial repositioning to the cortical cytoskeleton (Fig. S8F) and tumor cell invasion (Fig. 4I) in the presence of PI3K therapy.

To begin elucidating the signaling requirements of adaptive mitochondrial trafficking and tumor cell invasion, we next targeted the PI3K–Akt–mTOR axis, which becomes reactivated in response to PI3K therapy (8, 9). Knockdown of Akt1 or Akt2 (Fig. S9A), mTOR (Fig. S9B), or FAK (Fig. S9C) independently prevented the repositioning of mitochondria to the cortical cytoskeleton (Fig. 4J and K and Fig. S9D) and suppressed tumor cell invasion (Fig. 4L and Fig. S9G) induced by PI3K antagonists. In contrast, knockdown of these molecules in the absence of PI3K inhibition had no effect on mitochondrial trafficking (Fig. S9E) or organelle morphology (Fig. S9F).

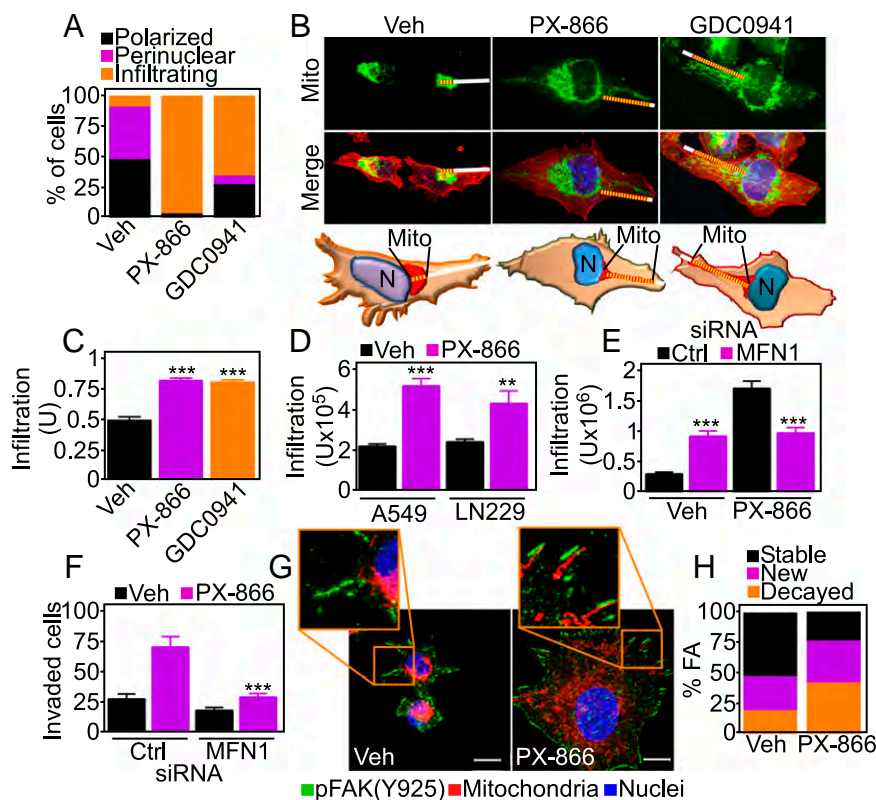


Fig. 3. Mitochondria fuel focal adhesion dynamics. (A) PC3 cells treated with vehicle or PI3K inhibitors for 48 h were stained with MitoTracker Red, phalloidin Alexa488, and DAPI, and full cell stacks were used to generate 3D max projection images that were scored for mitochondrial morphology (polarized, perinuclear, infiltrating). (B) Representative confocal 3D max projection images of PC3 cells treated with vehicle or the indicated PI3K inhibitors and stained as in A. (Bottom) Models for quantification of mitochondrial trafficking. Mito, mitochondria. White lines indicate the distance from nuclei to the cell border. Yellow lines indicate the length of mitochondrial infiltration into membrane lamellipodia. Magnification, 63 \times . (C) PC3 cells treated with vehicle or the indicated PI3K inhibitors were labeled as in A and quantified for mitochondrial infiltration into lamellipodia. At least 18 cells were analyzed at two independent lamellipodia, and data were normalized to total lamellipodia length. Mean \pm SEM ($n = 36$). *** $P < 0.0001$. (D) Lung adenocarcinoma A549 or glioblastoma LN229 cells were labeled as in A and scored for mitochondrial infiltration into membrane lamellipodia by fluorescence microscopy. Mean \pm SEM. ** $P = 0.0056$; *** $P < 0.0001$. (E) PC3 cells were transfected with control (Ctrl) or MFN1-directed siRNA, labeled as in A, and quantified for mitochondrial infiltration in the cortical cytoskeleton in the presence of vehicle or PX-866. Mean \pm SEM. *** $P < 0.0001$. (F) PC3 cells transfected with control or MFN1-directed siRNA were treated with vehicle or PX-866 and analyzed for Matrigel invasion after 48 h. Mean \pm SEM. *** $P = 0.0002$. (G) PC3 cells treated with vehicle or PI3K inhibitors for 48 h were replated onto fibronectin-coated slides for 5 h and labeled with an antibody to phosphorylated FAK (pY925) Alexa488, MitoTracker Red, and DAPI. Representative 1- μ m extended-focus confocal images with localization of mitochondria near FA complexes are shown. Magnification, 63 \times . (Scale bar, 10 μ m.) (H) PC3 cells expressing Talin-GFP to label FA were treated as indicated and quantified for decay, formation, and stability of FA complexes per cell over 78 min; $n = 631$. See also [Movie S2](#).

Discussion

In this study, we have shown that small-molecule PI3K inhibitors currently in the clinic induce global reprogramming of transcriptional and signaling pathways in tumor cells, paradoxically resulting in increased tumor cell motility and invasion. Mechanistically, this involves the trafficking of energetically active mitochondria to the cortical cytoskeleton of tumor cells, where they support membrane lamellipodia dynamics, turnover of FA complexes, and random cell migration and invasion. Conversely, interference with this spatiotemporal control of mitochondrial bioenergetics abolishes tumor cell invasion.

Although associated with important tumor traits, including “stemness” (20), malignant regrowth (21), and drug resistance (22), a general role of mitochondria in cancer has been difficult to determine (11). Whether these organelles play a role in tumor cell invasion and, therefore, metastatic competency has been equally controversial, with evidence that mitochondrial respiration is important (23), not important (24), or must be dysfunctional (25) to affect cell movements. Here disabling cellular respiration with depletion of mitochondrial DNA (26) or targeting an oxidative phosphorylation complex(es) (19) prevented

mitochondrial trafficking to the cortical cytoskeleton, abolished membrane dynamics of cell motility, and suppressed cell invasion. Conversely, scavenging of mitochondrial ROS, which are increased in response to PI3K therapy, did not affect organelle dynamics and tumor cell invasion. Together, these data suggest that oxidative phosphorylation contributes to cancer metabolism and provides a “regional” and potent ATP source to fuel highly energy-demanding processes of cell movements and invasion (27).

This “spatiotemporal” model of mitochondrial bioenergetics is reminiscent of the accumulation of mitochondria at subcellular sites of energy-intensive processes in neurons (28), including synapses, active growth cones, and branches (29). Whether the cytoskeletal machinery that transports mitochondria along the microtubule network in neurons (30) is also exploited in cancer (this study) is currently unknown. However, there is evidence that comparable mechanisms of organelle dynamics (31) support mitochondrial redistribution in lymphocytes (32) and may contribute to directional migration of tumor cells (33). Consistent with this model (31), interference with the mitochondrial fusion machinery, namely mitofusins, suppressed mitochondrial

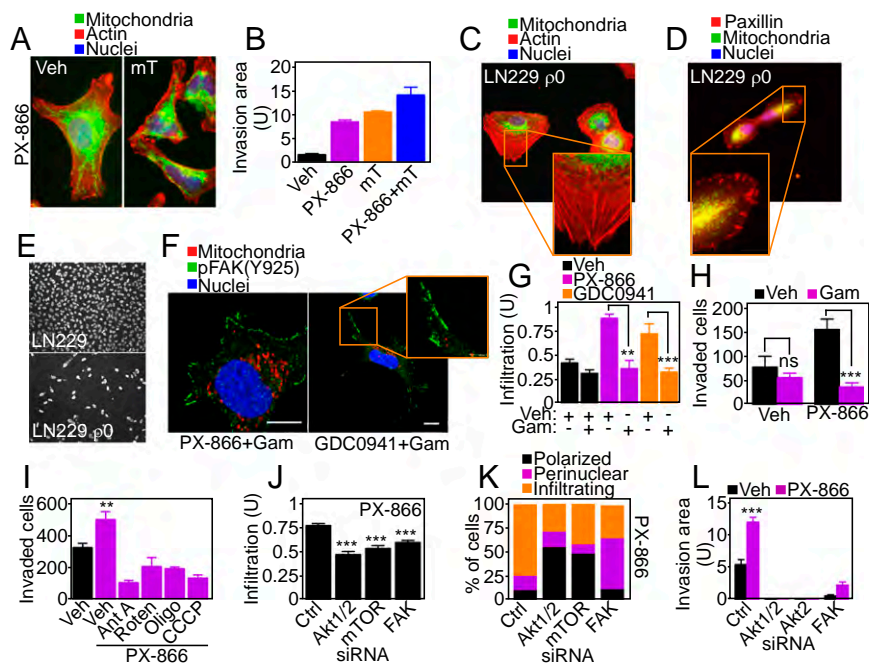


Fig. 4. Control of tumor cell invasion by spatiotemporal mitochondrial bioenergetics. (A) PC3 cells were labeled with MitoTracker Red, phalloidin Alexa488, and DAPI, treated with PX-866, and analyzed for mitochondrial infiltration into the peripheral cytoskeleton in the presence of vehicle or the mitochondrial-targeted ROS scavenger mitoTEMPO (mT; 50 μ M). (B) PC3 cells were incubated with the indicated agents alone or in combination (PX-866+mT) and analyzed for tumor cell invasion across Matrigel. Mean \pm SEM. P (ANOVA) < 0.0001. (C and D) Mitochondrial (mt)DNA-depleted LN229 (ρ 0) cells were stimulated with NIH 3T3 conditioned media for 2 h, labeled with MitoTracker Red, DAPI, and either phalloidin Alexa488 (C) or an antibody to FAK-associated paxillin (D), and analyzed by fluorescence microscopy. Representative pseudocolored images are shown. Magnification, 60 \times . (E) WT or ρ 0 LN229 cells were analyzed for invasion across Matrigel-coated Transwell inserts. Representative images of invasive cells stained with DAPI are shown. Magnification, 20 \times . (F) PC3 cells treated with vehicle or PI3K inhibitors in combination with the mitochondrial-targeted small-molecule Hsp90 inhibitor Gamitrinib (Gam) were labeled with anti-pY925-FAK Alexa488 followed by fluorescence microscopy. Representative 1- μ m extended-focus confocal images are shown. Magnification, 63 \times . (Scale bar, 10 μ m.) (G) PC3 cells treated with vehicle or PI3K inhibitors with or without Gamitrinib (1 μ M) were labeled with MitoTracker Red, phalloidin Alexa488, and DAPI and quantified after 48 h for mitochondrial infiltration into lamellipodia by fluorescence microscopy; n = 48. Mean \pm SEM. ** P = 0.0044; *** P < 0.0009. (H) PC3 cells were treated with vehicle or PX-866 (5 μ M) with or without Gamitrinib and quantified for invasion across Matrigel. Mean \pm SEM of replicates (n = 2). *** P < 0.0001. ns, not significant. (I) PC3 cells were incubated with vehicle or PX-866 alone or in combination with the various mitochondrial respiratory chain inhibitors and analyzed for Matrigel invasion. Ant A, Antimycin A; Oligo, Oligomycin; Roten, Rotenone. Mean \pm SEM. ** P = 0.006. (J) PC3 cells transfected with control siRNA or siRNA to Akt1/2, mTOR, or FAK were labeled as in C, treated with PX-866, and quantified for mitochondrial infiltration into lamellipodia; n = 44. Mean \pm SEM. *** P < 0.0001. (K) siRNA-transfected PC3 cells labeled as in C were treated with PX-866 (5 μ M) and analyzed for mitochondrial morphology (polarized, perinuclear, infiltrating) by fluorescence microscopy; n = 21. (L) PC3 cells transfected with the indicated siRNAs were quantified for invasion across Matrigel in the presence of vehicle or PX-866. Mean \pm SEM (n = 4). *** P < 0.0001.

repositioning to the cortical cytoskeleton and tumor cell invasion mediated by PI3K therapy.

In addition to oxidative phosphorylation, Akt/mTOR signaling was identified here as a key regulator of mitochondrial trafficking and tumor cell invasion. This is consistent with a pivotal role of PI3K in directional cell movements (34), supporting chemotaxis at the leading edge of migration (35) and Rac1 activation (36). A third signaling requirement of this pathway involved FAK activity (18), which has also been implicated in cytoskeletal dynamics (37).

Despite hopes for “personalized” medicine (4), small-molecule PI3K inhibitors have produced modest and short-lived patient responses in the clinic (5). Our data suggest that these agents potentially activate global adaptive mechanisms in tumors (7), unexpectedly centered on mitochondrial reprogramming in cell survival/bioenergetics (9) and subcellular trafficking (this study). In this context, the increased tumor cell motility and invasion stimulated by PI3K inhibitors may create an “escape” mechanism for tumor cells to elude therapy-induced environmental stress, reminiscent of the heightened metastatic propensity associated with other unfavorable conditions of hypoxia (38), acidosis (39), and antiangiogenic therapy (40, 41). Although this adaptive response to PI3K therapy may paradoxically promote more aggressive tumor traits and further compromise clinical

outcomes, disabling mitochondrial adaptation is feasible (19) and may provide a viable strategy to increase the anticancer efficacy of PI3K antagonists in the clinic.

Methods

Two-Dimensional Chemotaxis. Cells were treated with PI3K inhibitors for 48 h and seeded in 2D chemotaxis chambers (Ibidi) in 10% (vol/vol) FBS medium. After a 6-h attachment, cells were washed and the reservoirs were filled with 0.1% BSA/RPMI, followed by gradient setup by addition of NIH 3T3 conditioned medium. Video microscopy was performed over 8 h, with a time-lapse interval of 10 min. At least 30 cells were tracked using the WimTaxis module (Wimasis), and the tracking data were exported into Chemotaxis and Migration Tool v2.0 (Ibidi) for graphing and statistical testing. Experiments were repeated twice (n = 3).

FA Dynamics. Cells growing in high-optical-quality 96-well μ -plates (Ibidi) were transduced with Talin-GFP BacMam virus (50 particles per cell) for 18 h and imaged with a 40 \times objective on a Nikon TE300 inverted time-lapse microscope equipped with a video system containing an Evolution QEi camera and a time-lapse video cassette recorder. The atmosphere was equilibrated to 37 $^{\circ}$ C and 5% CO₂ in an incubation chamber. Time-lapse fluorescence microscopy was carried out for the indicated times at 1 min per frame. Sequences were aligned in Image-Pro Plus 7 (Media Cybernetics) and imported into ImageJ (NIH) for further analysis. The initial and final frames were duplicated and assembled as composite images. FA complexes were manually counted and classified according to presence in some or all of the

time frames: decaying, newly formed, stable sliding (FA moves to a different position over time), and stable mature (merged areas). The rate of decay and assembly of FA complexes was calculated for each cell as the number of FA complexes changing per h. At least 400 FA complexes from 10 cells were analyzed from 5 independent time lapses per condition.

Tumor Cell Invasion. Experiments were carried out essentially as described (42). Briefly, 8- μ m PET Transwell migration chambers (Corning) were coated with 150 μ L 80 μ g/mL Matrigel (Becton Dickinson). Tumor cells were seeded in duplicates onto the coated Transwell filters at a density of 1.25×10^5 cells per well in media containing 2% (vol/vol) FCS (FCII; HyClone), and media containing 20% (vol/vol) FCS were placed in the lower chamber as chemo-attractant. Cells were allowed to invade and adhere to the bottom of the plate, stained in 0.5% crystal violet/methanol for 10 min, rinsed in tap water, and analyzed by bright-field microscopy. Digital images were batch-imported into ImageJ, thresholded, and analyzed with the Analyze Particles function. For analysis of tumor cell invasion in 3D spheroids, tissue culture-treated 96-well plates were coated with 50 μ L 1% Difco Agar Noble (Becton Dickinson). LN229 cells were seeded at 5,000 cells per well and allowed to form spheroids over 72 h. Spheroids were harvested, treated with PX-866 (0–10 μ M), and placed in a collagen plug containing Eagle's minimum essential medium (EMEM), FBS, L-glutamine, sodium bicarbonate, and collagen type I (Gibco; 1.5 mg/mL). The collagen plug was allowed to set and 1 mL DMEM with 5% (vol/vol) FBS was added to the top of the plug. Cell invasion was analyzed every 24 h and quantified using Image-Pro Plus 7, as described (42).

Patient Samples. For studies using human samples, informed consent was obtained from all patients enrolled, and the study was approved by an Institutional Review Board of the Fondazione IRCCS Ca' Granda. The clinicopathological features of GBM patients used in this study are summarized in Table S1.

Statistical Analysis. Data were analyzed using either two-sided unpaired *t* test (for two-group comparisons) or one-way ANOVA test with Dunnett's multiple comparison posttest (for more than two-group comparisons) using a GraphPad software package (Prism 6.0) for Windows. Data are expressed as mean \pm SD or mean \pm SEM of multiple independent experiments. A *P* value of <0.05 was considered statistically significant.

ACKNOWLEDGMENTS. We thank James Hayden and Frederick Keeney of the Wistar Imaging Facility for outstanding help with time-lapse imaging. This work was supported by National Institutes of Health Grants P01 CA140043 (to D.C.A. and L.R.L.), R01 CA78810 and CA190027 (to D.C.A.), F32 CA177018 (to M.C.C.), and R01 CA089720 (to L.R.L.), the Office of the Assistant Secretary of Defense for Health Affairs through the Prostate Cancer Research Program under Award W81XWH-13-1-0193 (to D.C.A.), and a Joint Grant in Molecular Medicine 2013 from Fondazione IRCCS Ca' Granda and Istituto Nazionale Genetica Molecolare (to V.V.). Support for the core facilities used in this study was provided by Cancer Center Support Grant CA010815 to The Wistar Institute.

- Engelman JA, Luo J, Cantley LC (2006) The evolution of phosphatidylinositol 3-kinases as regulators of growth and metabolism. *Nat Rev Genet* 7(8):606–619.
- Manning BD, Cantley LC (2007) AKT/PKB signaling: Navigating downstream. *Cell* 129(7):1261–1274.
- Vivanco I, Sawyers CL (2002) The phosphatidylinositol 3-kinase AKT pathway in human cancer. *Nat Rev Cancer* 2(7):489–501.
- Rodon J, Dienstmann R, Serra V, Tabernero J (2013) Development of PI3K inhibitors: Lessons learned from early clinical trials. *Nat Rev Clin Oncol* 10(3):143–153.
- Fruman DA, Rommel C (2014) PI3K and cancer: Lessons, challenges and opportunities. *Nat Rev Drug Discov* 13(2):140–156.
- Jänne PA, Gray N, Settleman J (2009) Factors underlying sensitivity of cancers to small-molecule kinase inhibitors. *Nat Rev Drug Discov* 8(9):709–723.
- Cohen AA, et al. (2008) Dynamic proteomics of individual cancer cells in response to a drug. *Science* 322(5907):1511–1516.
- Chakrabarty A, Sánchez V, Kuba MG, Rinehart C, Arteaga CL (2012) Feedback upregulation of HER3 (ErbB3) expression and activity attenuates antitumor effect of PI3K inhibitors. *Proc Natl Acad Sci USA* 109(8):2718–2723.
- Ghosh JC, et al. (2015) Adaptive mitochondrial reprogramming and resistance to PI3K therapy. *J Natl Cancer Inst* 107(3):dju502.
- Ward PS, Thompson CB (2012) Metabolic reprogramming: A cancer hallmark even Warburg did not anticipate. *Cancer Cell* 21(3):297–308.
- Wallace DC (2012) Mitochondria and cancer. *Nat Rev Cancer* 12(10):685–698.
- Frezza C, et al. (2011) Haem oxygenase is synthetically lethal with the tumour suppressor fumarate hydratase. *Nature* 477(7363):225–228.
- Vaira V, et al. (2010) Preclinical model of organotypic culture for pharmacodynamic profiling of human tumors. *Proc Natl Acad Sci USA* 107(18):8352–8356.
- Roussos ET, Condeelis JS, Patsialou A (2011) Chemotaxis in cancer. *Nat Rev Cancer* 11(8):573–587.
- Hinz B, Alt W, Johnen C, Herzog V, Kaiser H-W (1999) Quantifying lamella dynamics of cultured cells by SACED, a new computer-assisted motion analysis. *Exp Cell Res* 251(1):234–243.
- Petrie RJ, Doyle AD, Yamada KM (2009) Random versus directionally persistent cell migration. *Nat Rev Mol Cell Biol* 10(8):538–549.
- Youle RJ, van der Blik AM (2012) Mitochondrial fission, fusion, and stress. *Science* 337(6098):1062–1065.
- Sulzmaier FJ, Jean C, Schlaepfer DD (2014) FAK in cancer: Mechanistic findings and clinical applications. *Nat Rev Cancer* 14(9):598–610.
- Chae YC, et al. (2013) Landscape of the mitochondrial Hsp90 metabolome in tumours. *Nat Commun* 4:2139.
- Janiszevska M, et al. (2012) Imp2 controls oxidative phosphorylation and is crucial for preserving glioblastoma cancer stem cells. *Genes Dev* 26(17):1926–1944.
- Viale A, et al. (2014) Oncogene ablation-resistant pancreatic cancer cells depend on mitochondrial function. *Nature* 514(7524):628–632.
- Haq R, et al. (2013) Oncogenic BRAF regulates oxidative metabolism via PGC1 α and MITF. *Cancer Cell* 23(3):302–315.
- LeBleu VS, et al. (2014) PGC-1 α mediates mitochondrial biogenesis and oxidative phosphorylation in cancer cells to promote metastasis. *Nat Cell Biol* 16(10):992–1003.
- Shiraishi T, et al. (2015) Glycolysis is the primary bioenergetic pathway for cell motility and cytoskeletal remodeling in human prostate and breast cancer cells. *Oncotarget* 6(1):130–143.
- Porporato PE, et al. (2014) A mitochondrial switch promotes tumor metastasis. *Cell Reports* 8(3):754–766.
- Olgun A, Akman S (2007) Mitochondrial DNA-deficient models and aging. *Ann N Y Acad Sci* 1100:241–245.
- De Bock K, et al. (2013) Role of PFKFB3-driven glycolysis in vessel sprouting. *Cell* 154(3):651–663.
- Lee CW, Peng HB (2006) Mitochondrial clustering at the vertebrate neuromuscular junction during presynaptic differentiation. *J Neurobiol* 66(6):522–536.
- Saxton WM, Hollenbeck PJ (2012) The axonal transport of mitochondria. *J Cell Sci* 125(Pt 9):2095–2104.
- Birsa N, Norkett R, Higgs N, Lopez-Domench G, Kittler JT (2013) Mitochondrial trafficking in neurons and the role of the Miro family of GTPase proteins. *Biochem Soc Trans* 41(6):1525–1531.
- Zhao J, et al. (2013) Mitochondrial dynamics regulates migration and invasion of breast cancer cells. *Oncogene* 32(40):4814–4824.
- Morlino G, et al. (2014) Miro-1 links mitochondria and microtubule dynein motors to control lymphocyte migration and polarity. *Mol Cell Biol* 34(8):1412–1426.
- Desai SP, Bhatia SN, Toner M, Irimia D (2013) Mitochondrial localization and the persistent migration of epithelial cancer cells. *Biophys J* 104(9):2077–2088.
- Kölsch V, Charest PG, Firtel RA (2008) The regulation of cell motility and chemotaxis by phospholipid signaling. *J Cell Sci* 121(Pt 5):551–559.
- Weiger MC, et al. (2009) Spontaneous phosphoinositide 3-kinase signaling dynamics drive spreading and random migration of fibroblasts. *J Cell Sci* 122(Pt 3):313–323.
- Kraynov VS, et al. (2000) Localized Rac activation dynamics visualized in living cells. *Science* 290(5490):333–337.
- Fabry B, Klemm AH, Kienle S, Schäffer TE, Goldmann WH (2011) Focal adhesion kinase stabilizes the cytoskeleton. *Biophys J* 101(9):2131–2138.
- Pennacchiotti S, et al. (2003) Hypoxia promotes invasive growth by transcriptional activation of the met protooncogene. *Cancer Cell* 3(4):347–361.
- Gatenby RA, Gillies RJ (2004) Why do cancers have high aerobic glycolysis? *Nat Rev Cancer* 4(11):891–899.
- Ebos JM, et al. (2009) Accelerated metastasis after short-term treatment with a potent inhibitor of tumor angiogenesis. *Cancer Cell* 15(3):232–239.
- Pàez-Ribes M, et al. (2009) Antiangiogenic therapy elicits malignant progression of tumors to increased local invasion and distant metastasis. *Cancer Cell* 15(3):220–231.
- Caino MC, et al. (2013) Metabolic stress regulates cytoskeletal dynamics and metastasis of cancer cells. *J Clin Invest* 123(7):2907–2920.
- Kang BH, et al. (2009) Combinatorial drug design targeting multiple cancer signaling networks controlled by mitochondrial Hsp90. *J Clin Invest* 119(3):454–464.
- Ortensi B, et al. (2012) Rai is a new regulator of neural progenitor migration and glioblastoma invasion. *Stem Cells* 30(5):817–832.
- Vaira V, et al. (2012) miR-296 regulation of a cell polarity-cell plasticity module controls tumor progression. *Oncogene* 31(1):27–38.
- Livak KJ, Schmittgen TD (2001) Analysis of relative gene expression data using real-time quantitative PCR and the 2- $\Delta\Delta$ CT method. *Methods* 25(4):402–408.
- Benjamini Y, Hochberg Y (1995) Controlling the false discovery rate: A practical and powerful approach to multiple testing. *J R Stat Soc Series B Stat Methodol* 57(1):289–300.
- Louis DN, et al. (2007) The 2007 WHO classification of tumors of the central nervous system. *Acta Neuropathol* 114(2):97–109.

CANCER

Survivin promotes oxidative phosphorylation, subcellular mitochondrial repositioning, and tumor cell invasion

Dayana B. Rivadeneira,^{1,2} M. Cecilia Caino,^{1,2} Jae Ho Seo,^{1,2} Alessia Angelin,³ Douglas C. Wallace,³ Lucia R. Languino,⁴ Dario C. Altieri^{1,2*}

Survivin promotes cell division and suppresses apoptosis in many human cancers, and increased abundance correlates with metastasis and poor prognosis. We showed that a pool of survivin that localized to the mitochondria of certain tumor cell lines enhanced the stability of oxidative phosphorylation complex II, which promoted cellular respiration. Survivin also supported the subcellular trafficking of mitochondria to the cortical cytoskeleton of tumor cells, which was associated with increased membrane ruffling, increased focal adhesion complex turnover, and increased tumor cell migration and invasion in cultured cells, and enhanced metastatic dissemination *in vivo*. Therefore, we found that mitochondrial respiration enhanced by survivin contributes to cancer metabolism, and relocalized mitochondria may provide a “regional” energy source to fuel tumor cell invasion and metastasis.

INTRODUCTION

The inhibitor of apoptosis (IAP) family member survivin functions in multiple mechanisms, including chromosomal segregation, microtubule dynamics, apoptosis resistance, and cellular stress responses (1). The transcription of the gene encoding survivin is greater in tumors than in normal tissues, and the presence of survivin in cancer has been linked to metastatic disease (2), but the underlying mechanism(s) has not been clearly defined. In tumors, a pool of survivin localizes to the mitochondria (3), where it promotes resistance to apoptosis (4) and influences organelle bioenergetics (5), thus acting as a potential cancer driver.

Although indispensable for normal tissue and organ bioenergetics, the role of mitochondria in cancer has been debated (6). Most tumors rewire their energy sources toward aerobic glycolysis at the expense of mitochondrial respiration (7), the so-called Warburg effect (8), a process that is important for disease progression (9). Further, mutations in oxidative phosphorylation genes produce “oncometabolites” (10) or stabilize oncogenes, such as HIF1 α (11), suggesting that mitochondrial respiration may have limited roles in cancer bioenergetics (12), and, at least in some cases, actually function as a “tumor suppressor” (13).

Conversely, there is evidence that oxidative phosphorylation remains an important source of ATP (adenosine 5'-triphosphate) for many tumors (14) and may affect important cancer traits, such as “stemness” (15), tumor repopulation after oncogene ablation (16), and resistance to therapy (17). Whether there are cancer-specific regulators of mitochondrial respiration is presently unknown, but protein folding quality control within the unique anatomy of mitochondria (18) is required to buffer the risk of proteotoxic stress (19), and provides a key requirement for oxidative phosphorylation in tumors (20). Mechanistically, this involves the chaperone activity of heat shock protein 90 (Hsp90) family proteins, which accumulate in tumor mitochondria compared to normal tissues (21), and maintain the stability

and folding of multiple bioenergetics effectors, including succinate dehydrogenase (SDH), an iron- and sulfur-containing subunit of oxidative phosphorylation Complex II (22). Here, we explored a link between mitochondrial survivin, tumor metabolic reprogramming, and metastatic competency.

RESULTS

Survivin-mediated regulation of tumor bioenergetics

We began this study by examining the distribution of mitochondrial survivin in androgen-independent prostate cancer PC3 cells (3). Analysis of sub-mitochondrial fractions revealed that survivin localized to the inner membrane and matrix, but not to outer membrane or intermembrane space (fig. S1A). With this topography, survivin colocalized with effectors of mitochondrial protein folding, including the AAA+ matrix protease CLPP and the molecular chaperones Hsp90 and TRAP-1 [tumor necrosis factor receptor (TNFR)-associated protein 1] (fig. S1A) (23).

Transfection of PC3 cells with a previously characterized small interfering RNA (siRNA) directed against survivin (24) efficiently depleted the mitochondrial pool of survivin (fig. S1B). In addition, treatment of PC3 cells with YM155, a small-molecule survivin “suppressant” currently in clinical trials (2), also abrogated the mitochondrial pool of survivin (fig. S1C). At the low concentrations of YM155 used and short incubation times, survivin targeting did not affect mitochondrial membrane potential (fig. S1D), nuclear morphology (fig. S1E), or cell cycle transitions (fig. S1F), and only modestly reduced cell proliferation (fig. S1G).

To determine whether mitochondrial survivin affected bioenergetics, we next profiled the metabolome of PC3 cells transfected with control or survivin-directed siRNA. Survivin silencing induced defective mitochondrial bioenergetics, with increased concentrations of various oxidative phosphorylation metabolites, including succinate and pyruvate, and a trend of increased α -ketoglutarate concentrations, associated with a substantial depletion of glutamine (Fig. 1, A and B, and table S1), suggestive of compensatory glutaminolysis. Although increased succinate has been linked to a tumorigenic, “pseudohypoxic” state (6), survivin knockdown did not affect HIF1 α protein abundance (fig. S1H), which mediates transcriptional responses to hypoxia (11). Consistent with impaired mitochondrial

¹Prostate Cancer Discovery and Development Program, The Wistar Institute, Philadelphia, PA 19104, USA. ²Tumor Microenvironment and Metastasis Program, The Wistar Institute, Philadelphia, PA 19104, USA. ³Center for Mitochondrial and Epigenomic Medicine, The Children's Hospital of Philadelphia, Philadelphia, PA 19104, USA. ⁴Department of Cancer Biology, Sidney Kimmel Cancer Center, Thomas Jefferson University, Philadelphia, PA 19107, USA.

*Corresponding author. E-mail: daltieri@wistar.org

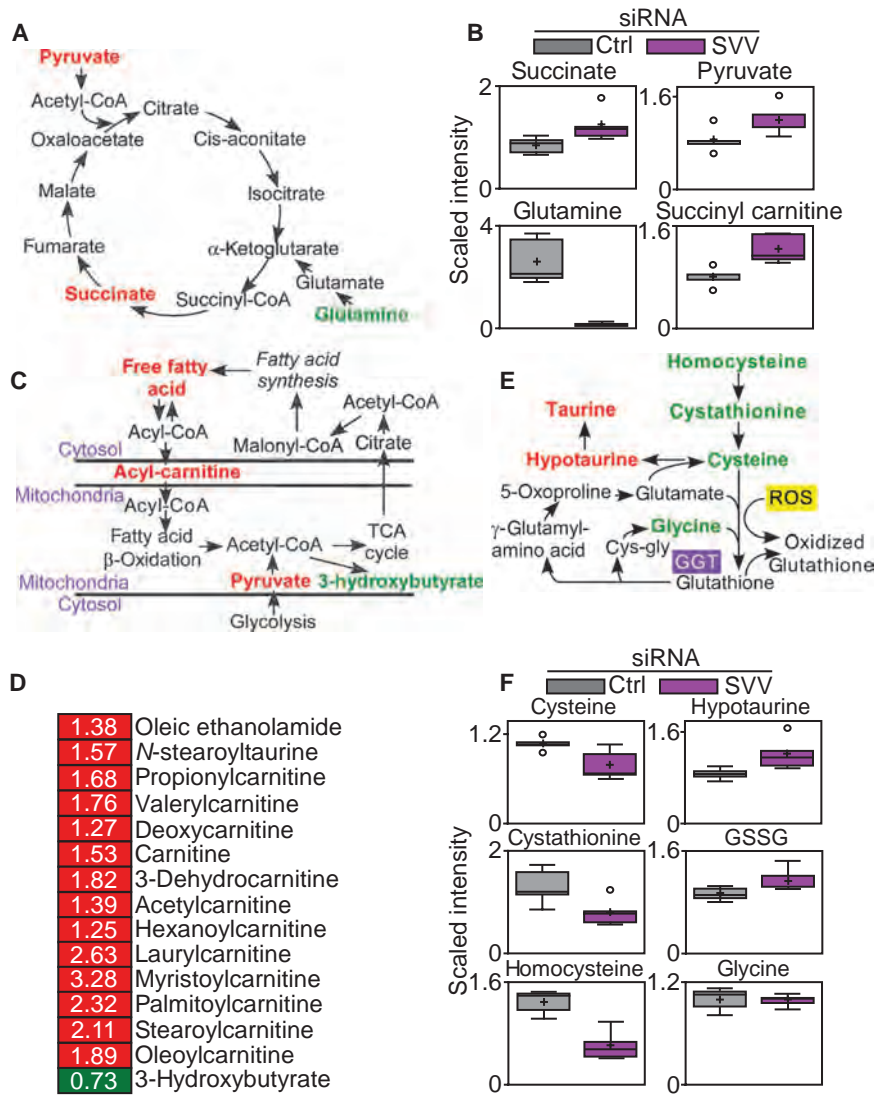


Fig. 1. Survivin targeting impairs mitochondrial metabolism. (A to F) Global metabolomics screening of PC3 cells transfected with control or survivin-directed (SVV) siRNA ($n = 5$ biological replicates; see also table S1). Changes in the concentrations of metabolites implicated in oxidative phosphorylation (A and B), fatty acid β oxidation (C and D), or glutathione metabolism (E and F) are shown. For the heat map (D), red indicates increased concentration, and green indicates decreased concentration. Only significant changes ($P < 0.05$) are shown. For box plots (B and F), relative metabolite abundance is represented. The limit of upper and lower quartiles, median values (straight line), and maximum and minimum distribution are shown. Cross, mean value; circle, extreme data point; Ctrl, control.

bioenergetics, survivin-silenced cells accumulated certain species of long-chain fatty acids (Fig. 1C and table S1), with increased concentrations of several carnitine-conjugated lipids involved in fatty acid import into mitochondria, and reduced concentrations of the ketone body 3-hydroxybutyrate (Fig. 1D and table S1). In addition, survivin depletion in PC3 cells decreased the concentrations of homocysteine, cystathionine, and glycine, all of which are implicated in redox mechanisms (Fig. 1, E and F, and table S1); reduced isoleucine and leucine, which are involved in the metabolism of branched-chain amino acids (fig. S1I and table S1); and reduced aspartate, ornithine, and putrescine concentrations and a

trend of decreased concentrations of proline, which are implicated in arginine metabolism (fig. S1J and table S1).

Modulation of oxidative phosphorylation by mitochondrial survivin

Consistent with the metabolomics data, siRNA-mediated silencing of survivin in prostate adenocarcinoma PC3 or DU145, or glioblastoma LN229 cells decreased oxygen (O_2) consumption (Fig. 2A), and oxygen consumption rates as assessed by real-time analysis of cellular respiration (Fig. 2B and fig. S2A). Targeting survivin with YM155 comparably suppressed O_2 consumption in PC3 cells (Fig. 2C). Impaired bioenergetics in survivin-targeted PC3 cells correlated with reduced production of ATP, compared to control cultures (Fig. 2D). Silencing of survivin with an independent, previously characterized siRNA sequence (24) (fig. S2C) also inhibited ATP production (Fig. 2E).

To examine the specificity of these findings, we next reconstituted PC3 cells silenced for endogenous survivin by siRNA with a mitochondrial-targeted survivin variant (3) that accumulates in mitochondria (fig. S2D) and localizes to the inner membrane and matrix in a similar manner to endogenous survivin (fig. S2E). Reconstitution of survivin-silenced PC3 cells with mitochondrial-targeted survivin (fig. S2F) restored ATP production to that of control cultures (Fig. 2F). Similarly, transfection of mitochondrial-targeted survivin increased ATP production in breast adenocarcinoma MCF-7 cells (fig. S2G) as well as rat insulinoma INS-1 cells (fig. S2H) that lack mitochondrial survivin (3). Furthermore, reconstitution of survivin-depleted PC3 cells with adenovirus (pAd) encoding mitochondrial-targeted survivin (3) (pAd-mt-SVV) stimulated O_2 consumption (Fig. 2G). In contrast, PC3 cells transfected with nontargeting siRNA and reconstituted with pAd-mt-survivin or pAd-mt-GFP [pAd-mitochondrial-targeted green fluorescent protein (GFP)] had comparable O_2 consumption (Fig. 2G). Accordingly, recombinant survivin accumulated to a greater extent in mitochondrial fractions compared to cytosol of PC3 cells (fig. S2I). Functionally, accumulation of mitochondrial survivin in MCF-7 or INS-1 cells did not change cell cycle transitions as assessed by propidium iodide staining (fig. S2J) or cell proliferation as assessed by BrdU (5-bromo-2'-deoxyuridine) incorporation (fig. S2, K and L).

Consistent with impaired mitochondrial bioenergetics, siRNA (Fig. 2H) or YM155 (Fig. 2I) targeting of survivin induced hallmarks of cellular starvation, including increased phosphorylation of the energy sensor AMP (adenosine 5'-monophosphate)-activated kinase (AMPK), induction of autophagy as assessed by microtubule-associated light chain 3 (LC3) conversion (Fig. 2H), and the appearance of punctate GFP-LC3 fluorescence corresponding to autophagosome formation (Fig. 2J). The response to YM155 was accompanied by decreased mammalian target of rapamycin (mTOR) signaling, as indicated by reduced phosphorylation of the downstream effectors 4EBP1 and p70S6 kinase (Fig. 2K).

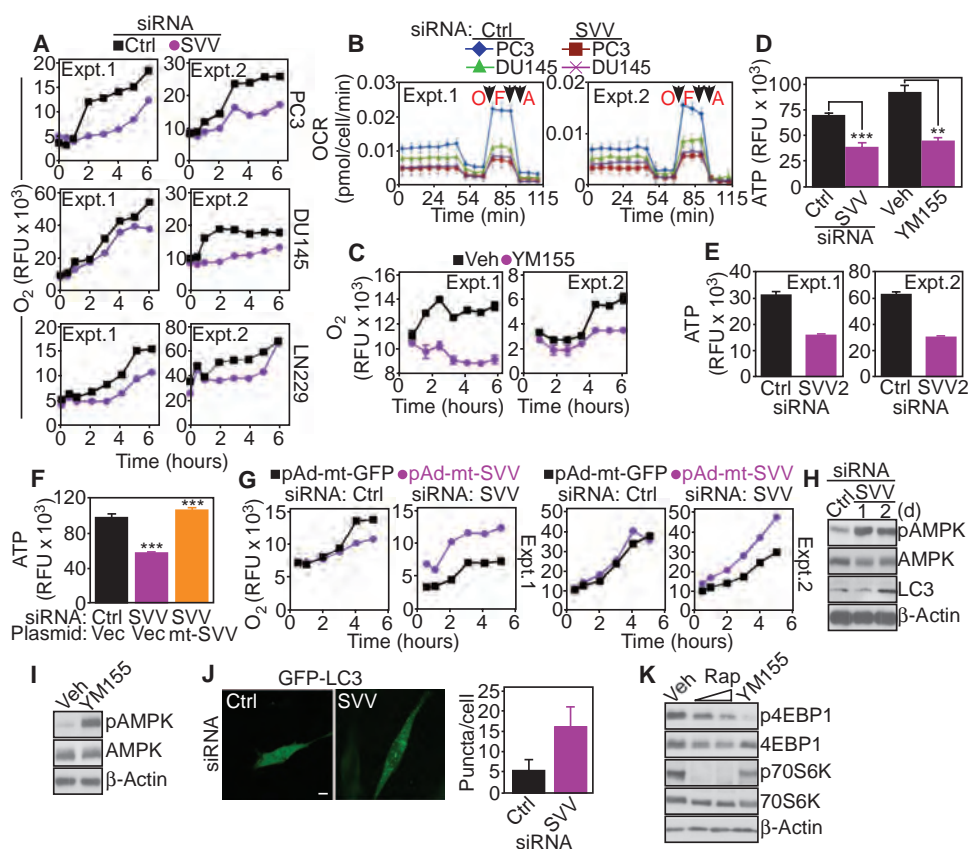


Fig. 2. Survivin regulation of mitochondrial bioenergetics. (A) Prostate cancer cell lines PC3 or DU145 or glioblastoma LN229 cells transfected with control (Ctrl) or survivin (SVV)-directed siRNA were analyzed for oxygen (O_2) consumption. RFU, relative fluorescence units. The results of two independent experiments are shown. (B) siRNA-silenced cells as in (A) were analyzed for O_2 consumption rates (OCR) under basal conditions or in response to oligomycin (O), FCCP (F), or antimycin (A). Arrows indicate time of drug addition. Extramitochondrial respiration after addition of antimycin was subtracted as background. The profiles of two independent experiments (Expt.) are shown. (C) PC3 cells were treated with vehicle (Veh) or small-molecule survivin suppressant YM155 and analyzed for O_2 consumption. Two independent experiments (Expt.) are shown. (D) PC3 cells transfected with the indicated siRNA or treated with vehicle (Veh) or YM155 were analyzed for ATP production. Graph shows means \pm SEM from three independent experiments. *** $P < 0.0001$; ** $P = 0.0011$. (E) PC3 cells transfected with control siRNA (Ctrl) or a second independent siRNA to survivin (SVV2) were analyzed for ATP production. Two independent experiments (Expt.) are shown. (F) PC3 cells transfected with control (Ctrl) or survivin-directed siRNA were reconstituted with vector or mitochondrial-targeted survivin cDNA and analyzed for ATP production. Graph shows means \pm SEM from three independent experiments. *** $P < 0.0001$. (G) PC3 cells were transfected with control siRNA (Ctrl) or survivin-directed siRNA, reconstituted with pAd-mt-GFP or pAd-mt-SVV, and analyzed for O_2 consumption. Two independent experiments (Expt.) are shown. (H and I) PC3 cells transfected with control or survivin-directed siRNA (H) or treated with vehicle or YM155 (I) were analyzed by Western blotting. d, days; p, phosphorylated. Blots are representative of two independent experiments. (J) PC3 cells transfected with control (Ctrl) or survivin (SVV)-directed siRNA plus GFP-LC3 were analyzed by fluorescence microscopy. Right: The number of GFP-LC3 puncta (autophagosomes) per cell was quantified ($n = 50$ cells imaged per transfection condition in two independent experiments). Scale bar, 10 μ m. (K) PC3 cells treated with vehicle (Veh), rapamycin (Rap), or YM155 were analyzed by Western blotting after 24 hours. p, phosphorylated. Blots are representative of two independent experiments.

Survivin-mediated regulation of mitochondrial oxidative phosphorylation complex II

We next examined the role of survivin on the function of individual oxidative phosphorylation complexes. High-resolution respirometry of permeabilized PC3 cells showed that targeting survivin with YM155 inhibited the activities of complex II (Fig. 3A) and complex I (fig. S3A), but not that of complex III (fig. S3B). Similarly, immunocaptured complex II from PC3 cells silenced for endogenous survivin by siRNA (Fig. 3B) showed reduced SDH activity (Fig. 3C), whereas citrate synthase or complex I activity was not affected (fig. S3C).

Next, we asked how survivin affected mitochondrial complex II activity. PC3 cells exposed to YM155 exhibited time-dependent degradation of complex II-associated proteins, but not of other mitochondrial phosphorylation complexes (Fig. 3D), a response that involved the SDHB and SDHC subunits of complex II, but not the SDHA subunit (Fig. 3E). Conversely, transfection of mitochondrial-targeted survivin in survivin-silenced PC3 cells was sufficient to increase the abundance of SDHB and SDHC subunits, but not that of SDHA subunit (Fig. 3F). To determine whether changes in SDH abundance reflected protein (mis) folding, we next quantified the amount of complex II proteins that remained insoluble over a broad range of detergent concentrations. Survivin silencing in PC3 cells increased the amount of detergent-insoluble complex II proteins, compared to control transfectants (fig. S3D), suggestive of protein misfolding. Complex V abundance was also modestly reduced, whereas the abundance of complex I, III, or IV was not affected (fig. S3D). In terms of individual subunits, loss of survivin increased the detergent insolubility of SDHB and SDHC, but not that of SDHA (Fig. 3G and fig. S3D).

Complex II–SDHB protein folding requires the mitochondrial chaperone Hsp90 and its homolog TRAP-1 (22). In co-immunoprecipitation experiments from mitochondrial extracts, survivin formed a complex with TRAP-1 (Fig. 3H). Similarly, recombinant survivin bound to glutathione *S*-transferase (GST)–TRAP-1, but not to GST, in pull-down experiments *in vitro*, indicating that this interaction was direct (Fig. 3I). Survivin immune complexes also contained the complex II subunits SDHA and SDHB (Fig. 3J). Silencing of TRAP-1 by siRNA (Fig. 3K) or inhibiting its chaperone activity with the mitochondrial-targeted

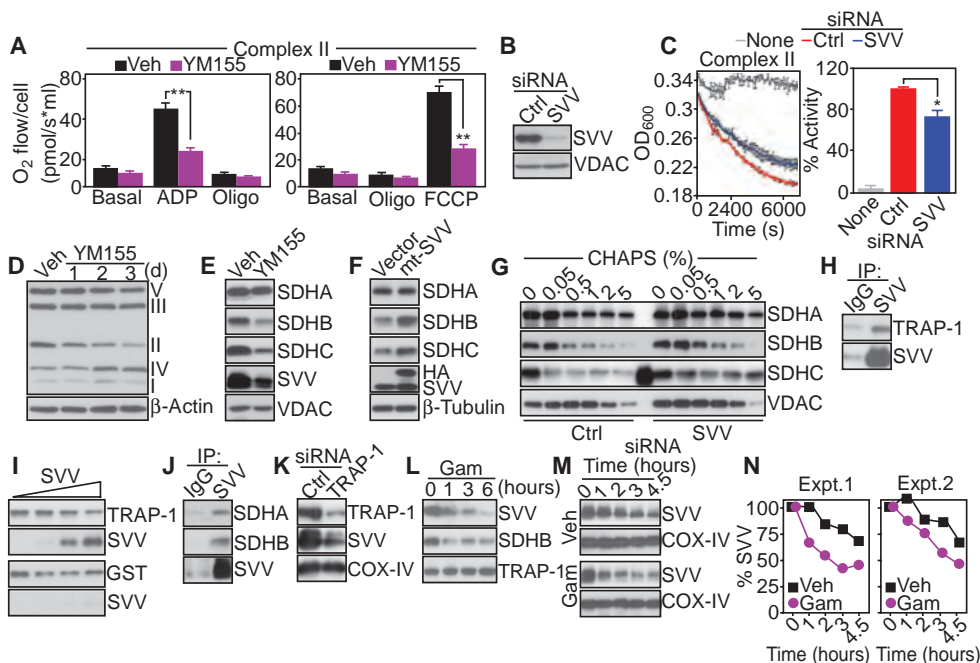


Fig. 3. Survivin regulation of mitochondrial complex II. (A) PC3 cells treated with vehicle (Veh) or YM155 were permeabilized with digitonin and analyzed for complex II activity in the presence of succinate and rotenone. Oligo, oligomycin. Graphs shows means \pm SEM from three independent experiments. $**P < 0.01$. (B) PC3 cells transfected with control (Ctrl) or survivin (SVV)-directed siRNA were analyzed by Western blotting. Blots are representative of two independent experiments. (C) Mitochondrial complex II was immunoprecipitated from siRNA-transfected PC3 cells as in (B) and analyzed for enzymatic activity. Right: Quantification. Graph shows means \pm SEM from three independent experiments. $*P = 0.037$. (D) Mitochondria from PC3 cells treated with vehicle (Veh) or YM155 were analyzed by Western blotting. The position of oxidative phosphorylation complex subunits is indicated. d, days. Blots are representative of two independent experiments. (E and F) PC3 cells treated with vehicle (Veh) or YM155 (E), or MCF-7 cells transfected with vector or mitochondrial-targeted survivin (mt-SVV) cDNA (F) were analyzed by Western blotting. In (F), the position of endogenous (SVV) or transfected (HA) survivin is indicated. Blots in (E) and (F) are representative of two independent experiments. (G) PC3 cells were transfected with the indicated siRNAs, and proteins remaining insoluble at increasing detergent concentrations (CHAPS) were analyzed by Western blotting. The extra band in the SDHC lane corresponds to nonspecific reactivity with a molecular weight marker. Blots are representative of two independent experiments. (H) Mitochondrial extracts from PC3 cells were immunoprecipitated (IP) with immunoglobulin G (IgG) or an antibody to survivin, and pellets were analyzed by Western blotting. Blots are representative of two independent experiments. (I) Aliquots of GST-TRAP-1 (top) or GST (bottom) were incubated with recombinant survivin (SVV), and bound proteins were analyzed by Western blotting. The molar ratio of survivin to TRAP-1 was 0, 0.1, 0.5, and 1. Blots are representative of two independent experiments. (J) PC3 mitochondrial extracts were immunoprecipitated (IP) with IgG or an antibody to survivin, and pellets were analyzed by Western blotting. Blots are representative of two independent experiments. (K and L) PC3 cells were transfected with control (Ctrl) or TRAP-1-directed siRNA (K), or treated with mitochondrial-targeted small-molecule Hsp90 inhibitor, gamitrinib (Gam) (L), and extracts were analyzed after 48 hours (K) or at the indicated time intervals (L) by Western blotting. Blots are representative of two independent experiments for (K) and (L). (M and N) PC3 cells were treated with vehicle (Veh) or gamitrinib (Gam), then cycloheximide, and analyzed by Western blotting (M), with quantification of survivin half-life by densitometry (N). The quantification from two independent experiments (Expt.) is shown.

small-molecule ATPase (adenosine triphosphatase) antagonist gamitrinib (20) (Fig. 3L) induced time-dependent degradation of mitochondrial survivin. Accordingly, gamitrinib treatment shortened the half-life of mitochondrial survivin from >4.5 hours to about 2.4 hours (Fig. 3, M and N), suggesting that survivin is a “client protein” of TRAP-1 in mitochondria. Consistent with chaperone-dependent SDHB folding (22), gamitrinib decreased SDHB abundance in

PC3 cells (Fig. 3L). In contrast, recombinant survivin did not affect TRAP-1 ATPase activity in vitro (fig. S3F).

Association between survivin-mediated regulation of bioenergetics and subcellular mitochondrial trafficking

Next, we asked whether survivin-directed bioenergetics affected tumor cell behavior. We found that chemotactic stimuli changed the morphology of mitochondria in PC3 cells, with the appearance of elongated organelles that infiltrated regions of the cortical cytoskeleton, close to membrane protrusions that participate in cell motility (Fig. 4A and fig. S4A). In contrast, YM155 inhibited the subcellular trafficking of mitochondria (Fig. 4A and fig. S4A) and depleted the number of mitochondria associated with the cortical cytoskeleton after chemoattractant stimulation (Fig. 4C) without affecting total mitochondrial content (Fig. 4D). Reciprocally, transfection of MCF-7 cells with mitochondrial-targeted survivin cDNA (complementary DNA) increased the localization of elongated mitochondria to paxillin-positive regions of the cortical cytoskeleton (Fig. 4, E and F) corresponding to focal adhesion complexes (25), compared to control transfectants.

Next, we looked at the requirements of mitochondrial trafficking to the cortical cytoskeleton in PC3 cells. Dissipation of mitochondrial membrane potential with carbonyl cyanide *m*-chlorophenylhydrazone (CCCP; Fig. 4G), inhibition of complex II activity with the small-molecule SDHB antagonist thenoyltrifluoroacetone (TTFA) (22) (Fig. 4H), or induction of SDHB degradation by gamitrinib (22) (Fig. 4I) suppressed mitochondrial trafficking to the cortical cytoskeleton (Fig. 4, G and H). These responses were associated with a reduction in mitochondrial content (Fig. 4K), potentially reflecting organelle fragmentation (fig. S4B). At the concentrations used, TTFA did not affect PC3 cell proliferation (fig. S4C).

Regulation of membrane dynamics by cortical mitochondria

We reasoned that redistribution of mitochondria to the cortical cytoskeleton near focal adhesion complexes (Fig. 4, E and F) could fuel the energy-intensive process of tumor cell movements. Consistent with this possibility, targeting survivin with YM155 or inhibiting SDHB with TTFA in PC3 cells suppressed membrane lamellipodia dynamics (Fig. 5, A and B, and fig. S5A), which are required, but not sufficient, for cell motility (25). Single-cell stroboscopic microscopy demonstrated that either treatment

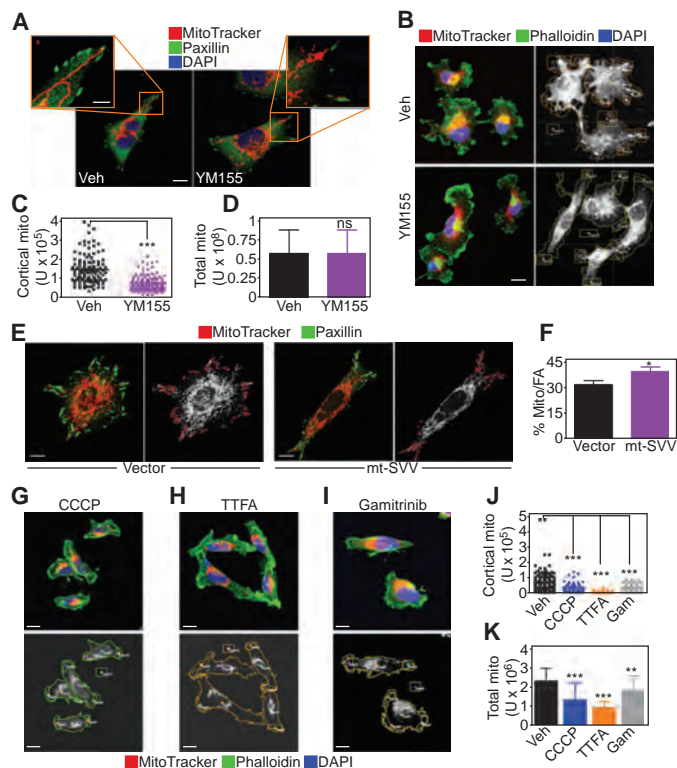


Fig. 4. Surivin-mediated regulation of subcellular mitochondrial trafficking. (A) PC3 cells were treated with vehicle (Veh) or YM155, labeled for mitochondria (MitoTracker, red), focal adhesion (FA) complexes (paxillin, green), and DNA [4',6-diamidino-2-phenylindole (DAPI), blue], and analyzed by confocal microscopy. Twenty cells per treatment condition imaged in two independent experiments. Scale bar, 10 μ m; insets, 5 μ m. (B) PC3 cells treated as in (A) were labeled for mitochondria (MitoTracker, red), actin (phalloidin, green), and DNA (DAPI, blue), and analyzed by confocal microscopy (left). Right: Masked images used to quantify mitochondrial localization to phalloidin-positive protrusions. Twenty cells per treatment condition imaged in two independent experiments. Scale bar, 10 μ m. (C and D) The conditions are as in (B), and the amount of cortical mitochondria (C) or total mitochondria (D) was quantified in the presence of vehicle or YM155. Each point corresponds to an individual measurement. Forty-five cells per treatment condition imaged in two independent experiments. *** $P < 0.0001$; ns, not significant. (E and F) MCF-7 cells were transduced with vector or mt-SVV, labeled for mitochondria (MitoTracker, red) and paxillin (green), and analyzed by fluorescence microscopy (E). Right: Masked (right panels) images were used to quantify mitochondrial localization to paxillin-containing regions (F). Data are expressed as percent of mitochondria localization to paxillin-containing focal adhesion (FA) complexes per cell. Mean \pm SEM. Vector, $n = 26$ cells; mt-SVV, $n = 27$; imaged in two independent experiments. * $P = 0.0013$. Scale bars, 10 μ m. (G to I) The conditions are as in (B) except that PC3 cells were treated with the mitochondrial uncoupler CCCP (G), the small-molecule complex II inhibitor TTFA (H), or gamitrinib (I) and analyzed by confocal microscopy (top). Bottom: Masked images used to quantify mitochondria localization to phalloidin-positive cellular protrusions. Forty-five cells per treatment condition imaged in two independent experiments. Scale bars, 10 μ m. (J and K) Treated PC3 cells were analyzed by confocal microscopy as in (G) to (I), and the amount of cortical mitochondria (J) or total mitochondria (K) was quantified. Each point corresponds to an individual measurement. *** $P < 0.0001$; ** $P = 0.0013$. Forty-five cells per treatment condition imaged in two independent experiments.

decreased the formation (Fig. 5C), total distance traveled (Fig. 5D), and total persistence of membrane ruffles (Fig. 5E). As a result, individual ruffles that formed in the presence of YM155 or TTFA extended for shorter distances (fig. S5, B and C) with slower retraction speed (fig. S5, D and E). In this analysis, average ruffling persistence did not change (fig. S5, F and G). Instead, a post-analysis of cumulative ruffling dynamics that takes into account all ruffling events (20 to 60 ruffles measured per cell in a 5-min time interval) showed that YM155 or TTFA treatment reduced the overall distance and persistence of cell dynamics (Fig. 5, D and E). In contrast, control cells exposed to conditioned medium used as a chemotactic stimulus exhibited vigorous membrane lamellipodia dynamics (Fig. 5A and fig. S5A).

Focal adhesion kinase (FAK) is a key effector of membrane dynamics, focal adhesion complexes, and cell motility that becomes activated through autophosphorylation at Tyr³⁹⁷ and Src-mediated phosphorylation at Tyr⁹²⁵ in response to growth factor stimulation and cell–extracellular matrix contact (26). Treatment with YM155 (Fig. 5F) or TTFA (fig. S5H) suppressed the autophosphorylation of FAK (26) at Tyr³⁹⁷ without affecting phosphorylation of Tyr⁹²⁵ (Fig. 5F). In contrast, YM155 did not affect the phosphorylation of Src or Akt, kinases that have also been implicated in cell motility, and total FAK abundance was unchanged (Fig. 5F). Consistent with these results, YM155 reduced the recruitment of phosphorylated FAK to focal adhesion complexes (Fig. 5G) while increasing the persistence of mature complexes (Fig. 5H and fig. S5I) (25). In contrast, vehicle-treated cells assembled focal adhesion complexes at cellular protrusions that contained Tyr³⁹⁷-phosphorylated FAK (Fig. 5G).

Control of tumor cell invasion and metastasis by mitochondrial survivin

Next, we asked whether survivin bioenergetics and regulation of membrane dynamics affected PC3 cell movements. When analyzed for two-dimensional chemotaxis, survivin targeting with siRNA (Fig. 6A) or YM155 (fig. S6A) decreased PC3 cell velocity and distance traveled, as assessed by time-lapse videomicroscopy in scratch closure assays (Fig. 6B and fig. S6B), which mimic wound healing in vitro. In addition, YM155 (Fig. 6C) or survivin silencing by siRNA (fig. S6C and Fig. 6, D and E) inhibited PC3 cell invasion across Matrigel-coated inserts, whereas reconstitution of survivin knockdown cells with mitochondrial-targeted survivin partially restored PC3 cell invasion (Fig. 6F). Furthermore, stable expression of mitochondrial-targeted survivin in poorly migratory INS-1 or MCF-7 cells was sufficient to increase their invasive ability (Fig. 6G). In contrast, expression of a mitochondrial-targeted survivin Cys⁸⁴→Ala (C84A) dominant negative mutant, which accumulated in the mitochondria, but not the cytosol of MCF-7 cells (fig. S6C), did not increase invasion (fig. S6D). To determine whether survivin regulation of tumor cell invasion was important in vivo, we measured liver metastasis in immunocompromised mice injected with MCF-7 cells in the spleen. Mice injected with mitochondrial-targeted survivin-expressing cells had more liver metastases with greater surface area than those injected with vector-expressing cells (Fig. 6, H to J).

Finally, we asked whether oxidative phosphorylation was required for tumor cell invasion mediated by mitochondrial survivin. As expected, treatment of PC3 cells with the complex I inhibitor rotenone or the complex III inhibitor antimycin A suppressed ATP production (fig. S7A). Inhibition of the respiratory chain with rotenone (Fig. 7A), TTFA (which inhibits the SDHB subunit of complex II) (Fig. 7B), or antimycin A (Fig. 7C) reduced PC3 cell invasion. Furthermore, siRNA-directed silencing of SDHB (fig. S7B) increased the phosphorylation of AMPK in PC3 cells (fig. S7B), which occurs under conditions of nutrient deprivation, and inhibited the invasion (Fig. 7D and fig. S7C) and migration (Fig. 7E) of PC3 and breast adenocarcinoma MDA-231 cells. Consistent with a requirement of FAK in this response (Fig. 5F), transfection of PC3 cells with a cDNA encoding

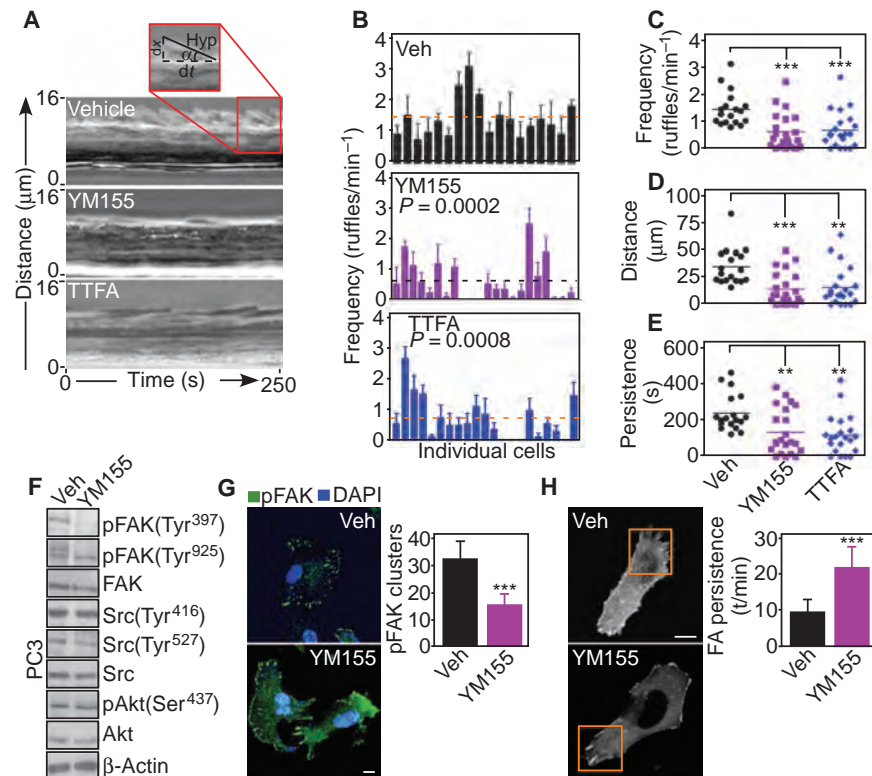


Fig. 5. Mitochondrial bioenergetics requirements of membrane dynamics. (A) Representative stroboscopic images of fetal bovine serum (FBS)-stimulated PC3 cells treated with vehicle, YM155, or the complex II inhibitor TTFA. Inset, stroboscopic analysis of cell dynamics (SACED) parameters of cell protrusion dynamics. (B) Quantification of membrane ruffle frequency in PC3 cells treated with vehicle (Veh), YM155, or TTFA. Each bar corresponds to an individual cell. Cells were imaged in two independent experiments. Broken lines, average values. The *P* values in YM155- or TTFA-treated cultures compared to Veh are indicated. (C–E) PC3 cells treated with vehicle (Veh), YM155, or TTFA were analyzed by SACED stroboscopic microscopy for average frequency of membrane ruffling (C), ruffle distance traveled (D), or ruffle persistence time (E). The quantified values are as follows (number of cells examined in parentheses): frequency of membrane ruffling (C), Veh, 1.44 ± 0.14 ($n = 18$); YM155, 0.61 ± 0.14 ($n = 22$), $P = 0.0002$; TTFA, 0.68 ± 0.14 ($n = 21$), $P = 0.0008$; ruffle distance traveled (D), Veh, 35 ± 3.9 ($n = 18$); YM155, 14.2 ± 3.2 ($n = 22$), $P = 0.0002$; TTFA, 16 ± 3.89 ($n = 21$), $P = 0.0016$; time of ruffle persistence (E), Veh, 243.3 ± 24.3 ($n = 18$); YM155, 136.4 ± 26.9 ($n = 22$), $P = 0.006$; TTFA, 120.3 ± 24.1 ($n = 21$), $P = 0.001$. Cells were imaged in two independent experiments. (F) PC3 cells treated with vehicle (Veh) or YM155 were analyzed by Western blotting. p, phosphorylated. Blots are representative of two independent experiments. (G) PC3 cells were treated with vehicle (Veh) or YM155, labeled with an antibody to phosphorylated FAK (pFAK, Tyr³⁹⁷), and analyzed by confocal microscopy. DNA was stained with DAPI. Right: Quantification of phosphorylated FAK clusters. Mean \pm SEM. *** $P < 0.0001$. Twenty cells per treatment condition imaged in two independent experiments. Scale bar, 10 μ m. (H) PC3 cells treated as in (G) were transfected with α -actinin–GFP cDNA and analyzed by confocal microscopy. Ten cells (10 movies) per treatment condition imaged in two independent experiments. *** $P < 0.0001$. Scale bar, 10 μ m. Right, FA dynamics quantified by time-lapse videomicroscopy. FA complexes examined: Veh, $n = 42$; YM155, $n = 47$.

wild-type FAK that could be phosphorylated on Tyr³⁹⁷ (fig. S7D) partially or fully reversed the inhibitory effect of YM155 (Fig. 7F) or SDHB knockdown (Fig. 7G) on tumor cell invasion. In contrast, siRNA-mediated silencing of FIP200 (fig. S7E), an upstream autophagy initiator and endogenous inhibitor of FAK (27), did not rescue the inhibition of tumor cell in-

vasion mediated by YM155 (fig. S7F). Similarly, inhibition of nuclear factor κ B (NF- κ B) signaling, which has been implicated in the regulation of cell motility by cytosolic survivin (28), by transfection of an I κ B α super-repressor mutant, did not rescue the inhibition of tumor cell invasion mediated by YM155 (fig. S7G).

DISCUSSION

Here, we showed that a mitochondrial pool of survivin (3) cooperates with Hsp90 chaperones in the folding of the oxidative phosphorylation complex II subunits SDHB and SDHC. Genetic, molecular, or pharmacologic interference with this pathway impaired mitochondrial respiration, lowered ATP production, and produced a phenotype of cellular starvation characterized by phosphorylation of AMPK and suppression of mTOR signaling. Conversely, oxidative phosphorylation supported by survivin enabled the trafficking of mitochondria to the cortical cytoskeleton of tumor cells, which may provide a “regional” energy source to fuel membrane lamellipodia dynamics, disassembly of FAK-containing focal adhesion complexes, increased tumor cell migration and invasion, and heightened metastatic dissemination in vivo.

IAP proteins, including survivin (28), have been implicated in cell motility (29). The mechanistic underpinnings of this pathway have not been completely elucidated, because at least under certain conditions, IAPs can inhibit cell migration, potentially through ubiquitination of Rac1 (30) or stimulation of RAF destruction (31). However, most data point to IAPs (32, 33), including survivin (28), as evolutionarily conserved (34) activators of cell migration, invasion, and metastatic dissemination (29). In the case of survivin, this response has been linked to the formation of an survivin–XIAP (X-linked inhibitor of apoptosis protein) complex (35), promoting NF- κ B–dependent activation of a process that promotes cell motility, including increased production and deposition of fibronectin (28).

The data here uncover a mechanism by which survivin promotes tumor cell invasion through mitochondrial bioenergetics. Accordingly, a pool of survivin localized to tumor mitochondria (3), and previously implicated in apoptosis resistance upon discharge in the cytosol (4), emerged here as an intrinsic regulator of oxidative phosphorylation in tumors. We showed that mitochondrial survivin cooperated with the chaperone TRAP-1 (23) to maintain SDH folding and complex II activity in tumors, consistent with a role of protein quality control in preserving organelle bioenergetics (22). This finding conflicts with other

data showing that mitochondrial survivin promotes mitochondrial fission, inhibits complex I–dependent respiration, and enhances aerobic glycolysis (5).

How survivin affects a TRAP-1–SDH interaction (22) in maintaining mitochondrial protein folding quality control remains to be elucidated. Several chaperones, including Hsp90 (36), the aryl hydrocarbon receptor–interacting

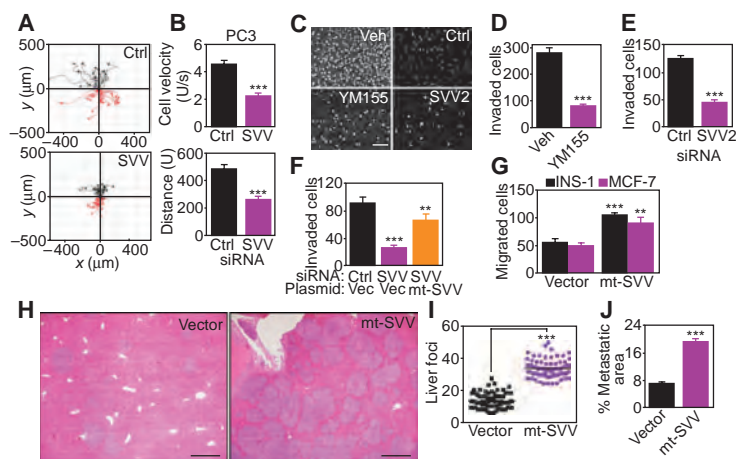


Fig. 6. Regulation of tumor cell motility, invasion, and metastasis by mitochondrial survivin. (A) siRNA-transfected PC3 cells were analyzed in a scratch closure assay, and individual cell movements were tracked by time-lapse videomicroscopy. Ctrl siRNA, number of cells examined ($n = 29$); survivin (SVV) siRNA, $n = 30$; imaged in two independent determinations. (B) Average cell velocity (top) or total distance traveled (bottom) of the cells in (A) was quantified per each condition. Mean \pm SEM. $P < 0.0001$. (C to E) PC3 cells treated with vehicle (Veh) or YM155 or transfected with survivin-directed siRNA (SVV2) were analyzed for Matrigel invasion. DAPI-stained nuclei of invaded cells (C) after YM155 treatment (D) or survivin knockdown (E) were quantified. Mean \pm SEM. $***P < 0.0001$. One hundred to 250 cells per treatment or transfection condition imaged in two independent experiments. Scale bar, 200 μ m. (F) PC3 cells silenced for survivin by siRNA were reconstituted with vector or mt-SVV cDNA and analyzed for Matrigel invasion. Mean \pm SEM. $**P = 0.0026$; $***P < 0.0001$. One hundred to 250 cells per treatment or transfection condition imaged in two independent experiments. (G) INS-1 or MCF-7 cells transfected with vector or mt-SVV cDNA were analyzed for Matrigel invasion. Mean \pm SEM. $**P = 0.003$; $***P < 0.0001$. One hundred to 250 cells per treatment or transfection condition imaged in two independent experiments. (H) MCF-7 cells transfected with vector or mt-SVV cDNA were injected in the spleen of immunocompetent mice (three mice per transfection condition). Representative images of hematoxylin and eosin-stained liver sections ($n = 15$ per each transfection condition). Scale bars, 500 μ m. (I and J) Morphometric quantification of total number of metastatic foci (I) and metastatic surface area (J) in serial liver sections ($n = 15$ per each transfection condition). Mean \pm SEM. $***P < 0.0001$.

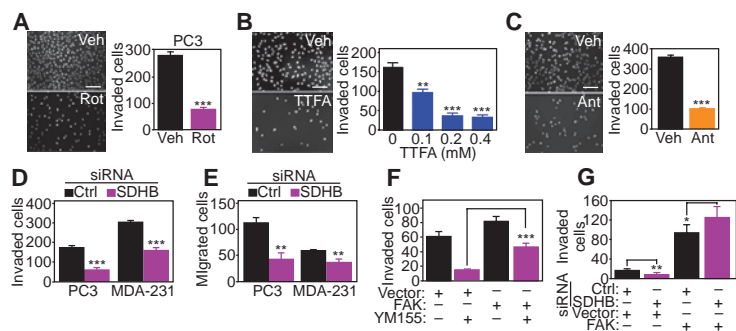


Fig. 7. Requirements of mitochondrial regulation in tumor cell invasion. (A to C) PC3 cells were incubated with vehicle or the complex I inhibitor rotenone (Rot) (A), the complex II inhibitor TTFA (B), or the complex III inhibitor antimycin A (C), and analyzed for Matrigel invasion. Right panels: Quantification of DAPI-stained nuclei of invaded cells in the presence of the various inhibitors. Mean \pm SEM. $**P = 0.0053$; $***P < 0.0001$. One hundred to 250 cells per treatment condition imaged in two independent experiments. Scale bar, 200 μ m. (D and E) PC3 or MDA-231 cells were transfected with control (Ctrl) or SDHB-directed siRNA, and analyzed for Matrigel invasion (D) or cell migration (E). Mean \pm SEM. $**P = 0.001$ to 0.0028 ; $***P < 0.0001$. One hundred to 250 cells per treatment condition imaged in two independent experiments. (F and G) PC3 cells transfected with vector or FAK cDNA were treated with vehicle (Veh) or YM155 (F), or silenced for SDHB by siRNA (G) and quantified for Matrigel invasion. Mean \pm SEM. $*P = 0.03$; $**P = 0.0032$; $***P < 0.0001$. One hundred to 250 cells per treatment condition imaged in two independent experiments.

protein (AIP) (37), and Hsp60 (38) associate with survivin, regulating protein stability and subcellular trafficking. In the case of TRAP-1, the recruitment of survivin to this complex may protect co-associated SDH subunits (22) from the mitochondrial protein degradation machinery. This scenario is reminiscent of how cytosolic survivin prevents access of the ubiquitin-conjugating enzyme UbcH5 to XIAP, maintaining XIAP stability and increasing apoptosis resistance (35).

A role of mitochondrial respiration in cancer metabolism has been debated (6) against the backdrop of the Warburg effect (8). Whether this process contributes to tumor cell motility, and potentially, metastasis, has also been controversial (39), with findings suggesting that oxidative phosphorylation is important (40), not important (41), or must be dysfunctional (42) to support tumor cell invasion. In addition, a prevailing model is that metabolites that accumulate in a highly glycolytic (43) and hypoxic (44) microenvironment suppress mitochondrial respiration (7) and enhance metastatic competency in vivo. The data here suggest a complementary scenario, in which oxidative phosphorylation maintained by survivin-TRAP-1 protein folding is integral to cancer metabolism (39) and enables the repositioning of energetically active mitochondria to the cortical cytoskeleton of tumor cells, where they provide a concentrated, regional energy source to support cell motility (25). Targeting mitochondrial survivin, destabilizing complex II, or inhibiting different steps in oxidative phosphorylation interfered with this pathway, prevented the accumulation of cortical mitochondria, suppressed the formation of membrane lamellipodia (45) and focal adhesion dynamics (26), and inhibited tumor cell migration and invasion. There is precedent for a model of regional mitochondrial bioenergetics to support highly energy-intensive cellular tasks. For instance, neurons reposition mitochondria (46) to subcellular sites of high ATP demands, providing an efficient energy source to power synapses, growth cones, and dendritic branching (47). Whether the same machinery controlling mitochondrial trafficking in neurons is exploited for metastatic competency in tumors is unknown. However, mitochondrial dynamics has been implicated in tumor cell migration (48), and asymmetric mitochondrial distribution toward the leading edge may contribute to the directionality of tumor cell movements (49).

These observations thus identify survivin as a potential cancer therapeutic target (1). Accordingly, expression of mitochondrial survivin was sufficient to convert poorly migratory MCF-7 cells into cells with an invasive and metastatic phenotype in vivo, in line with clinical data that link survivin abundance to metastatic dissemination in humans (2). Although the specificity of YM155 as a survivin antagonist (50) remains to be fully elucidated (51), our data show that this agent disrupted mitochondrial bioenergetics, suppressed cell invasion, and activated tumor suppressor mechanisms, namely, AMPK activation or mTOR inhibition.

In summary, we have demonstrated that survivin controls mitochondrial respiration, enabling organelle trafficking and potentially regional bioenergetics to fuel tumor cell motility and metastasis. These observations reinforce a key role of mitochondrial bioenergetics as a driver of tumor progression (22) and open new prospects for targeting oxidative phosphorylation as a cancer therapeutic strategy (52).

MATERIALS AND METHODS

Antibodies and reagents

The following antibodies to survivin (Novus Biologicals), SDHB (Abcam), SDHA (Abcam), SDHC (Abcam), Cox-IV (Cell Signaling), Thr¹⁷²-phosphorylated AMPK α (Cell Signaling), AMPK α (Cell Signaling), Tyr³⁹⁷-phosphorylated FAK (Invitrogen), Tyr⁹²⁵-phosphorylated FAK (Cell Signaling), FAK (Cell Signaling), Tyr⁴¹⁶-phosphorylated Src (Cell Signaling), Tyr⁵²⁷-phosphorylated Src (Cell Signaling), Src (Cell Signaling), Ser⁴⁷³-phosphorylated Akt (Cell Signaling), Akt (Cell Signaling), FIP200 (Novus Biologicals), LC-3B (Cell Signaling), TRAP-1 (BD Biosciences), Hsp90 (BD Biosciences), Thr^{37/46}-phosphorylated 4EBP1 (Cell Signaling), 4EBP1 (Cell Signaling), Thr³⁸⁹-phosphorylated p70S6 kinase (Cell Signaling), 70S6 kinase (Cell Signaling), VDAC (Cell Signaling), Cox-IV (Cell Signaling), CypD (Millipore), CLPP (Santa Cruz Biotechnology), β -actin (Sigma-Aldrich), and β -tubulin (Sigma-Aldrich) were used. An oxidative phosphorylation antibody cocktail (MitoSciences) directed against the 20-kD subunit of complex I (20 kD), cytochrome c oxidase subunit II of complex IV (22 kD), SDHB subunit of complex II (30 kD), core 2 of complex III (~50 kD), and F1 α (ATP synthase) of complex V (~60 kD) was used.

The complete chemical synthesis, high-performance liquid chromatography profile, and mass spectrometry of mitochondrial-targeted small-molecule Hsp90 antagonist gamitrinib (GA mitochondrial matrix inhibitors) has been previously reported (53). The gamitrinib variant containing triphenylphosphonium as a mitochondrial-targeting moiety was used in this study (53). Oligomycin, carbonyl cyanide *p*-trifluoromethoxyphenylhydrazone (FCCP), CCCP, antimycin A, and TTEA were obtained from Sigma-Aldrich. Antimycin A and rotenone were obtained from Abcam Biochemicals. A small-molecule survivin suppressant, YM155, which inhibits Sp1-dependent transcription of the *survivin* locus (50), was from Selleckchem. In all experiments, TTEA was used at concentrations of 100 to 400 μ M, and YM155 was used at 10 nM. All chemicals were of the highest purity commercially available.

Cell culture

Human glioblastoma LN229, prostate adenocarcinoma PC3 and DU145, and breast adenocarcinoma MCF-7, MCF-10A, and MDA-MB231 cells were obtained from the American Type Culture Collection (Manassas, VA) and maintained in culture according to the supplier's specifications. Rat insulinoma INS-1 cells stably transfected with vector or mitochondrial-targeted survivin have been previously described (3).

Transfections

For gene knockdown experiments, tumor cells were transfected using control, nontargeting siRNA pool (Dharmacon, catalog no. D-001810), two independent custom-prepared survivin-directed siRNA with the sequence GAGCCAAGAACAAAUUGC (SVV) or GGACCACCGCAUCUCUACA (SVV2) (Thermo Scientific) characterized in previous studies (24), or siRNA pools targeting TRAP-1 (Dharmacon, catalog no. L-010104) or FIP200 (Dharmacon, catalog no. L-021117), as described (54). The various siRNAs were transfected at 10 to 30 nM in the presence of Lipofectamine RNAiMAX in a 1:1 ratio (Invitrogen). Cells were incubated for 48 hours, validated for target protein knockdown by Western

blotting, and processed for subsequent experiments. Plasmid DNA transfections were carried out using X-tremeGENE HP DNA Transfection Reagent (Roche). A replication-deficient adenovirus (pAd) encoding mitochondrial-targeted GFP (pAd-GFP) or mitochondrial-targeted GFP-survivin (pAd-mt-SVV) has been previously described (3). For reconstitution experiments, PC3 cells were silenced for endogenous survivin by siRNA and transfected with plasmid encoding mitochondrial-targeted survivin or, alternatively, pAd-mt-SVV. In some experiments, MCF-7 or MCF-10A cells were transfected with vector, or mitochondrial-targeted wild-type survivin or mitochondrial-targeted Cys⁸⁴→Ala (C84A) survivin dominant negative mutant, characterized in previous studies (55). For rescue experiments, PC3 cells treated with vehicle or YM155, or, alternatively, silenced for endogenous SDHB expression by siRNA, were transfected with vector or cDNA encoding FAK, FIP200 (54), or I κ B α super-repressor mutant (28) characterized in previous studies before analysis of Matrigel invasion.

Quantification of autophagy

PC3 cells were cotransfected with siRNA against survivin and plasmid encoding GFP fused to human dynein LC3 cDNA in the presence of Lipofectamine 2000 Transfection Reagent (Invitrogen). After 48 hours, transfected cells were fixed in 4% paraformaldehyde for 15 min at 37°C, washed, and examined by confocal microscopy (Leica, SP5). The numbers of GFP-LC3 punctate dots per cell were determined from two independent experiments. A minimum of 50 GFP-LC3-positive cells assessed from at least 10 random fields per sample were counted in triplicate per each condition, as previously described (20).

Cell proliferation, cell cycle analysis, and mitochondrial membrane potential

Potential changes in cell proliferation in various tumor cell types (2×10^4 to 1.25×10^5 cells) were evaluated after 48 to 72 hours by direct cell counting. Alternatively, tumor cells were labeled with 1:1000 dilution BrdU (Amersham Pharmacia Biotech) in cultured medium for 1 hour and analyzed by multiparametric flow cytometry with quantification of BrdU⁺ cells. In some experiments, tumor cell types (1×10^6) were fixed in glacial 70% ethanol for 24 hours, followed by incubation with propidium iodide (2.5 μ g/ml) in the presence of ribonuclease A for 10 min at room temperature. Twenty thousand events were acquired on a Calibur flow cytometer, with quantification of individual cell cycle transitions using CellQuest Pro software (Becton Dickinson), as previously described (20).

In some experiments, PC3 cells grown at low confluency (1×10^4 to 2×10^4 per well) on optical-grade coverslips were transfected with control or survivin-directed siRNA or treated with vehicle or YM155 (10 nM) for 24 hours, fixed in 4% formaldehyde for 15 min at 37°C, washed in phosphate-buffered saline (PBS), pH 7.4, and permeabilized with 0.1% Triton X-100 for 5 min at 22°C. Slides were washed in PBS, pH 7.4, blocked in 1% bovine serum albumin (BSA)/PBS for 30 min, and analyzed for changes in nuclear morphology by DAPI staining on a Leica TCS SP5 fluorescence microscope with a 100 \times oil objective. To test the impact of survivin targeting on mitochondrial inner membrane potential, PC3 cells were treated with 10 nM YM155 for 16 hours or transfected with siRNA against survivin for 48 hours, incubated with 0.1 μ M tetramethylrhodamine methyl ester, and analyzed for changes in fluorescence emission by flow cytometry.

Subcellular fractionation

Mitochondrial fractions were isolated from treated cells as previously described (20). Briefly, the various tumor cell types were mechanically disrupted by 70 strokes with a Dounce homogenizer in isolation buffer containing protease inhibitor cocktail. Cell debris was removed by centrifugation at 700g for 10 min. The supernatant was further centrifuged at

3000g for 15 min, and supernatants or mitochondrial pellets were processed for further analysis.

Protein analysis

For Western blotting, protein lysates were prepared from the different cell types in radioimmunoprecipitation assay buffer (150 mM NaCl, 1.0% Triton X-100, 0.5% sodium deoxycholate, 0.1% SDS, 50 mM Tris, pH 8.0) containing EDTA-free Protease Inhibitor Cocktail (Roche) and Phosphatase Inhibitor Cocktail 2 and 3 (Sigma-Aldrich). Equal amounts of protein lysates were separated by SDS gel electrophoresis, transferred to polyvinylidene difluoride membranes, and incubated with primary antibodies of various specificities. Protein bands were visualized by chemiluminescence. In some experiments, mitochondria were isolated from PC3 cells and lysed in 0.5% CHAPS buffer, containing 1% *n*-dodecyl- β -D-maltopyranoside plus protease inhibitors (Roche) for 30 min at 4°C under constant agitation. For immunoprecipitation experiments, aliquots (500 μ g) of isolated mitochondrial extracts were incubated with nonbinding IgG or an antibody to survivin for 16 hours at 4°C. Immune complexes were coupled with protein A Sepharose beads (Calbiochem) for 2 hours at 4°C. After washes in TBST, the immune complexes were separated by SDS gel electrophoresis and analyzed by Western blotting.

Mitochondrial protein folding

Mitochondrial protein folding assays were performed as previously described (20, 22). Briefly, mitochondrial fractions were isolated after 24 to 48 hours from PC3 cells transfected with control nontargeting or survivin-directed siRNA and suspended in equal volume of mitochondrial fractionation buffer containing increasing concentrations of CHAPS (0, 0.05, 0.5, 1, 2, or 5%) or NP-40 (0, 0.05, 0.2, 0.5, or 2%). Samples were incubated for 25 min on ice with vortexing every 5 min, and detergent-insoluble protein aggregates were isolated by centrifugation (20,000g) for 20 min, separated on SDS polyacrylamide gels, and analyzed by Western blotting. In some experiments, PC3 cells were treated with 5 μ M gamitrinib for 6 hours and incubated with the protein synthesis inhibitor cycloheximide (100 μ g/ml), and aliquots of mitochondrial extracts were collected at T_0 and after 1, 2, 3, and 4.5 hours, followed by Western blotting. Protein bands at the indicated time intervals were quantified by densitometry, and survivin half-life was calculated.

Submitochondrial fractionation

Purified mitochondrial pellets isolated by sucrose step gradient were suspended in swelling buffer [10 mM KH_2PO_4 (pH 7.4) plus protease inhibitors] and incubated for 20 min at 0°C with gentle mixing, as previously described (21). Mitochondria were mixed with equal volume of shrinking buffer [10 mM KH_2PO_4 (pH 7.4), 32% sucrose, 30% glycerol, 10 mM MgCl_2 , and protease inhibitors] for 20 min at 0°C. After centrifugation at 10,000g for 10 min, the supernatant was collected as containing outer membrane and intermembrane space fractions. Pellets were washed three times with 1:1 mixture of swelling-shrinking buffer, suspended in swelling buffer, and sonicated to disrupt the inner membrane, which was collected as containing inner membrane and matrix fractions. Aliquots containing outer membrane and intermembrane space fractions and inner membrane and matrix fractions were further fractionated by centrifugation at 150,000g for 1 hour at 4°C. The pellets were collected as outer membrane and intermembrane space fractions, respectively. Supernatants were concentrated using Centricon 10K and Microcon 10K centrifugal filters (Millipore) and collected as inner membrane and matrix fractions, respectively.

Metabolomics screen

A global metabolomics profiling to examine changes in expression of 301 individual metabolites in PC3 cells transfected with control nontargeting

siRNA or survivin-directed siRNA was performed by Metabolon, as previously described (22).

Tumor bioenergetics

Various tumor cell types treated with 10 nM YM155 for 16 hours or, alternatively, transfected with control nontargeting siRNA or survivin-directed siRNA for 48 hours were analyzed for oxygen consumption (Enzo Life Sciences, catalog no. ENZ-51045-1) or ATP generation (BioChain, catalog no. Z5030041), as previously described (20, 22). Aliquots of cultured medium were collected for analysis of glucose consumption (Enzyme, catalog no. CA-G005) or lactate production (Abcam, catalog no. ab65331), as previously described (20, 22).

Cellular respiration

Oxygen consumption rates were assayed in intact cells using an Extracellular Flux System 24 Instrument (Seahorse Bioscience), as previously described (22). Briefly, PC3 and DU145 cells in complete medium were transfected with the various siRNAs for 24 to 36 hours. After trypsinization and resuspension in growth medium, 2.5×10^4 cells were plated in each well of a Seahorse XF24 cell culture plate (100 μ l) in complete medium. After 4 hours of incubation to allow cells to adhere to plates, an additional 150 μ l of medium was added to each well, and cells were grown in 5% CO_2 for 24 hours at 37°C. The medium was then exchanged with unbuffered Dulbecco's modified Eagle's medium (DMEM) XF assay medium (Seahorse Bioscience) supplemented with 2 mM GlutaMAX, 1 mM sodium pyruvate, and 5 mM glucose (pH 7.4 at 37°C), and equilibrated for 30 min at 37°C and ~0.04% CO_2 before the experiment. Where indicated, the unbuffered DMEM XF assay medium was supplemented with high (10 mM) or low (1 mM) glucose concentrations. Cellular oxygen consumption was monitored at basal conditions (before any addition) and after addition of oligomycin (1.25 μ M), FCCP (0.4 μ M), and antimycin (1.8 μ M), all dissolved in dimethyl sulfoxide (DMSO). The three drugs were injected sequentially, and the oxygen consumption rate was measured with three cycles of mixing (150 s), waiting (120 s), and measuring (210 s). This cycle was repeated after each injection.

For quantification of cellular respiration in permeabilized cultures, PC3 cells were treated with vehicle (DMSO) or 10 nM YM155 in complete medium for 16 hours. After trypsinization, PC3 cells were suspended in MiR06 incubation medium (Oroboros Instruments) at a density of 1.5×10^6 cells/ml (3×10^6 cells total) and permeabilized with digitonin (10 μ g/ 1×10^6 cells), and oxygen consumption was measured at 37°C with an Oroboros Oxygraph-2k (Oroboros Instruments), two-chamber high-resolution respirometer, Clark-type oxygen electrode, in closed 2-ml chambers equipped with magnetic stirring. The respiration medium contained 10 mM glutamate and 2 mM malate (complex I assay), 10 mM succinate and 0.5 μ M rotenone (complex II assay), and 5 mM malonic acid and 10 mM glycerol phosphate (complex III assay). During the experiment, the following agents were added: ADP (adenosine 5'-diphosphate) (200 μ M), oligomycin (2.5 μ M), FCCP (1 μ M), and antimycin (2 μ M).

Mitochondrial respiration complex activity

PC3 cells were analyzed for changes in oxidative phosphorylation complex activity with Abcam reagents (catalog no. ab109721, complex I; catalog no. ab109908, complex II) using lysed isolated mitochondria, as described previously. Briefly, PC3 cells were transfected with control nontargeting or survivin-directed siRNA and validated for protein knockdown by Western blotting, and 2 μ g of mitochondrial extracts from each condition was assayed for Citrate Synthase activity (ScienCell). Aliquots of mitochondrial lysates with comparable citrate synthase activity were applied to mitochondrial complex-specific microplates for immunocapture, with continuous

quantification of enzymatic activity in a microplate reader for either an increase in absorbance at 450 nm (complex I) or a decrease in absorbance at 600 nm (complex II). NADH (reduced form of nicotinamide adenine dinucleotide) or ubiquinone was used as substrate for complex I or complex II activity, respectively. Relative complex activities were calculated by determining the change in absorbance over time in the linear range of the measurements.

Immunofluorescence

To quantify mitochondrial subcellular trafficking, PC3 cells were incubated with MitoTracker Red CM-H₂XRos (Invitrogen) diluted in conditioned medium for 1 hour at 37°C. Cells were fixed with 3.7% paraformaldehyde for 20 min, permeabilized in 0.2% Triton X-100 for 15 min, washed with 100 mM glycine, blocked with 1% BSA/0.05% Triton X-100 for 30 min, and further incubated with Alexa Fluor 488 phalloidin (Life Technologies) in blocking buffer for 20 min. After three washes in PBS, coverslips were mounted in ProLong Gold mounting medium with DAPI (Invitrogen). In some experiments, cells were treated with the mitochondrial uncoupler CCCP (12.5 μM), the SDHB inhibitor TTFA (200 μM), or the mitochondrial-targeted small-molecule Hsp90 inhibitor gamitrinib (5 μM) for 16 hours before immunofluorescence staining. For analysis of phosphorylated FAK clusters, PC3 cells were seeded on fibronectin (10 μg/ml) for 2 hours in the presence of vehicle (DMSO) or YM155 (10 nM). Cells were fixed with 3.7% paraformaldehyde for 20 min, permeabilized in 0.2% Triton X-100 for 15 min, washed with 100 mM glycine, blocked with 1% BSA/0.05% Triton X-100 for 30 min, and incubated with an antibody to phosphorylated FAK (Tyr³⁹⁷) for 1 hour (1:100) in blocking buffer. After three washes in PBS, cells were incubated with a fluorescein isothiocyanate-conjugated secondary antibody (1:1000) for 1 hour and washed, and coverslips were mounted in ProLong Gold mounting medium containing DAPI (Invitrogen) for analysis by confocal microscopy. For quantification of mitochondria-containing focal adhesion complexes, MCF-7 cells were transfected with vector or mitochondrial-targeted wild-type survivin cDNA for 48 hours. Cells were then seeded on fibronectin-covered coverslips, incubated with MitoTracker Red for 1 hour at 37°C, and stained with an antibody to paxillin (1:100) as a marker for focal adhesions before analysis by confocal fluorescence microscopy.

For quantification of microscopy data, a minimum of 50 cells per experiment were imaged using a Leica TCS SP5 II Scanning Laser Confocal Microscope system with an HCX PL APO CS 63× 1.40 numerical aperture (NA) oil ultraviolet (UV) objective using the same laser intensity and exposure time. A full-cell Z-stack of a minimum of 11 sequential steps of 0.5-μm size was collected. Total fluorescence intensity of mitochondria for whole cell and within the lamellipodia regions was obtained by creating masks for each cell and areas of interests for lamellipodia, determined by costaining with phalloidin. For scoring of phosphorylated FAK-containing clusters per cell, or focal adhesions per cell, an automated counting was applied by thresholding phosphorylated FAK-containing clusters or focal adhesions based on fluorescence intensity using ImagePro software. Outlines of focal adhesions were created and overlaid on images showing mitochondrial staining, and intensity measurements of MitoTracker in the outlines of focal adhesions were obtained to quantify positive staining in focal adhesion regions. Control images were additionally taken for subtraction of background signal.

Stroboscopic analysis of cell dynamics

Quantification of membrane ruffle dynamics in live cells was carried out as described previously (54). Briefly, 3×10^4 to 5×10^4 cells were grown on high optical quality 96-well μ-plates (Ibidi) and imaged with a 40× objective on a Nikon TE300 inverted time-lapse microscope equipped with a video system containing an Evolution QEi camera and a time-lapse video cassette

recorder. The atmosphere was equilibrated to 37°C and 5% CO₂ in an incubation chamber. Phase-contrast images were captured at 0.5-s intervals for 250 s (500 frames) and merged into sequence files using ImagePro Plus 7. To monitor dynamics of a particular region by SACED (54), the sequence files were imported into ImageJ, and a particular region of 16.2 mm × 0.162 mm (“SACED line”) was selected, duplicated, and montaged in sequence to display the region over time in a stroboscopic image. This process was repeated to obtain four SACED lines and therefore four stroboscopic images per cell, and structures such as protruding lamellipodia and ruffles were manually labeled. For each cell, the frequency of ruffles per minute, the ruffling retraction speed (μm/min), the ruffle migration distance (nm), and the time of ruffle persistence (ms) were calculated. Mean values were calculated from at least 18 cells from two separate wells. All experiments were repeated at least twice.

Time-lapse analysis of focal adhesion complex dynamics

PC3 cells were transfected with a GFP-α-actinin cDNA for 48 hours. Cells were seeded on glass plates coated with fibronectin (10 μg/ml), treated with 10 nM YM155 or vehicle (DMSO) for 4 hours, and kept at 37°C and 5% CO₂ during imaging. Time-lapse videomicroscopy was done using a Leica TCS SP5 II Scanning Laser Confocal Microscope system with an HCX PL APO CS 63× 1.40 NA oil UV objective. Acquisition of live cells using an integrated Leica LAS software was performed every 1 min for a total interval of 30 min using an argon laser at 476 nm for detection of GFP-α-actinin. Actinin-positive focal adhesion complexes were identified on the basis of fluorescence intensity, thresholded, and masked using FIJI software. Identified focal adhesion complexes for every cell were tracked using generated masks through every image taken at each minute of the experiment, and individual focal adhesion life spans and newly formed focal adhesion complexes were recorded throughout the 30-min time-lapse interval. The analysis was carried out in 10 cells per condition in 10 independent time-lapse experiments using a FIJI software package.

Cell migration and invasion

Tumor cell lines were treated as indicated in each experiment, suspended in 0.1% BSA/DMEM, and seeded (1.6×10^3 to 3.2×10^3 cells/mm², depending on the cell line) in the upper compartments of 8-μm pore diameter BD Transwells. NIH3T3 conditioned medium was placed in the lower compartment as a chemoattractant, as previously described (54). Except for the complex I inhibitor, rotenone (4 μM), which was preincubated with PC3 cells, YM155 (10 nM), or inhibitors of complex II—SDHB, TTFA (100 to 400 μM), or complex III (antimycin A, 30 μM) were added to the top and bottom chambers. After 6 to 18 hours of incubation at 37°C, Transwell membranes were recovered, and cells on the upper side (nonmigratory) were wiped off the surface. Cells on the lower side of the membrane were fixed in methanol, rinsed in water, and mounted on glass slides with Vectashield medium containing DAPI (Vector Laboratories). Migrated cells on each membrane were counted by fluorescence microscopy in five different fields. For cell invasion assays, Transwell membranes were coated with Matrigel and processed as described above (54). For cell migration using a scratch closure assay, PC3 cells were transfected with control nontargeting siRNA or survivin-directed siRNA, or, alternatively, treated with vehicle or YM155, and seeded in 24-well plates (5×10^5 per well). Scratch “wounds” were made with a 10-μl pipette tip, cell debris was washed off, and cultures were maintained in complete medium containing 10% FBS at 37°C and 5% CO₂ for 24 hours. Time-lapse imaging of migrating cells was performed with a TE300 Inverted Microscope (Nikon) equipped with an incubator set at 37°C, 5% CO₂, and 95% relative humidity. Each image was acquired using a 10× objective of the same fields every 10-min time interval for a total 24 hours. Velocity of cell migration and distance traveled were quantified

under the different conditions using ImageJ's Chemotaxis and Migration Tool, version 1.01. A minimum of 30 cells per condition were individually tracked between frames, generating a live track for each individual cell. Each track was then uploaded to the Migration Tool yielding average velocity and distance traveled.

Liver metastasis model

All in vivo experiments were carried out in accordance with the *Guide for the Care and Use of Laboratory Animals* of the National Institutes of Health (NIH). Protocols were approved by an Institutional Animal Care and Use Committee at The Wistar Institute. A liver metastasis model was carried out generally as previously described (28). Briefly, 6- to 8-week-old female SCID (severe combined immunodeficient)/beige mice (three mice per experimental condition) were anesthetized with ketamine hydrochloride, the abdominal cavity was exposed by laparotomy, and 1.5×10^6 MCF-7 cells transfected with vector or mitochondrial-targeted survivin cDNA were injected into the spleen. Spleens were removed the first day after injection to minimize potentially confounding effects on metastasis due to variable growth of primary tumors. Animals were sacrificed 11 days after injection, and their livers were resected, fixed in formalin, and paraffin-embedded. Serial liver sections 500 μ m apart ($n = 15$ per each condition) were stained with hematoxylin and eosin and analyzed histologically. Metastatic foci were quantified by morphometry and expressed as number of lesions and surface areas of tumor growth compared to total surface area, as previously described (28).

Statistical analysis

Data were analyzed using the two-sided unpaired *t* tests or analysis of variance (ANOVA) using a GraphPad software package (Prism 4.0) for Windows. Data are expressed as means \pm SD or means \pm SEM of at least three independent experiments. A *P* value of <0.05 was considered statistically significant. For a metabolomics screening, missing values (if any) were assumed to be below the level of detection. However, biochemicals that were detected in all samples from one or more groups, but not in samples from other groups, were assumed to be near the lower limit of detection in the groups in which they were not detected. In this case, the lowest detected level of these biochemicals was imputed for samples in which that biochemical was not detected. After log transformation and imputation with minimum observed values for each compound, Welch's two-sample *t* test was used to identify biochemicals that differed significantly between experimental groups. The false discovery rate in the metabolomics screen was estimated using the *q* value per each compound detected. Pathways were assigned for each metabolite, allowing examination of overrepresented pathways. For classification studies, random forest analyses were performed. Statistical analyses were performed with the program "R" (<http://cran.r-project.org/>).

SUPPLEMENTARY MATERIALS

www.sciencesignaling.org/cgi/content/full/8/389/ra80/DC1

Fig. S1. Mitochondrial survivin.

Fig. S2. Survivin regulation of mitochondrial bioenergetics.

Fig. S3. Modulation of oxidative phosphorylation by survivin.

Fig. S4. Survivin regulation of mitochondrial trafficking.

Fig. S5. Regulation of membrane dynamics by survivin.

Fig. S6. Expression of mitochondrial-targeted survivin dominant negative mutant.

Fig. S7. Mitochondrial survivin-complex II regulation of tumor cell motility.

Table S1. Heat map of statistically significant biochemicals profiled in this study.

REFERENCES AND NOTES

1. D. C. Altieri, Survivin—The inconvenient IAP. *Semin. Cell Dev. Biol.* **39**, 91–96 (2015).
2. S. Fulda, D. Vucic, Targeting IAP proteins for therapeutic intervention in cancer. *Nat. Rev. Drug Discov.* **11**, 109–124 (2012).

3. T. Dohi, E. Beltrami, N. R. Wall, J. Plescia, D. C. Altieri, Mitochondrial survivin inhibits apoptosis and promotes tumorigenesis. *J. Clin. Invest.* **114**, 1117–1127 (2004).
4. T. Dohi, F. Xia, D. C. Altieri, Compartmentalized phosphorylation of IAP by protein kinase A regulates cytoprotection. *Mol. Cell* **27**, 17–28 (2007).
5. J. Hagenbuchner, A. V. Kuznetsov, P. Obexer, M. J. Ausserlechner, BIRC5/Survivin enhances aerobic glycolysis and drug resistance by altered regulation of the mitochondrial fusion/fission machinery. *Oncogene* **32**, 4748–4757 (2013).
6. D. C. Wallace, Mitochondria and cancer. *Nat. Rev. Cancer* **12**, 685–698 (2012).
7. N. C. Denko, Hypoxia, HIF1 and glucose metabolism in the solid tumour. *Nat. Rev. Cancer* **8**, 705–713 (2008).
8. M. G. Vander Heiden, L. C. Cantley, C. B. Thompson, Understanding the Warburg effect: The metabolic requirements of cell proliferation. *Science* **324**, 1029–1033 (2009).
9. G. Kroemer, J. Pouyssegur, Tumor cell metabolism: Cancer's Achilles' heel. *Cancer Cell* **13**, 472–482 (2008).
10. S. Turcan, D. Rohle, A. Goenka, L. A. Walsh, F. Fang, E. Yilmaz, C. Campos, A. W. Fabius, C. Lu, P. S. Ward, C. B. Thompson, A. Kaufman, O. Guryanova, R. Levine, A. Heguy, A. Viale, L. G. Morris, J. T. Huse, I. K. Mellinghoff, T. A. Chan, IDH1 mutation is sufficient to establish the glioma hypermethylator phenotype. *Nature* **483**, 479–483 (2012).
11. M. A. Selak, S. M. Armour, E. D. MacKenzie, H. Boulahbel, D. G. Watson, K. D. Mansfield, Y. Pan, M. C. Simon, C. B. Thompson, E. Gottlieb, Succinate links TCA cycle dysfunction to oncogenesis by inhibiting HIF- α prolyl hydroxylase. *Cancer Cell* **7**, 77–85 (2005).
12. P. S. Ward, C. B. Thompson, Metabolic reprogramming: A cancer hallmark even warburg did not anticipate. *Cancer Cell* **21**, 297–308 (2012).
13. E. Gottlieb, I. P. Tomlinson, Mitochondrial tumour suppressors: A genetic and biochemical update. *Nat. Rev. Cancer* **5**, 857–866 (2005).
14. C. Jose, N. Bellance, R. Rosignol, Choosing between glycolysis and oxidative phosphorylation: A tumor's dilemma? *Biochim. Biophys. Acta* **1807**, 552–561 (2011).
15. M. Janiszewska, M. L. Suvà, N. Riggi, R. H. Houtkooper, J. Auwerx, V. Clément-Schatto, I. Radovanovic, E. Rheinbay, P. Provero, I. Stamenkovic, Imp2 controls oxidative phosphorylation and is crucial for preserving glioblastoma cancer stem cells. *Genes Dev.* **26**, 1926–1944 (2012).
16. A. Viale, P. Pettazoni, C. A. Lyssiotis, H. Ying, N. Sánchez, M. Marchesini, A. Carugo, T. Green, S. Seth, V. Giuliani, M. Kost-Alimova, F. Muller, S. Colla, L. Nezi, G. Genovese, A. K. Deem, A. Kapoor, W. Yao, E. Brunetto, Y. Kang, M. Yuan, J. M. Asara, Y. A. Wang, T. P. Heffernan, A. C. Kimmelman, H. Wang, J. B. Fleming, L. C. Cantley, R. A. DePinho, G. F. Draetta, Oncogene ablation-resistant pancreatic cancer cells depend on mitochondrial function. *Nature* **514**, 628–632 (2014).
17. A. Roesch, A. Vultur, I. Bogeski, H. Wang, K. M. Zimmermann, D. Speicher, C. Körbel, M. W. Laschke, P. A. Gimotty, S. E. Philipp, E. Krause, S. Pätzold, J. Villanueva, C. Krepler, M. Fukunaga-Kalabis, M. Hoth, B. C. Bastian, T. Vogt, M. Herlyn, Overcoming intrinsic multidrug resistance in melanoma by blocking the mitochondrial respiratory chain of slow-cycling JARID1B^{high} cells. *Cancer Cell* **23**, 811–825 (2013).
18. W. E. Balch, R. I. Morimoto, A. Dillin, J. W. Kelly, Adapting proteostasis for disease intervention. *Science* **319**, 916–919 (2008).
19. C. M. Haynes, D. Ron, The mitochondrial UPR—Protecting organelle protein homeostasis. *J. Cell Sci.* **123**, 3849–3855 (2010).
20. Y. C. Chae, M. C. Caino, S. Lisanti, J. C. Ghosh, T. Dohi, N. N. Danial, J. Villanueva, S. Ferrero, V. Vaira, L. Santambrogio, S. Bosari, L. R. Languino, M. Herlyn, D. C. Altieri, Control of tumor bioenergetics and survival stress signaling by mitochondrial HSP90s. *Cancer Cell* **22**, 331–344 (2012).
21. B. H. Kang, J. Plescia, T. Dohi, J. Rosa, S. J. Doxsey, D. C. Altieri, Regulation of tumor cell mitochondrial homeostasis by an organelle-specific Hsp90 chaperone network. *Cell* **131**, 257–270 (2007).
22. Y. C. Chae, A. Angelin, S. Lisanti, A. V. Kossenkov, K. D. Speicher, H. Wang, J. F. Powers, A. S. Tischler, K. Pacak, S. Fliedner, R. D. Michalek, E. D. Karoly, D. C. Wallace, L. R. Languino, D. W. Speicher, D. C. Altieri, Landscape of the mitochondrial Hsp90 metabolome in tumours. *Nat. Commun.* **4**, 2139 (2013).
23. L. A. Lavery, J. R. Partridge, T. A. Ramelot, D. Elnatan, M. A. Kennedy, D. A. Agard, Structural asymmetry in the closed state of mitochondrial Hsp90 (TRAP1) supports a two-step ATP hydrolysis mechanism. *Mol. Cell* **53**, 330–343 (2014).
24. E. Beltrami, J. Plescia, J. C. Wilkinson, C. S. Duckett, D. C. Altieri, Acute ablation of survivin uncovers p53-dependent mitotic checkpoint functions and control of mitochondrial apoptosis. *J. Biol. Chem.* **279**, 2077–2084 (2004).
25. E. T. Roussos, J. S. Condeelis, A. Patsialou, Chemotaxis in cancer. *Nat. Rev. Cancer* **11**, 573–587 (2011).
26. F. J. Sulzmaier, C. Jean, D. D. Schlaepfer, FAK in cancer: Mechanistic findings and clinical applications. *Nat. Rev. Cancer* **14**, 598–610 (2014).
27. T. Hara, A. Takamura, C. Kishi, S. Iemura, T. Natsume, J. L. Guan, N. Mizushima, FIP200, a ULK-interacting protein, is required for autophagosome formation in mammalian cells. *J. Cell Biol.* **181**, 497–510 (2008).
28. S. Mehrotra, L. R. Languino, C. M. Raskett, A. M. Mercurio, T. Dohi, D. C. Altieri, IAP regulation of metastasis. *Cancer Cell* **17**, 53–64 (2010).

29. S. Fulda, Regulation of cell migration, invasion and metastasis by IAP proteins and their antagonists. *Oncogene* **33**, 671–676 (2014).
30. T. K. Oberoi, T. Dogan, J. C. Hocking, R. P. Scholz, J. Mooz, C. L. Anderson, C. Karreman, D. Meyer zu Heringdorf, G. Schmidt, M. Ruonala, K. Namikawa, G. S. Harms, A. Carpy, B. Macek, R. W. Köster, K. Rajalingam, IAPs regulate the plasticity of cell migration by directly targeting Rac1 for degradation. *EMBO J.* **31**, 14–28 (2012).
31. T. Dogan, G. S. Harms, M. Hekman, C. Karreman, T. K. Oberoi, E. S. Alnemri, U. R. Rapp, K. Rajalingam, X-linked and cellular IAPs modulate the stability of C-RAF kinase and cell motility. *Nat. Cell Biol.* **10**, 1447–1455 (2008).
32. J. Liu, D. Zhang, W. Luo, Y. Yu, J. Yu, J. Li, X. Zhang, B. Zhang, J. Chen, X. R. Wu, G. Rosas-Acosta, C. Huang, X-linked inhibitor of apoptosis protein (XIAP) mediates cancer cell motility via Rho GDP dissociation inhibitor (RhoGDI)-dependent regulation of the cytoskeleton. *J. Biol. Chem.* **286**, 15630–15640 (2011).
33. J. Yu, D. Zhang, J. Liu, J. Li, Y. Yu, X. R. Wu, C. Huang, RhoGDI SUMOylation at Lys-138 increases its binding activity to Rho GTPase and its inhibiting cancer cell motility. *J. Biol. Chem.* **287**, 13752–13760 (2012).
34. E. R. Geisbrecht, D. J. Montell, A role for *Drosophila* IAP1-mediated caspase inhibition in Rac-dependent cell migration. *Cell* **118**, 111–125 (2004).
35. T. Dohi, K. Okada, F. Xia, C. E. Wilford, T. Samuel, K. Welsh, H. Marusawa, H. Zou, R. Armstrong, S. Matsuzawa, G. S. Salvesen, J. C. Reed, D. C. Altieri, An IAP-IAP complex inhibits apoptosis. *J. Biol. Chem.* **279**, 34087–34090 (2004).
36. P. Fortugno, E. Beltrami, J. Plescia, J. Fontana, D. Pradhan, P. C. Marchisio, W. C. Sessa, D. C. Altieri, Regulation of survivin function by Hsp90. *Proc. Natl. Acad. Sci. U.S.A.* **100**, 13791–13796 (2003).
37. B. H. Kang, F. Xia, R. Pop, T. Dohi, M. Socolovsky, D. C. Altieri, Developmental control of apoptosis by the immunophilin aryl hydrocarbon receptor-interacting protein (AIP) involves mitochondrial import of the survivin protein. *J. Biol. Chem.* **286**, 16758–16767 (2011).
38. J. C. Ghosh, T. Dohi, B. H. Kang, D. C. Altieri, Hsp60 regulation of tumor cell apoptosis. *J. Biol. Chem.* **283**, 5188–5194 (2008).
39. A. S. Tan, J. W. Baty, M. V. Berridge, The role of mitochondrial electron transport in tumorigenesis and metastasis. *Biochim. Biophys. Acta* **1840**, 1454–1463 (2014).
40. V. S. LeBleu, J. T. O'Connell, K. N. Gonzalez Herrera, H. Wikman, K. Pantel, M. C. Haigis, F. M. de Carvalho, A. Damascena, L. T. Domingos Chinen, R. M. Rocha, J. M. Asara, R. Kalluri, PGC-1 α mediates mitochondrial biogenesis and oxidative phosphorylation in cancer cells to promote metastasis. *Nat. Cell Biol.* **16**, 992–1003 (2014).
41. T. Shiraishi, J. E. Verdone, J. Huang, U. D. Kahlert, J. R. Hernandez, G. Torga, J. C. Zarif, T. Epstein, R. Gatenby, A. McCartney, J. H. Elisseeff, S. M. Mooney, S. S. An, K. J. Pienta, Glycolysis is the primary bioenergetic pathway for cell motility and cytoskeletal remodeling in human prostate and breast cancer cells. *Oncotarget* **6**, 130–143 (2014).
42. P. E. Porporato, V. L. Payen, J. Perez-Escuredo, C. J. De Saedeleer, P. Danhier, T. Copetti, S. Dhup, M. Tardy, T. Vazelle, C. Bouzin, O. Feron, C. Michiels, B. Gallez, P. Sonveaux, A mitochondrial switch promotes tumor metastasis. *Cell Rep.* **8**, 754–766 (2014).
43. R. A. Gatenby, R. J. Gillies, Why do cancers have high aerobic glycolysis? *Nat. Rev. Cancer* **4**, 891–899 (2004).
44. G. L. Semenza, HIF-1 mediates metabolic responses to intratumoral hypoxia and oncogenic mutations. *J. Clin. Invest.* **123**, 3664–3671 (2013).
45. C. Wu, S. B. Asokan, M. E. Berginski, E. M. Haynes, N. E. Sharpless, J. D. Griffith, S. M. Gomez, J. E. Bear, Arp2/3 is critical for lamellipodia and response to extracellular matrix cues but is dispensable for chemotaxis. *Cell* **148**, 973–987 (2012).
46. I. R. Boldogh, L. A. Pon, Mitochondria on the move. *Trends Cell Biol.* **17**, 502–510 (2007).
47. W. M. Saxton, P. J. Hollenbeck, The axonal transport of mitochondria. *J. Cell Sci.* **125**, 2095–2104 (2012).
48. J. Zhao, J. Zhang, M. Yu, Y. Xie, Y. Huang, D. W. Wolff, P. W. Abel, Y. Tu, Mitochondrial dynamics regulates migration and invasion of breast cancer cells. *Oncogene* **32**, 4814–4824 (2013).
49. S. P. Desai, S. N. Bhatia, M. Toner, D. Irimia, Mitochondrial localization and the persistent migration of epithelial cancer cells. *Biophys. J.* **104**, 2077–2088 (2013).
50. D. N. Church, D. C. Talbot, Survivin in solid tumors: Rationale for development of inhibitors. *Curr. Oncol. Rep.* **14**, 120–128 (2012).
51. A. Rauch, D. Hennig, C. Schafer, M. Wirth, C. Marx, T. Heinzl, G. Schneider, O. H. Kramer, Survivin and YM155: How faithful is the liaison? *Biochim. Biophys. Acta* **1845**, 202–220 (2014).
52. S. Fulda, L. Galluzzi, G. Kroemer, Targeting mitochondria for cancer therapy. *Nat. Rev. Drug Discov.* **9**, 447–464 (2010).
53. B. H. Kang, J. Plescia, H. Y. Song, M. Meli, G. Colombo, K. Beebe, B. Scroggins, L. Neckers, D. C. Altieri, Combinatorial drug design targeting multiple cancer signaling networks controlled by mitochondrial Hsp90. *J. Clin. Invest.* **119**, 454–464 (2009).
54. M. C. Caino, Y. C. Chae, V. Vaira, S. Ferrero, M. Nosotti, N. M. Martin, A. Weeraratna, M. O'Connell, D. Jernigan, A. Fatatis, L. R. Languino, S. Bosari, D. C. Altieri, Metabolic stress regulates cytoskeletal dynamics and metastasis of cancer cells. *J. Clin. Invest.* **123**, 2907–2920 (2013).
55. F. Li, E. J. Ackermann, C. F. Bennett, A. L. Rothermel, J. Plescia, S. Tognin, A. Villa, P. C. Marchisio, D. C. Altieri, Pleiotropic cell-division defects and apoptosis induced by interference with survivin function. *Nat. Cell Biol.* **1**, 461–466 (1999).

Acknowledgments: We thank J. Hayden and F. Keeney of the Wistar Imaging Shared Resource for excellent assistance. **Funding:** This work was supported by NIH grants P01 CA140043 (D.C.A. and L.R.L.), R01 CA78810 and CA190027 (D.C.A.), R01 CA089720 (L.R.L.), and F32 CA177018 (M.C.C.) and the Office of the Assistant Secretary of Defense for Health Affairs through the Prostate Cancer Research Program under award no. W81XWH-13-1-0193 (D.C.A.). Support for Core Facilities used in this study was provided by Cancer Center Support Grant CA010815 to The Wistar Institute. **Author contributions:** D.B.R., M.C.C., J.H.S., and D.C.A. designed the research; D.B.R., M.C.C., J.H.S., and A.A. performed the research; D.B.R., M.C.C., J.H.S., A.A., D.C.W., L.R.L., and D.C.A. analyzed the data; and D.B.R., M.C.C., J.H.S., and D.C.A. wrote the paper. **Competing interests:** The authors declare that they have no competing interests.

Submitted 19 March 2015
Accepted 22 July 2015
Final Publication 11 August 2015
10.1126/scisignal.aab1624

Citation: D. B. Rivadeneira, M. C. Caino, J. H. Seo, A. Angelin, D. C. Wallace, L. R. Languino, D. C. Altieri, Survivin promotes oxidative phosphorylation, subcellular mitochondrial repositioning, and tumor cell invasion. *Sci. Signal.* **8**, ra80 (2015).

Survivin promotes oxidative phosphorylation, subcellular mitochondrial repositioning, and tumor cell invasion

Dayana B. Rivadeneira, M. Cecilia Caino, Jae Ho Seo, Alessia Angelin, Douglas C. Wallace, Lucia R. Languino and Dario C. Altieri (August 11, 2015)

Science Signaling **8** (389), ra80. [doi: 10.1126/scisignal.aab1624]

The following resources related to this article are available online at <http://stke.sciencemag.org>.
This information is current as of September 29, 2015.

Article Tools	Visit the online version of this article to access the personalization and article tools: http://stke.sciencemag.org/content/8/389/ra80
Supplemental Materials	"Supplementary Materials" http://stke.sciencemag.org/content/suppl/2015/08/07/8.389.ra80.DC1
Related Content	The editors suggest related resources on <i>Science's</i> sites: http://stke.sciencemag.org/content/sigtrans/7/329/ra56.full http://stke.sciencemag.org/content http://www.sciencemag.org/content/sci/334/6054/376.full http://stm.sciencemag.org/content/scitransmed/4/133/133ra56.full
References	This article cites 55 articles, 14 of which you can access for free at: http://stke.sciencemag.org/content/8/389/ra80#BIBL
Permissions	Obtain information about reproducing this article: http://www.sciencemag.org/about/permissions.dtl